Hungarian University of Agriculture and Life Sciences

Doctoral School of Environmental Sciences

Integration of Remote Sensing and Field Data for Monitoring the Environmental Impact of Wetlands Restoration

Case Study: Al-Hammar Marshland, Southern Iraq

Doctoral Dissertation (PhD)

Sadiq Al-Maliki

GÖDÖLLŐ, HUNGARY

2023

Hungarian University of Agriculture and Life Sciences, Hungary

Name of Doctoral School: Doctoral School of Environmental Sciences

Discipline: Environmental Sciences / Water Resources Management Engineering

Head of Doctoral School: Csákiné Dr Erika Michéli PhD
Professor, head of department
Department of Soil Science and Agrochemistry
Faculty of Agricultural and Environmental Sciences
Institute of Environmental Sciences

Supervisor(s): Professor Zoltán Vekerdy PhD, Department of Water Management and Climate Adaptation, Hungarian University of Agriculture and Life Sciences.

Professor Gusztáv Jakab PhD, Department of Water Management and Climate Adaptation, Hungarian University of Agriculture and Life Sciences.

Approval of Supervisor(s) Approval of Head of Doctoral School

Professor Zoltán Vekerdy PhD Professor Csákiné Erika Michéli PhD

…….

Professor Gusztáv Jakab PhD

……

TABLE OF CONTENTS

LIST OF ABBREVIATIONS

Abbreviation	Description
ADCP	Acoustic Doppler Current Profile
BCM	Billion cubic meters
CMEWQIM	Canadian Council of Ministers of the Environment Water Quality Index Model
CRIM	Center for the Restoration of Iraqi Marshes
CRIMW	Center for the Restoration of Iraqi Marshes & Wetlands
DEM	Digital Elevation Model
DO	Dissolved Oxygen
EC	Electric Conductivity
ET	Evapotranspiration
ET_0	Reference Evapotranspiration
ET_a	Actual Evapotranspiration
ETM+	Enhanced Thematic Mapper
FAO	Food and Agriculture Organization of the United Nations
GIS	Geographical Information System
GPS	Global Positioning System
LEDAPS	Landsat Ecosystem Disturbance Adaptive Processing System
LSM	Land surface models
LCLU	Land Cover and Land Use
BCM	Billion Cubic Meters
MoWR	Ministry of Water Resources in Iraq
m.a.m.s.l.	Meter Above Mean Sea Level
MOD	Main Outfall Drain
MODIS	Moderate Resolution Imaging Spectroradiometer
MSS	Multispectral scanner
NDVI	Normalised Difference Vegetation Index
NDWI	Normalised Water Difference Index
NDMI	Normalised Difference Moisture Index
IWRM	Integrated Water Resources Management
OM	Organic Matter
OLI	Operational Land Imager

PET	Potential evapotranspiration
RS	Remote Sensing
SEBS	Surface Energy Balance System
SSEBop	Operational Simplified Surface Energy Balance System
SPSS	Statistical Package for the Social Sciences Software
SS	Soil Salinity
TDS	Total Dissolved Solids
TIRS	Thermal Infrared Sensor
TM	Thematic Mapper
UNEP	United Nations Environment Programme
UNESCO	United Nations Educational, Scientific and Cultural Organization
UTM-WGS84	Universal Transverse Mercator- World Geodetic System
WQI	Water Quality Index
WHO	Would Health Organization

LIST OF TABLES

LIST OF FIGURES

1 INTRODUCTION

1.1 Background

Diminishing water resources lead to water scarcity worldwide, especially in semi-arid and arid climatic zones with high evaporation rates. The combined evaporation and transpiration from soil moisture, open water surfaces, and vegetation are frequently referred to as evapotranspiration (ET). It is an intricate process driven by the available energy covering latent heat. Also, it is limited by water availability, the evaporating surface's resistance, and the atmosphere's vapour deficit. Accurate analysis and modelling of regional hydrological processes require detailed knowledge about the spatiotemporal distribution of this flux (Bashford *et al.*, 2002). Regional evapotranspiration cannot be directly measured due to its complexity. Several approaches exist for describing its components, using state and rate variables measured at different spatial and temporal scales. Practical limitations are also frequently imposed by missing data and varying inaccuracies in the measurements of the parameters. In arid regions, the modelled ET is more sensitive to uncertainties in the net radiation, and in humid circumstances, it is more sensitive to uncertainties in precipitation (Jung *et al.*, 2019).

Estimating actual ET in agricultural and environmental monitoring is fundamental, based on various land cover/land use (LCLU) types in the different climatic zones and meteorological data availability. Several empirical ET estimation methods have been created (Bastiaanssen *et al.*, 1998; Oberg and Melesse, 2006) based on various land cover land uses for different climatic zones and the availability of meteorological data. These methods are usually valid for small areas due to static data of point measurements. The calculation and estimation of ET need several parameters from metrological stations. Sometimes the missing data, uncorrected measurements, especially from pan evaporation, and uncertainties in the measurements of solar radiation, humidity, and wind speed cause four times larger errors in the estimation of ET than the error due to air temperature (Tabari *et al.*, 2012). Furthermore, the most frequently available in situ evaporation data originated from uncorrected evaporation pan measurements, leading to inaccurate estimates of the regional ET since those point measurements do not properly represent the processes in large areas.

Significant changes in land cover occur all around the world. These changes cause, among others, many environmental problems, such as erosion and increased surface runoff, and have complex interactions with drought, climate, and biodiversity (Mas, 1999). The information on LCLU is

important on large and small scales to understand the influences of many environmental factors such as climate change, desertification, and others (Yesuph and Dagnew, 2019).

Wetlands play an essential role in the local and regional water cycles, especially in arid and semi-arid regions. They are considered natural water reservoirs, habitats for many plants and animals, and carbon stores and thus play a significant role in reducing global warming (Tiner, Lang and Klemas, 2015).

Due to major anthropogenic interventions within their catchments, many rivers that feed marshes in these areas undergo significant changes in land cover and land use over time. Many of the interventions focused on controlling and altering the natural hydrology of these rivers and ultimately modifying the flooding regimes. Surface water resources from rivers, streams, and reservoirs are at risk and are mainly used for irrigated areas in these regions (Wu *et al.*, 2015). The changes have negatively impacted the marshland's water availability and quality. This leads to unsecured preserving marshlands in arid and semi-arid areas because of the imbalance between potential evapotranspiration (ET) and precipitation, resulting in a considerable ET deficit (Gokmen *et al.*, 2013). The use of remote sensing data becomes essential to capture the interventions on the marshes. Remote sensing data are optimal for covering the spatial extent of large marshlands and monitoring their complex ecosystems (Guo *et al.*, 2017). Therefore, due to the complexity of these areas, there is a need to follow scientific ways to monitor this ecosystem based on their land cover.

The calculation of ET in a wetland is complex because of the extreme dynamics of the land cover related to changes in vegetation (merged, submerged), open water, and soil moisture. There are several methods to calculate and estimate evaporation and evapotranspiration. Modellers of hydrological processes must balance the simple approaches based on a few parameters and the physically more explicit models, which need complex parameterisation (Polhamus *et al.*, 2013). Simple techniques are based fully or partially on empirical methods, depending on different meteorological and surface-related parameters.

Remote sensing gives much information about the Earth's surface and can be used to estimate ET over larger areas. Complex models can still be spatially limited, but nowadays, the spatial distribution of many parameters can be defined explicitly using remote sensing images captured by sensors on satellites or aeroplanes.

The increasing number of remote sensing models, satellite sensors, and no-cost satellite data for monitoring the surface temperature and vegetation parameters formed the basis for developing surface energy balance (SEB) models. SEB calculation needs a larger number of various parameters (many defined by RS data with different assumptions), like the Operational Simplified Surface Energy Balance (SSEBop) and the Energy Balance Algorithm for Land (SEBAL). Full automation is complex due to the complex processes that need local parameterisation. For monitoring and modelling wetlands, a good compromise is needed between the complexity of the applied algorithm and the need for simplicity for automatic processing (Tucker, 1979; Wan and Li, 1997; Xie and Arkin, 1997; Bastiaanssen W.G.M. *et al.*, 1998; Roerink, Su and Menenti, 2000; Su, 2002; Bastiaanssen *et al.*, 2005; Gowda *et al.*, 2008; Kalma, McVicar and McCabe, 2008; Chávez *et al.*, 2009; Glenn, Nagler and Huete, 2010; USGS, 2016; Jana *et al.*, 2016).

Several studies that compared the performance of various single-source energy balance models have arrived at different results for estimating ET. Lian (2016) and Bhattarai *et al.* (2016) found that using SSEB and METRIC methods based on Landsat 7 ETM data in oasis-desert regions provides good results.

According to Senay (2011), a valuable method to understand the limitations, strengths, and suitability of modelling for estimating actual ET is the comparison of the results with measured actual ET, which provides information for developers and users to understand better the uncertainties of model components and their effects on the ET values (Allen *et al.*, 2011). However, it is challenging to compare ET models because each model uses a different combination of factors.

Guo et al. (2017) found that remote sensing is extensively used to assess wetlands across the globe, with between 300 to 500 peer-reviewed articles published annually over the past five years. Their results also highlighted that high-resolution satellite images are essential, whereby out of the 5719 wetland research papers published globally, 1259 papers used Landsat data. Satellite images were taken by sensors on Landsat 4, 5, 7, 8, and other satellites, providing a rich global time series that spans over 31 years (1986-2017) (Guo *et al.*, 2017).

Besides water fluxes, water quality is also essential to aquatic ecosystems. Significant spatial and temporal variations characterise the water quality in wetland systems due to differences in

hydrological conditions and pollution sources. The distribution of water quality parameters (e.g., pH, sediments, algae, TDS, temperature) in wetland systems is complex and influenced by several processes, like adsorption, precipitation, filtration, excretion, biological uptake, and sedimentation/suspension; thus, monitoring the actual spatial distribution and the spatiotemporal changes of the water quality using RS and situ data are essential to support the water resources pollution control (Al-Mosewi, 2009; Al-Saad *et al.*; 2010; AL-Shamary A.Ch, 2012; Hashesh and Ahmed, 2018).

ET is one of the most significant fluxes in arid and semi-arid areas and the largest volume of flux because of the spatial spread energy flux due to different parts of the land cover of the Marshlands (deep water, shallow water, wet soil, dry soil or vegetations). This study focuses on (1) classifying and analysing the wetlands, (2) finding the best ET monitoring method by integrating the data from metrological and remote sensing to calculate actual ET with spatial distribution instead of using calculated ET from metrological data only, (3) then use the in situ data together with the classification results to analyse scenarios for water routing/management **Figure 1** Each part will be published as individual research. These three activities will be built on each other and complement each other; therefore, each chapter has a classical structure (such as problem definition, reviews, background and different methodology).

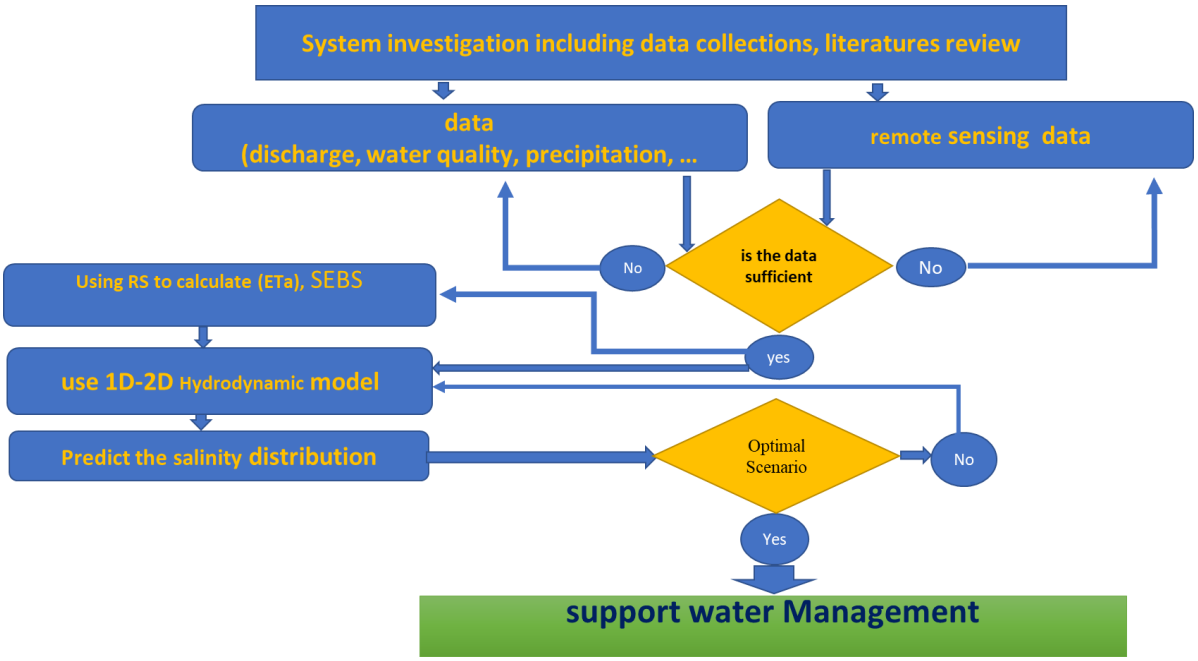

Figure 1: The research process.

1.2 Statement of the Research Problem

The diverse processes due to human and natural activities make the inventory of wetlands functioning complex, and special attention has to be paid to the spatial resolution of the data in

comparison to the spatial complexity of the ET. Satellite images provide a large amount of data but cannot offer information about all aspects of the evapotranspiration process. An integrated method is needed to provide sufficient information, so there is a need to integrate the data from satellite images and field measurements.

Conservation of wetlands and the optimal use of the available water resources require an integrated management system to ensure sustainability. The management system has to be based on extensive studies to reveal the hydrological and environmental characteristics of the wetlands. This approach secures the marshes' sustainability and meets the planning requirements by continuously monitoring the hydraulic and environmental components and maximising the information extracted from the available data.

In addition to considerations about the broad spatial coverage, the strong influence of the fluctuation of the flood cycle on the marshlands in these areas because of the availability of water upstream and due to the high ET, which exposes the soil to inundation and drought continuously and this make the annual inundation pattern complicates the inter-annual comparison, so the flood regime's effects must be accounted for. Given the concern that the weak spectral separability of wet soils from open water may prevent the accurate definition of land cover units in the post-flood state, so it is difficult to classify land cover in these areas using the two known methods (supervised and unsupervised Classification) and requires a fast approach there is a need for a new and straightforward approach to monitoring and classification. Also, studies to calculate ET in marshlands by different energy balance models and compare the results for validating the ET products are rare.

The Iraqi Marshlands form the largest wetland system in Southwest Asia. Geographically, it is extended over more than 20,000 km^2, surrounding the Tigris and Euphrates rivers' confluence in the southern part of Iraq and a part of southwestern Iran. The Tigris and the Euphrates rivers are primarily fed from the Taurus Mountain Range in Turkey. Additional parts of the rivers' transboundary water basins are in Iran, Syria, and Saudi Arabia. Turkey regulates between 80 to 95% of the Euphrates' flow, with an annual discharge of between 28.4 and 32.4 Billion Cubic Meters (BCM) per year **Figures 2** and **3**. The yearly natural variability of the Tigris River discharge was high, with rates ranging between 49.2 and 52.6 BCM before the upstream dam constructions, i.e., before the "Age of Dams" in the basin, that started in the late 1950s (Vinez and Leonard, 2010; Partow *et al*. 2005).

In the downstream area, the marshes function as flood retention basins for the excess upstream water, consisting of several once-interconnected wetland systems. Historically, the southernmost part of the system, the Al-Hammar marsh, reached 4500 km^2. Between 1991 and 1997, six canals (with a length of 5000 km) were constructed to drain the marshlands. As a result of these projects, the marshes were almost completely dry by 1999 (Munro and Touron, 1997; Vinez and Leonard, 2010; Becker, 2014). In 2001, the UNEP estimated that only 10% of the original marshlands remained. By 2003, the area of the Al-Hammar marsh decreased to 6% of its original size (Vinez and Leonard, 2010). In 2004 the Center for Restoration of Iraqi Marshes (CRIM) started re-flooding it. Nowadays, the area available for restoration does not exceed 1600 km^2 because many dried areas were recently utilised for agricultural, urban, and oil exploitation purposes **Figure 4.**

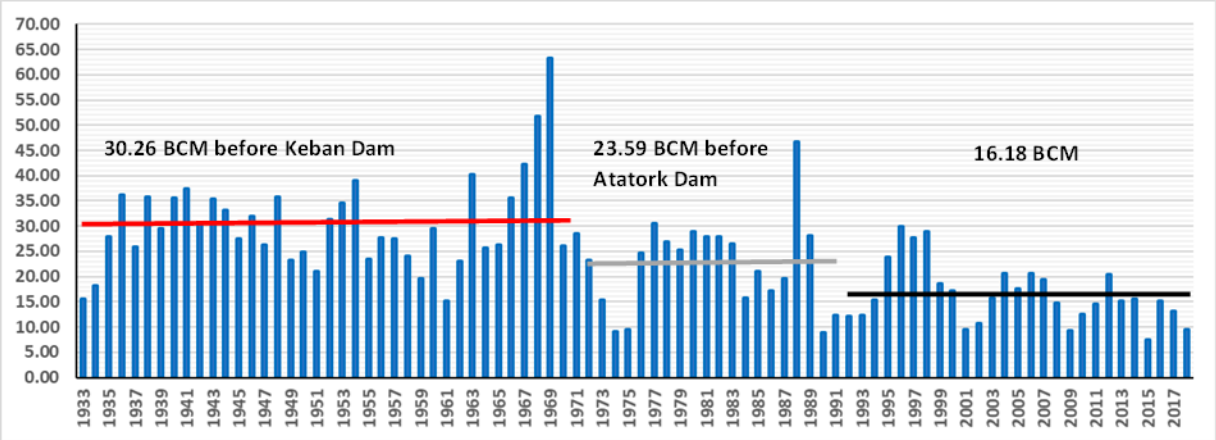

Figure 2: Annual discharge in Billion Cubic Meters (BCM) of the Euphrates River at the border of Turkey and Iraq in the period 1933-2011 (Source of data: Ministry of Water Resources, Iraq) (Al-Maliki, 2017).

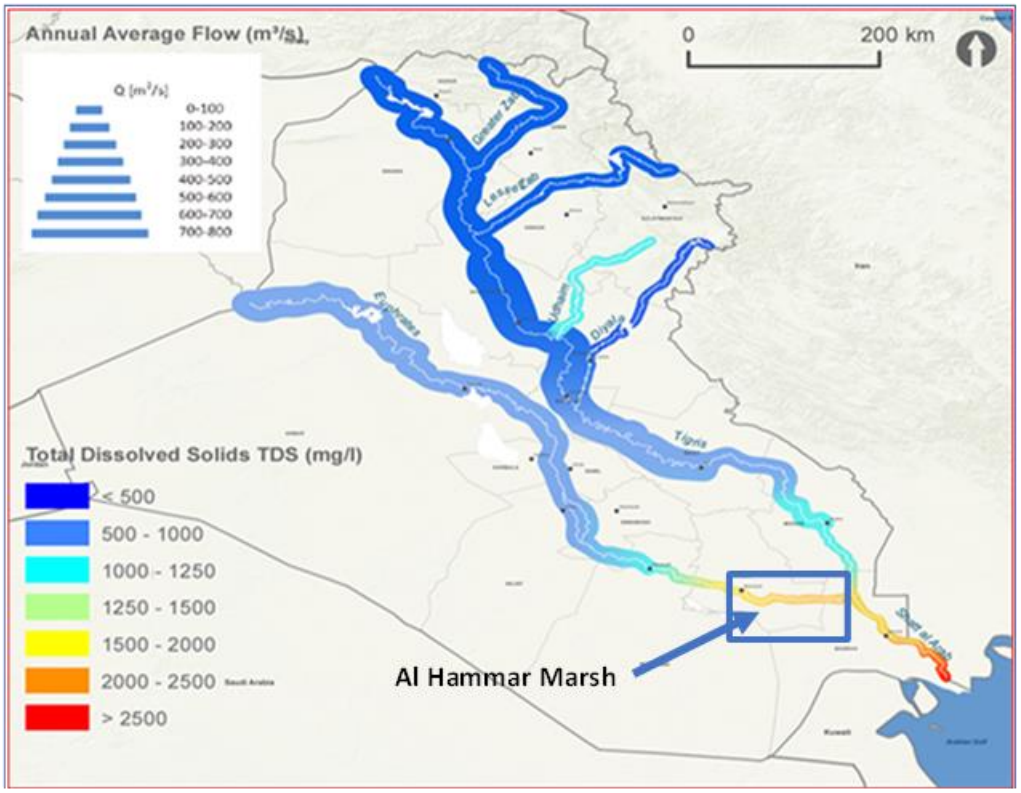

Figure 3: Present state of water quality and quantity of the main rivers (MoWR, 2014).

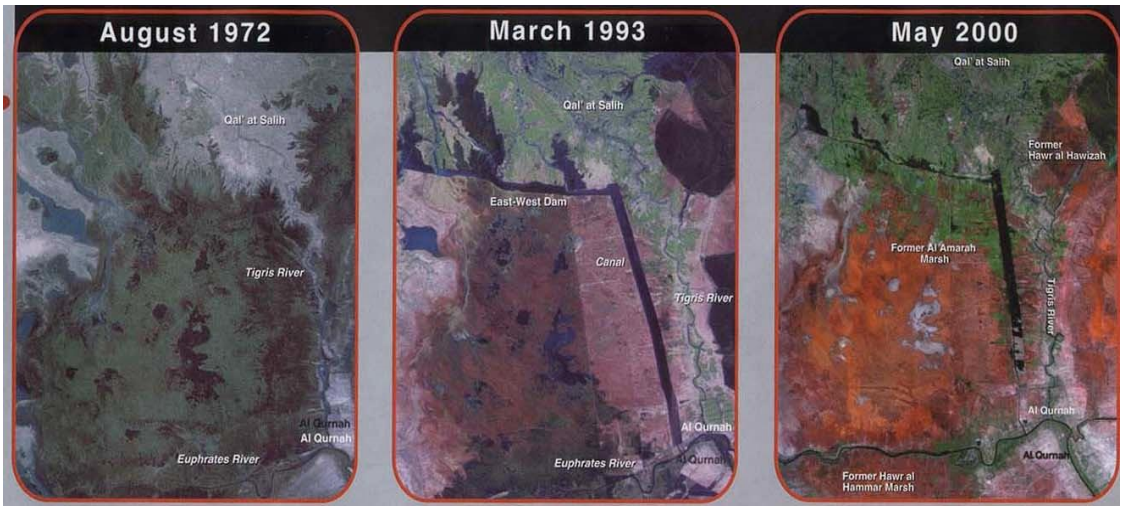

Figure 4: Deterioration of the Iraqi marshlands (UNEP, 2001).

As part of the restoration efforts, brackish effluent water from the upstream irrigation areas has been supplied to the western part of the Al-Hammar marsh since 2010 to overcome the problem of water supply shortage and prevent the wetland from drying out again. As a result, salts began accumulating in the marsh; therefore, a solution is required to limit the process and restrict the environmental effects. Brackish water is a broad term that refers to somewhat salty water, more

than freshwater but less saline than seawater. In the study area, the brackish water comes from upstream agricultural activities (drain water).

1.3 Research objective

The main research objective is to develop a remote sensing method based on data integration for analyses, classification, and monitoring of the environmental impact of wetlands restoration.

The test area of the research is the Mesopotamian marshlands (west part of Al-Hammar marsh).

1.3.1 Sub Objectives

1. Develop a fast wetland classification and monitoring method based on remote sensing data.
2. For evaluating and testing water balance scenarios under different operational conditions, calculate the time series of actual evapotranspiration from satellite images using different surface energy balance models, then compare them with the evapotranspiration calculated from metrological stations to find the optimal data processing method.
3. Analyse different water balance scenarios under various operational conditions based on field discharge measurements, collected water samples, and water losses by ET calculated from RS data.

1.3.2 Research Questions

During the research, the following questions will be answered:

- Related to sub-objective 1: How can RS data be used for quantifying the different features of land cover in wetlands for a consistent time series analysis?
- Related to sub-objective 2: How are the different actual evapotranspiration time series obtained from satellite images used?
- Related to sub-objective 2: Which is the most suitable surface energy balance model for the estimate of evapotranspiration of the marshlands, and which is the most sensitive to spatial differences?
- Related to sub-objective 3: Which strategy should be used to reduce the salinity in the Al-Hammar marshland to improve the environmental state of the wetland?

2 DESCRIPTION OF THE STUDY AREA

2.1 Location

The Al-Hammar marsh **Figure 5** is one of the largest regions of the remaining lower Mesopotamian marshlands (the largest wetland in Southwest Asia)**.** It is also the largest water body in southern Iraq. It extends from the Al-Nasiriyah Governorate in the west to the outskirts of Basra Governorate on the Shatt al-Arab River in the east. In the south, it is bordered by saline lakes and the sand dune belt of the southern desert. In the north, bordered by the Euphrates River. This marsh area covers approximately 2800 km^2 of permanent marsh and lake, expanding to over 4500 km^2 during seasonal and temporary inundation periods. At its largest extent, the marsh was approximately 120 km long and 25 km wide, with maximum water depth ranging from 1.8 to 3 m (CRIMW, 2007). The remaining marshland for restoration after 2003 is about 1762 km^2 (Aoki 2009; Guarasci *et al.* 2011; CRIM 2017) and comprises a system of deep and shallow lakes depending on the availability of water (Salim, 1962). It is located on the right side of the Euphrates River before it joins the Tigris River at Al Qurna City.

Al-Hammar marsh lies within a region of high evapotranspiration, approximately 3000 mm/year (CRIM, 2010). Al-Hammar marsh is divided into two parts; the first part (west) is located next to AL-Nassiriyah City and feeds from many rivers, while the second (east) is next to Al-Basrah City, and the tide of the Persian Gulf feeds it through the Shatt al-Arab River. The Al-Hammar Dike separates the eastern and western parts of the marsh. In the future, there is a plan to construct the Al-Hammar Barrage to connect the two parts of the marsh (CRIM, 2010). Each part of the Al-Hammar Marsh has its own hydrological properties. The western part **Figure 5** is supplied mainly from the Euphrates River by many rivers in addition to the water from the Main Outfall Drain (MOD) by Al Khamissiya Canal due to water shortage, which was completed by 2010 (brackish water); this canal has a maximum capacity of 40 m^3/s., bounded by Euphrates River in the north, Al Rumaila Oil Fields east, and Al Basrah Water Supply canal and the MOD from the south, and Suq AshShuyukh city from the west. The western part covers an area of about 1150 km^2 (CRIM, 2010).

There are many natural and artificial features in the marsh, such as islands, deep pools, security dikes, waterways, a railway, and several dikes surrounding the marsh and extending into it; these obstructions are shown in **Figures 6** and **7**.

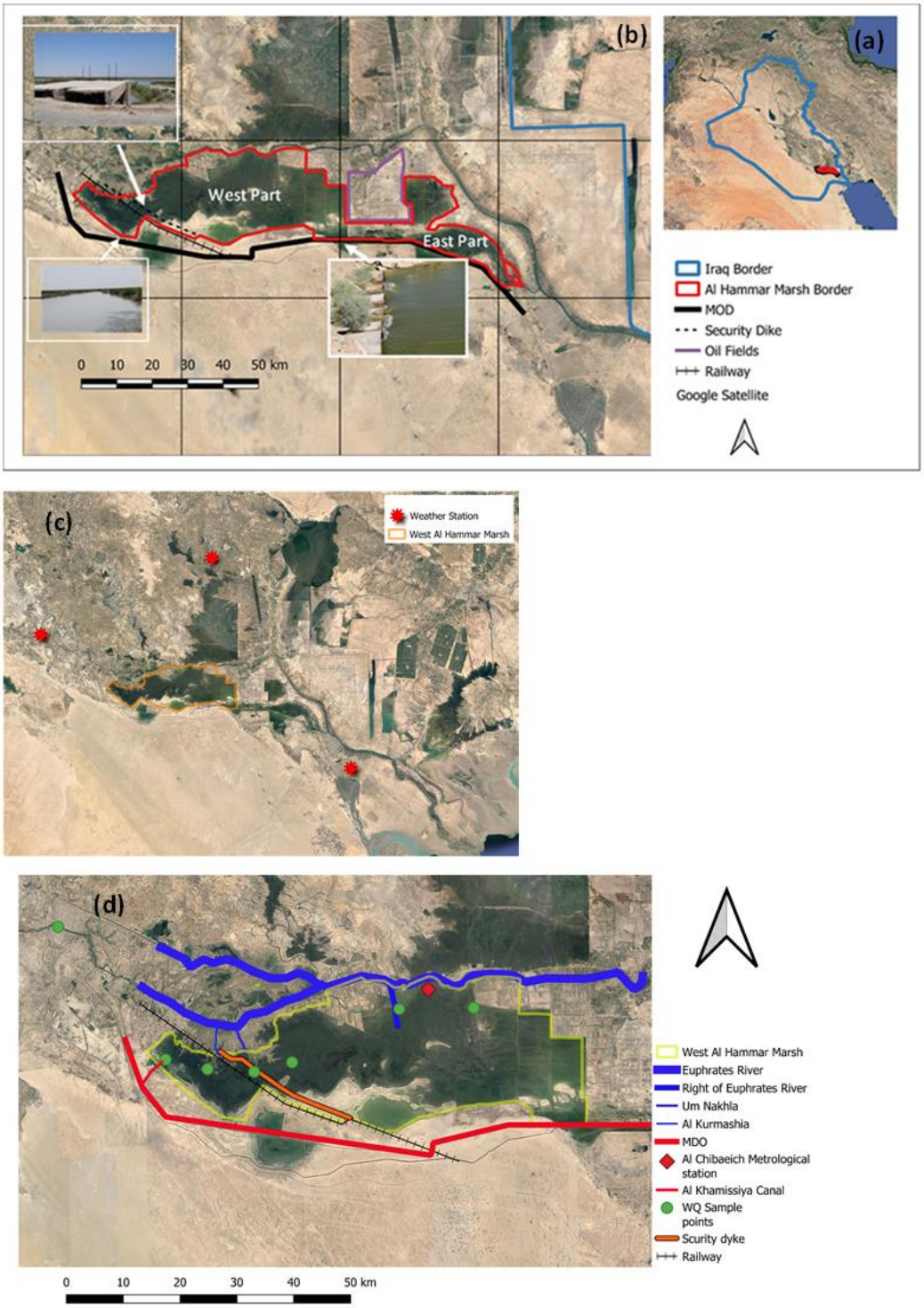

Figure 5: General layout of the study area shows (a)Iraq map, (b) Satellite image showing the geographic location and the boundary of the two parts of the Al-Hammar marsh with some hydraulic structures, (c) the boundary of west Al- Hammar marsh and the location of the weather stations, (d) A topographic map showing the different geographic objects: 1. Euphrates River, 2. Right of Euphrates River feeders, 3. Um Nakhla feeder, 4. Al Kumfeede feeder, 5. Main Outfall Drain (MOD), 6. Al Chibaeich Metrological station, 7. Al Khamissiya Canal, 8. The Water Quality locations samples, 9. The Security dyke, 10. The Railway which crosses the marsh.

2.2 Feeders and Outlets

The feeding and outlet river system of the Al-Hammar marsh is complex since some of these rivers once work as feeders and other times as outlets, according to the water levels in the marsh and these rivers.

A railway line **Figure 6(a**) crosses the north marsh boundary. Six culverts **Figure 6(b**), with varying capacities link the two sides of the marsh body along the railway.

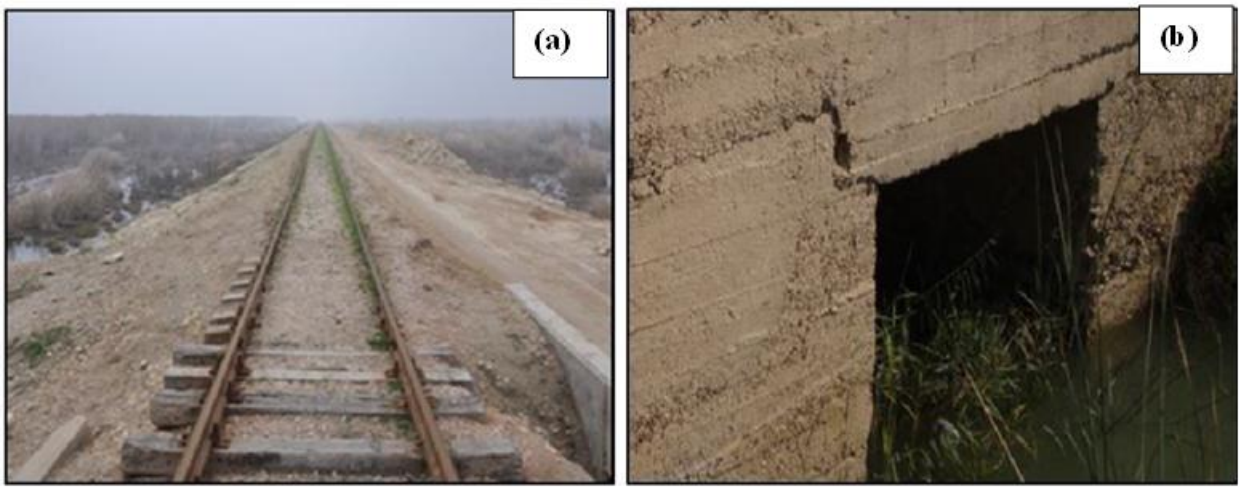

Figure 6: Railway through the Al-Hammar marsh, Aug. 2019, (a) General view (b) One of the culverts under the railway.

In addition to the railway, a dike, known as a security dike, crosses the marsh **Figure 7 (a)**. This dike crosses the north marsh boundary. Four culverts with varying capacities link the marsh along this dike **Figure 7(b)**.

Figure 7: The security dike through Al-Hammar marsh, Aug. 2019 (a) General view, (b) One of the culverts under the dike.

The discharge data of the Euphrates River were collected from the Center for the Restoration of Iraqi marsh and Wetland (CRIMW) National Center for Water Resources Management (NCWRM).

2.3 Hydraulic System

In the Al-Hammar marsh, the hydrodynamic regime is fed by water inputs from the surface flow of several rivers and precipitation. The volume of water in the marsh is governed by the balance between additions from water inflow and losses due to evaporation and outflow. The losses are usually more significant than the flow in the summer season due to ET, so the water level in the marsh gradually decreases.

2.4 Topography of the Marsh

The ground surface elevation of the marsh increases, in general, from south to northwest and northeast. The elevation generally ranges from -10 to 6 m a.m.s.l. The basic data of the digital elevation model (DEM) was obtained from the Shuttle Radar Topographical Mission Data of 90 meters resolution (CRIMW, 2006), and it was corrected in the eastern part with the data of the surveys conducted by CRIMW in different years.

Most of the marsh sediment is composed of clayey silt with some sand. Sediment within the rivers in the marsh is mainly composed of fine sands that become gradually finer as they move southwards (CRIMW, 2006). CRIMW represented Manning's Roughness Coefficients of the marsh bed using the roughness-depth relationship shown in **Figure 8**.

At an elevation of 1.2 m a.m.s.l., the western part of the Al-Hammar marsh area is kept as a permanent lake with an area of 250 km^2. At the elevation of 2 m a.m.s.l., the weir crest level of the proposed control structure separating the two parts of Al-Hammar marsh, the marsh area is 700 km^2 **Figure 9**.

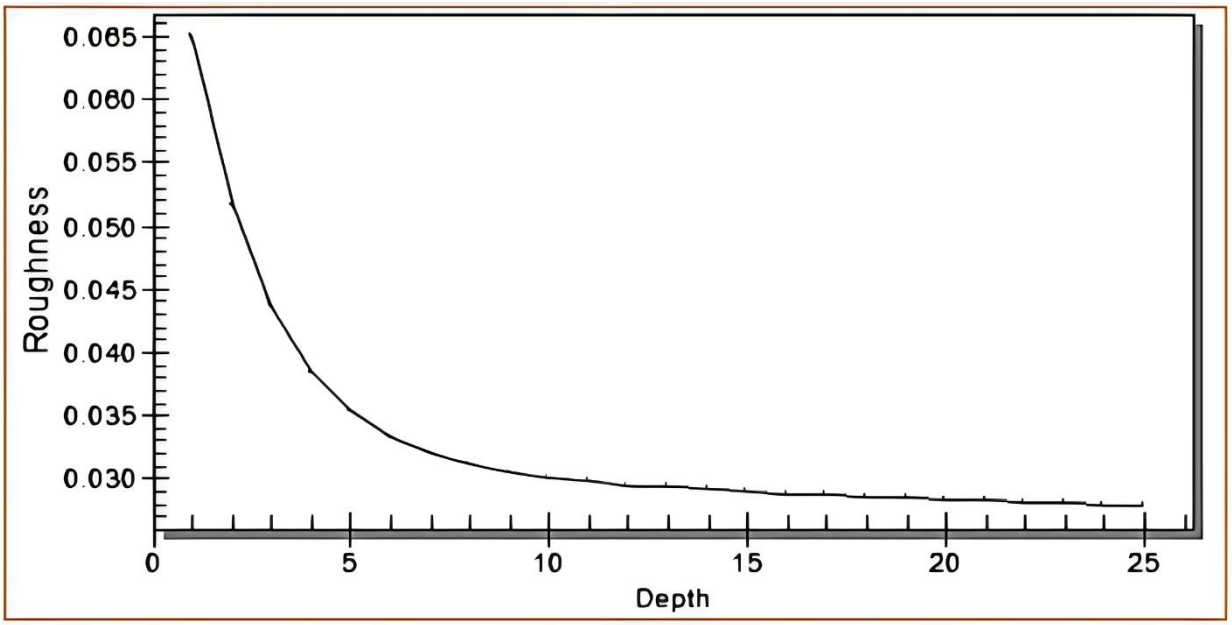

Figure 8: Manning's roughness coefficients of the bed of the Al-Hammar marsh (Center for Restoration of Iraqi marshes, 2017).

2.5 Area and Storage Rating Curves

Based on the DEM of the marsh, the elevation–area and the elevation–storage rating curves were obtained for the western part of the Al-Hammar marsh by CRIM (2010), as shown in **Figures 9** and **10**. Elevation refers to the elevation of the water surface.

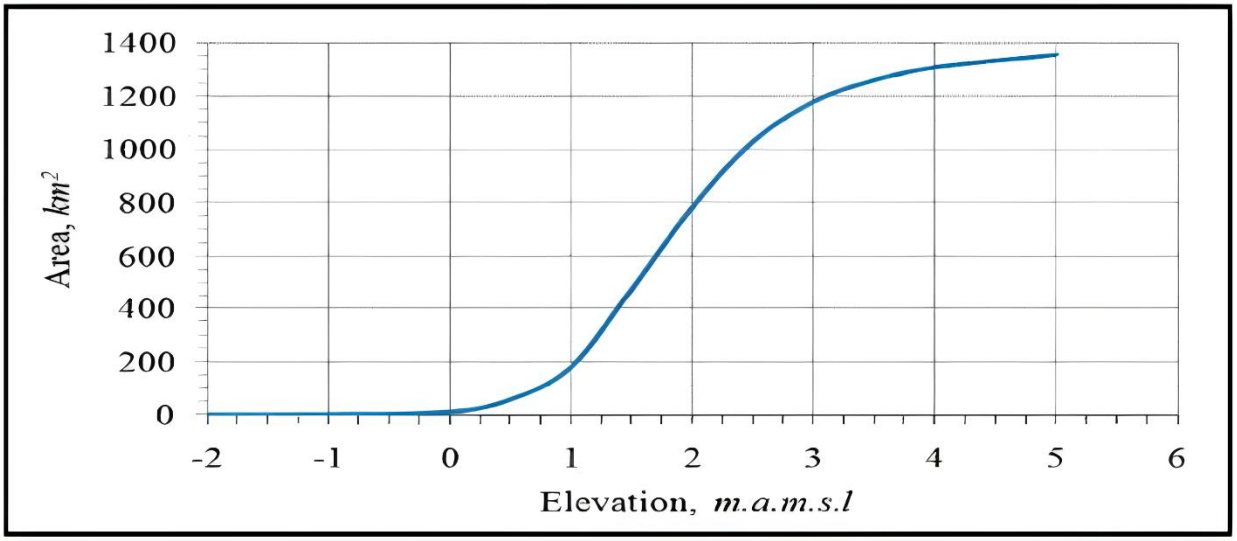

Figure 9: Area-elevation curve, CRIM, 2010.

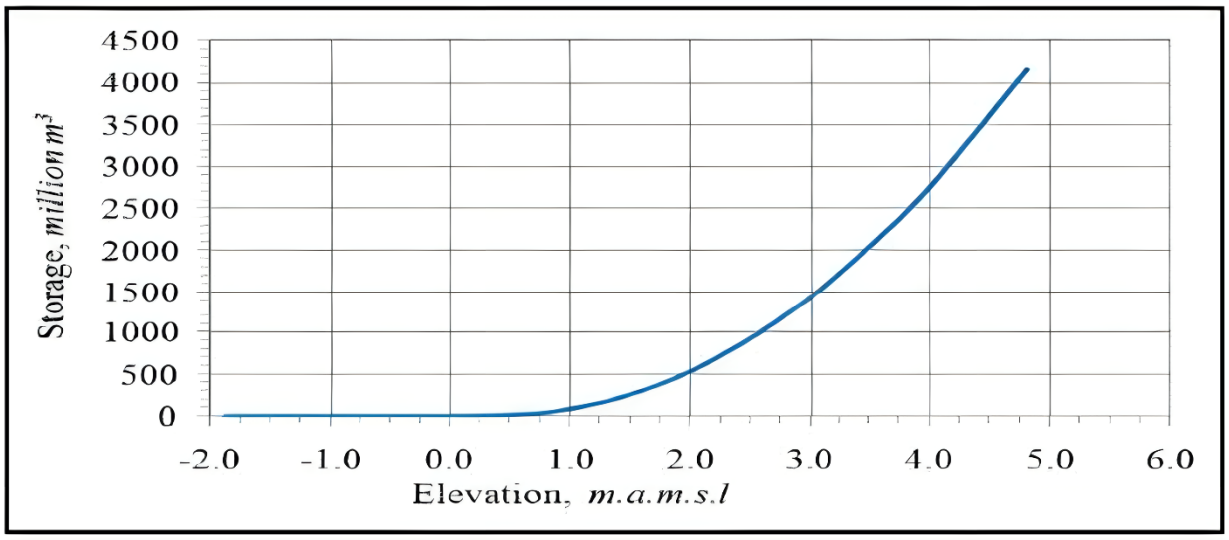

Figure 10: Storage-elevation curve, CRIM, 2010.

2.6 Vegetation

Natural wetland vegetation covers the bulk of the marsh area. Common reed dominates the core of the permanent marshes, gradually yielding to reed mace in the ephemeral seasonal zone. Temporarily inundated mudflats are overgrown with salt-tolerant vegetation of short sedges and bulrush. Deeper permanent lakes support rich submerged aquatic vegetation typified by species such as hornwort, eelgrass, pondweed, and bottom vegetation such as stonewort. In the smaller lakes and back swamps, floating vegetation of water lilies, water soldiers, and duckweed are common (Al-Hmedawy, 2008).

3 LITERATURE REVIEW

This chapter presents a summary of the earth Observation (EO) based monitoring methods already applied in the Mesopotamian marshes and then discusses the water quality aspects.

3.1 Monitoring of Marshlands

Munro and Touron (1997) conducted a study using satellite data to estimate the degradation rate in the Iraqi marshlands. Landsat TM images were used to calculate the Normalized Difference Vegetation Index (NDVI), representing the marsh's vegetation distribution. The results of NDVI analysis showed that 90% of the marshlands dried between 1992 and 1994, such as the Central marshes and Al-Hammar marsh. Due to the drainage operations in the region between 1992 and 1993, a significant vegetation collapse occurred. The changes in vegetation coverage between 1992 and 1994 were –82% in the Al-Hammar marsh, –38% in the Al Hawizeh marsh, and –92% in the Central marshes. Furthermore, the changes in the water coverage between 1992 and 1994 were –79% in the Al-Hammar marsh, +3% in the Al Hawizeh marsh, and –96% in the Central marshes. However, getting data from the field was difficult for practical reasons, making accuracy assessment impossible. This historical study characterised the degradation in the wetlands using a single indicator (NDVI) only, which resulted in generic categories (water and vegetation) without describing the differences within the categories.

Salih, Ziboon, and Salman (2006) carried out a study measuring different soil parameters in the Al-Hammar marsh, such as Total Dissolved Solids (TDS), Organic Matter (OM), and soil texture using Landsat ETM+ image. They used six training areas (vegetation, water, and soil with four subclasses types, including CL, SC/SM, CH, and ML). The study explained the relationship between the spectral reflectance in satellite images and the parameters. The results of the maximum and minimum concentrations of (TDS) for 25 samples of soil were 3.69 mg/l and 7.75 mg/l, respectively. The primary source of soil salinity (SS) was water feeding the marsh, i.e., water of the feeders, which has relatively high salinity concentrations. They also found that the unsupervised classification method is a valuable technique for preparing a schematic map for reconnaissance, soil survey, and collecting soil samples, reducing effort, time, and cost. In contrast, the supervised classification methods give an accuracy of about 99.7%. In this study, the authors used one satellite image for the classification, and the accuracy was very high, raising questions about the study’s reliability.

Abbas and Ziboon (2009) studied the utilisation of remote sensing and GIS to monitor the soils' physical properties in the Al-Hammar marsh. The study includes digital image processing (image enhancement and digital classification techniques of three bands of the Landsat 7 (ETM+)) using two methods to enhance the image (Convolution Filtering (Edge Enhancement), Histogram equalisation) by ERDAS software with matrix filter image and the outcome images with a resolution of 14.25 m after using a kernel of 7x7 to enhance the edges for the detection of the sudden changes in grey levels from one pixel to another. The study included GPS surveying the soil sampling locations and laboratory tests, including soil classification and spectral measurements. The results of this study show that the chosen visible bands are suitable for identifying soil types. They found that the soils of the study region have a high content of fine grains (clay and silt).

The study concluded that the differences in surface composition (grain size distribution of soils) and moisture content affect the soils' spectral reflectance. The soil moisture content of the surficial soil layer is a function, among others, of the soil texture. The finer the texture of the soil is, the greater its ability to keep high moisture content. The greater the soil moisture, the more it absorbs the incident energy and reflects less. Therefore, the soil appears darker when wet than when it is dry. Using high-pass convolution filtering (edge enhancement) is extremely useful for the visual interpretation of unsupervised classification. This study showed the possibility of classifying the soils from satellite images, but this method works only with bare soils. This study's reported land cover classification accuracy is unrealistically high, posing questions about those results. Moreover, the two papers above are part of a PhD thesis, and there is a similarity in their content, as they used one satellite image in 2004.

Based on RS data and GIS techniques, Al-Hmedawy (2008) analysed the geomorphology of the Al-Hammar marsh and its adjacent area. Remote sensing data of the MSS and ETM+ sensors, a DEM and topographic, geologic, and structural maps, as well as ground truth data, were used in the study. A radiometer with four filters was used to measure the spectral reflectance of the land targets. The satellite images were corrected geometrically and radiometrically using different techniques to support visual image interpretation and allow measurements. The change detection was monitored through six essential land cover classes: water, vegetation, (*sabkha*) “an area of coastal flats subject to periodic flooding and evaporation which result in the accumulation of aeolian clays, evaporites, and salts, found in North Africa and Arabia”, gravely sand, sand sheet, and salina from 1973-2003. These classes have been separated according to differences in spectral reflectance signatures. The spectral reflectance of eighteen essential land targets was measured

precisely in the field. Nine geomorphological units have been determined and classified based on their origin: aeolian, evaporitic, solutional, marine, fluvial-lacustrine, structural-denudational, structural, fluvial, and organic. A geomorphologic map was drawn showing the distribution of these main groups.

The results of digital image processing were used to separate the landcover and land use units and to define the basic geomorphologic units. The classification techniques gave good results in monitoring change detection, while the subtraction operator technique results were poor compared to other results.

The identification of the targets was done based on their spectral reflectance. The study showed an inverse relationship between spectral reflectance and soil moisture and proportional relation between the softness and sleekness from one side and reflectance from the other. Those relationships have helped to distinguish between different land targets.

The DEM showed that the general direction of the slope is southwest-northeast. Slope angles range between 0° and 1.3°. Most parts of the area slope gently except at the higher limbs of Jabal Sanam, where the slope angles reach about eight degrees. The topographic profiles drawn across a contour map showed the elevation of the Mesopotamian Plain about 7 m above sea level around the study area and the depression in the site Al-Hammar marshland and showed that the Al Batin alluvial fan consists of three sand terraces. The elevations of the first, second, and third terraces are about 33, 74, and 81 m.a.m.s.l, respectively. The dominance of the sedimentary processes and the low slope values along the rivers were clear, resulting in a dendritic drainage pattern. This geomorphological study integrated satellite images and GIS data to define the Al-Hammar marsh changes from 1973 to 2003 can conclude that geomorphologic classes cannot be determined from only satellite images since those highly depend on topographic features, too, i.e., DEMs or contour maps are also needed.

Hassan (2012) used remote sensing techniques and geographic information systems to study the extent of variations of the Al-Hammar marsh and its aquatic plant cover from 1973 to 2010 (eight satellite images were used from Landsat-MSS, TM, and ETM). They showed that in 1973 the marsh area was 2540 km^2, of which 1735 km^2 was covered with aquatic plants and 805 km^2 was covered with open water. The reduction in the marsh area started in 1990 and reached the minimum extent of 190 km^2, of which aquatic plants covered 45 km^2, and 145 km^2 was covered by

open water in 2000. After the restoration of the marsh, its area reached 1746 km^2 in 2006, of which 998 km^2 was covered with aquatic plants. In 2010, the area reached 676 km^2, of which 360 km^2 was covered with aquatic plants and 316 km^2 with open water. This historical study provides the baseline of the variations of the inundated area and the aquatic plants from 1973-2010.

Noticeable changes happened in the land use/land cover of the Al-Hammar marsh from 1975 to 2002, as Saleh (2012) showed by comparing two satellite images. There were increasing trends in the area of dry land and deep water while declining trends in the area of wet ground and shallow water. He showed that most of the marsh area was dry during 2002. Based on in situ data, it was also found that the concentrations of sulphates exceeded the allowable limits in 2002 according to the guidelines of the World Health Organization for drinking water (400 mg/l). The high concentrations of SO_4^{2-} were originated from severely burned organic matter in soils after the drainage period in the marsh after 1991. This study used two satellite images to demonstrate the surface temporal change, so this method is unsuitable for showing the whole dynamics of the changes in the region. This study used two satellite images in 1975 and 2002.

Based on the reviewed articles, the generic conclusion for monitoring the marshlands showed the potential to use satellite images to classify and monitor these areas. The supervised approach is more applicable than the unsupervised; the NDVI gave a good result for monitoring the vegetation area.

These studies used a few satellite images for comparison. Techniques such as supervised or unsupervised classification need field data for validation, which costs extra time and money. We need a free and fast methodology for classifying and monitoring the marshlands to help improve water management.

3.2 Water Quality

To address the possibilities of restoring the Iraqi marshes, Al-Ansari, Knutsson, and Ali (2012) evaluated water quality at several locations. To assess the water quality (WQ) during the summer, they took 154 water samples from the marshes at 48 sampling points. The water quality index (WQI) was calculated to characterise the water samples. Several parameters were taken into account in WQI, such as the potential of hydrogen pH, temperature, total dissolved solids, dissolved oxygen, etc. The result showed that the WQ was changing during the seasons in the marshes: in the summer, the water had poor quality, while the best water quality was in spring or

winter. The central marshes had bad water quality for every season except for the northern part. The worst WQ results for every season occurred in the Al-Hammar marsh due to the poor WQ of its feeders and the drop of the water stages in the Euphrates River, which is the primary source of the water flowing into the Al-Hammar marsh. In general, the poor WQ in the summer season is due to the high evaporation from the marshes and the decreased dilution factor in the Euphrates and Tigris rivers due to the low discharges. To improve the marshes' water quality, continuous water with good quality should flow into the marshes. The results showed that about 70-75% of the original Iraqi marshes could be restored. This study focused on the WQ defined from the in situ samplings in 2008 and showed that the WQ in the Al-Hammar marsh was bad even before using brackish water for restoration in 2010.

To study the water quality of the Al-Hammar marsh, Al-Mosewi (2009) analysed ten water samples to explain the variation of the parameters with the location within the Al-Hammar marsh. He found that the biochemical oxygen demand and dissolved oxygen are acceptable for drinking and agriculture use where the dissolved oxygen concentrations have a minimum value of 6 mg/l, which is a good range for drinking and agriculture uses, according to the World Health Organization (WHO). The results showed high concentrations of total dissolved solids TDS and high electrical conductivity (EC) at the upstream and downstream edges of the Al-Hammar marsh. The analyses showed a decrease in these parameters in the middle of the marsh. The analysis showed low concentrations of total suspended solids at the Al-Hammar marsh; it strongly depends on the water velocity in the marsh, which is considered low in the study region. This study showed high concentrations of TDS at the upstream and the downstream edges of the Al-Hammar marsh. The TDS concentration increased by using brackish water to restore the marsh.

Safiah (2010) investigated the hydrochemical changes and their effect on the Al-Hammar marsh. She collected water samples at eight locations within the marsh each month from 2009 to 2010. The water samples were tested for electrical conductivity, the total dissolved solids, pH, Na, Ca, Mg, HCO, Cl, and SO_4. She showed that the average values of these parameters at the eight locations measured during the study period, except the pH, were very high compared to their average values tested in 1973 before using brackish water to restore the marsh.

Al-Saboonchi et al. (2011) studied the present and restoration conditions of the southern Iraqi marshlands. They evaluated the water quality of the east, a part of Al-Hammar marsh, by applying the Canadian Council of Ministers of the Environment Water Quality Index Model (CMEWQIM).

The model applies two approaches based on the Canadian Council of Ministers of the Environment aquatic life guidelines as objectives and uses historical data. Variables included within the index calculation were dissolved oxygen, water temperature, pH, salinity, total nitrogen, nitrate, ammonia, sodium, and phosphorus. Based on the data recorded between 2005 and 2006, the water quality index (WQI) analysis in two approaches reflected that the water quality of the east part of Al-Hammar marsh is rated as poor, i.e., the conditions of the marsh are often below the natural or desirable levels, particularly concerning nitrogenous and sodium compounds; the marsh has not recovered yet. The results reflected that the water quality in the marshes remains far from the present criteria. This study focused on the eastern part of the Al-Hammar marsh.

A study by Al-Shamary (2012) analysed the water quality of the southern part of the Al-Hammar marsh. The water samples' physical and chemical parameters were collected from two stations within the southeastern part of the Al-Hammar marsh. Samples were collected monthly for one year, from November 2006 to November 2007. The studied physical and chemical parameters include the temperatures of air and water, total dissolved solids, pH, suspended solids, dissolved oxygen, biochemical oxygen demand, ammonia, NO_2, NO_3, PO_3, turbidity, and the velocity of flow. They found a significant difference between the tested parameters at the two stations. The highest water temperature at the two stations was recorded during August as 30ºC and 25ºC, respectively. The lowest value was recorded at the first station in February at 11ºC and the second station in January at 10ºC. Low values of ammonia and nitrite were recorded, and high concentrations of phosphates. There was a fluctuation in the values of the other tested parameters with no clear trend.

The reviewed WQ papers showed that all studies were built on in situ sampling and lab analysis; nowadays, the water salinity is a big problem, especially since the re-flooding started with brackish water and accumulated the salt inside the marsh without any outlet or methods to reduce it, and the lack of detailed information about the distribution of salinity.

3.3 Water Management

Several initiatives were made to assess the Iraqi marshlands' damages and design the restoration and rehabilitation. The Iraqi Ministry of Water Resources partly executed these initiatives through the Center for Restoration of Iraqi Marshlands and Wetlands with assistance from the international community (US, Canada, Italy, Japan, and several UN organisation, including UNEP, UNDP, and UNESCO). The restoration projects ranged from promoting ecological restoration to funding new

development projects and providing essential services in various hydrological, environmental, economic, and social fields. This also included efforts to promote multi-stakeholder processes, engage the international community through environmental agreements and develop a broader dialogue with other riparian states, particularly Turkey and Iran (CIDA, 2010; Guarasci, 2011).

The limited available water resources in the study region and the poor quality of the available water make it difficult, if not impossible, to expect complete restoration of the marshes. Moreover, the conversion of marshlands to agricultural lands, the discovery of oil, future climate change, salinisation of soils due to the adoption of poor irrigation technologies, and the executions of future upstream water impoundments (e.g., dams, dikes, and reservoirs) in Turkey, Syria, and Iraq add to the difficulty of the complete restoration (CIDA, 2010).

The most important restoration initiatives funded by the international community are presented below.

3.3.1 The Mesopotamian Marshlands: Demise of an Ecosystem

The DEWA/GRID-Geneva and UNEP conducted the study in cooperation with GRID-Sioux Falls and the Regional Office for West Asia (ROWA) (UNEP, 2001). The study's main goals were to provide scientific advice to decision-makers regarding water management in the Tigris-Euphrates River system. It examines the shrinking of the Iraqi marshlands and the causes of their degradation. The main causes of the marshlands' demise were linked to upstream dam construction and the drainage of marshlands. Note that the latter's effects are more direct on the wetlands, while regulating flows has restricted the amount and timing of the water flowing into the marshes. The study concluded that the construction of dams during the last century along the Tigris-Euphrates rivers had altered the overall water system of the region, especially the water supply to the marshlands. As a result, the spatial extent of the wetlands was reduced significantly by the year 2000. They estimated that by 2000, only 3.1%, 33.3%, and 6.4% of the 1973-1976 areas were still present for the Central, Huwaiza, and Al-Hammar marshes, respectively. In total, 7600 km^2 of wetland area disappeared between 1973 and 2000. The analysis of satellite imagery highlights the large-scale destruction of the marsh ecosystem by 2000, except in some regions across the Huwaiza marsh. This study documents the shrinkage of the Iraqi marshlands and identifies the causes of their degradation.

3.3.2 New Eden Plan

In 2006 the Iraqi Ministries of Water Resources, Environment, Municipalities and Public Works and the Italian Ministry for the Environment and Territory developed a master plan for the New Eden Project for integrated water resources management (IWRM) in the Iraqi marshlands (New Eden Team, 2006). The study aimed to develop quantitative hydrological models and help policymakers manage the complex hydrologic systems of the Mesopotamian Marshlands. Reliance on models is in line with the mission of this project to provide the Iraqi government with transparent methods that will provide reliable, fair, and consistent data to improve the quality of predictions while reducing the fiscal costs of implementation. The study implemented important tools, like hydrological models, for predicting water flows and planning water allocations to the marshes. The various control structures were suggested to achieve the goals of sustainable environmental restoration within the marshes and a detailed descriptive analysis of the ecological condition of the marshes. The primary conclusion of this study is that the restoration requires a proactive system of direct human interactions to control water input, flow, and discharge in the wetlands. Restoration cannot be achieved under a natural flood scenario, given the number of dams built upstream. Marsh restoration through direct manipulation is technically feasible and can be accomplished on a significant scale with considerably less volume of water than previously anticipated. This way, restoration can recover between 50% and 75% of the wetland extent recorded in 1970 without physically conflicting with existing land uses in Mesopotamian marshes. A variety of technically feasible water management strategies exist that decision-makers may utilise to achieve various targets. The Iraqi marshlands' hydrological situation was studied, several control structures were proposed, and an integrated management plan was suggested.

Main findings of the Eden Plan study

- Several restoration scenarios were proposed to fit the changing socio-economic conditions of the area. These scenarios target a boost for socio-economic conditions with emphasis on the marsh population and the return of refugees.
- Effective water use is critical in eliminating unproductive water use, particularly agricultural practices.
- Refugees can return to the marsh area under acceptable cultural, economic, and environmental conditions.
- Drinking water supply and wastewater treatment systems are the best alternatives for an optimal capital investment return to ensure healthy communities.

- Long-term investments are imperative for navigation along the downstream reaches of the ET Rivers (New Eden Team, 2006).

This master plan was worked out in 2006, and most of the recommendations of this study have not been implemented. Furthermore, the plan did not calculate a considerable deterioration of the water quality of those resources, which can be used for the restoration.

3.3.3 Support for Environmental Management – UNEP

UNEP developed a remote sensing-based system for monitoring the Mesopotamian marshlands (UNEP, 2009). Its objective was to support sustainable restoration by assisting in strategy formulation, monitoring marsh conditions, and supporting decision-makers. A summary of the main aspects of the study is shown below:

An integrative framework was used during this study covering several tools and analyses that covered mainly:

- Establish a marshlands Information Network (ESTIS) to define the marshlands and their activities, the progress achieved, and ways to enhance cooperation through information exchange.
- Phytotechnology project (wastewater treatment with wetlands).
- The use of remote sensing technology in the environmental monitoring of the marshlands.
- Establishment of an integrative management strategy.
- Monitoring the state of the marshes.
- Analyzing water quality and biodiversity.
- Assessment of re-flooding and habitat reconstruction.
- Assessment of socioeconomic conditions and waste generation.
- Monitoring the extent and distribution of re-flooding changes and associated variations in vegetation cover.

The major achievements and benefits reached during this study are:

- Improvement of access to adequate drinking water, sanitation, and wastewater.
- Improving the ecosystem and corresponding biodiversity.
- Assessment of water quality, remote sensing data, and policy institutional needs.
- Improving the capacity and knowledge of decision-makers and technical experts.
- Improvement of water quality and reduction of waterborne diseases.

- Documented the partial recovery of the marshlands between 2003 and 2006; a remarkable increase in water and vegetation cover. The methodology proposed was costly because it needed local validation.

3.3.4 Managing for Change: The Present and Future State of the Marshes

The Canadian International Development Agency (CIDA) conducted the study as part of the Canada-Iraq marshlands Initiative. The purpose of this study was to propose a scientific basis for the management and restoration of the marshlands. It reviewed alterations in the wetlands since 1973, targeting the extent of the marshes and key features to ensure their sustainable restoration CIDA (2010).

The health of the marshlands system was considered an indicator of the social and economic activities within the region as mentioned in the Ramsar Convention and included:

- Highlighting new evidence on the extent of the marshes in Southern Iraq and the changes that have occurred since 2003.
- Presenting the extent of the health of marshlands using data and information from the Canadian Marshlands Restoration Initiative.
- Developing future scenarios for marshland restoration and defining the best strategies for applying these scenarios.

The outcomes of this study were reached through the use of various tools and analytical processes:

- Development of an ecosystem health index.
- Presenting the key elements affecting the marshland restoration (e.g., establishing a base of scientific information that could help social and economic planning).

Future scenarios were generated based on gathered data and ecosystem factors (e.g., increased demands on water for agricultural, industrial, and domestic uses and more severe droughts caused by climate change). **Scenario (1):** used the land use of 1973 as a baseline and then compared that with the current conditions. The potential lands not converted to agriculture did not reach 70% of the 1973 levels due to agricultural development, new settlements, and other activities (such as oil drilling). The future size and health of the marshes in the remaining (non-developed) areas will depend on how much water is available. **Scenario (2):** Considering maintaining the high-water levels of 2008 and the efforts required to address transboundary water issues with Turkey and Iran to obtain the necessary water supply for this scenario. marsh extents were 38% of the similar land cover type in 1973. **Scenario (3):** A basic management alternative was implemented, and the

marshes were left to cope with the environmental conditions. Under that scenario, the wetlands would become much smaller except for a small part of the Al-Hammar Marsh, which would turn into a brackish marsh.

Besides the master plans and initiatives above, some researchers studied these areas.

According to (Altinbilek, 2004), assessments with issues related to the water management and development of the Euphrates and Tigris Rivers system. This study examined a history covering land resources development, hydrology, water, water conflict, and geography in riparian countries, namely Turkey, Syria, and Iraq. Accordingly, misconceptions and problems were examined in the context of water utilisation, availability, losses, rights, the role of dams and reservoirs, and the environmental problems of the Mesopotamian marshlands. Advantages and areas of cooperation between riparian stakeholders were equally reviewed. The main outcome showed that the Euphrates and Tigers basin water conflict requires a hydro-political approach that targets legal, political, technical, and economic aspects of its multi-dimensional characteristics. This study focused on the hydro-political and negotiation aspects.

CRIMW (2007) carried out a study that was a prelude to an initial study of each marsh and feeder. The focus was on environmental tests (biological samples and water amounted to approximately 30 elements) required to understand the marshes' environmental state. Finally, the results obtained from water testing were compared with the standard limits of concentrations of the Iraqi environmental legislation issued by the Iraqi Environment Ministry for the year 1990, especially Law No. 25 of 1967 (maintenance of rivers and public water pollution).

Jones et al. (2008) studied the impacts of hydraulic engineering projects on the Tigris-Euphrates River system and the Iraqi marshlands, including the Al-Hammar marsh. They constructed a catchment-based continuous rainfall-runoff model for the watershed area of 10^6 km^2 using the Soil Water Assessment Tool (SWAT) model based on the available data from 1964 to 1998. This study concludes with the effect of water projects in riparian countries of the marshland. The SWAT modelling showed that the discharges and the peak flow rates declined in the discussed periods. The dams built in the different modelled periods caused the decline. Comparing marsh extents from satellite images to the simulated flow proved that the Al-Hammar marsh shrinks with the declining flow. The simulation predicted that with the completion of the South Eastern Anatolya project, the Al-Hammar marsh would be reduced by at least an additional 550 km^2.

A study by the Center for the Restoration of Iraqi marsh CRIM (2007) for the restoration of Al-Hammar marsh presented the hydrological and topographical survey data, hydrological and hydraulic models that were used in the study, evaluation of the main irrigation canals, and irrigation projects within the marsh and their effects on the quantity and quality of the supplied water to the marsh, and the hydraulic structures proposed to control the Al-Hammar marsh. The study concluded that 1552 km^2 limits Al-Hammar marsh's restoration area, which forms about 52% of its original area in 1980, due to the existing constraints of productive agricultural projects, oil fields, and the Al-Basra water project. The study assigned the maximum, minimum, and average required net inflow discharges for three degrees of restoration depending on the water availability, full, moderate, and dry years. Evapotranspiration is kept minimal by minimising the water surface during hot seasons. The water circulation within the marsh will be better if more than one feeder is used to supply the marsh with the required flow rates.

Amin (2008) developed volume-elevation and elevation-area relationships based on a DEM to restore the Al-Hammar marsh. These relationships were part of a water balance model including the evapotranspiration losses to compute the required inflow into the Al-Hammar marsh for three restoration scenarios suitable for dry, moderate, and wet years with 50%, 70%, and 90% of the total area of the marsh. The inflow required for the marsh was distributed over the feeders, which are, in general, former irrigation canals for agricultural projects constructed inside the marsh area before 2003. A new feeding source was proposed from the Euphrates River to supply marsh water during flooding. The study suggests expanding the capacity of the head regulator of the Al-Kurmashia Canal to increase the water discharges that reach the marsh. Also, the study proposed a control structure on the Shatt Al-Arab River or at the outlet of the Al-Hammar marsh to control the water intruding into the marsh during ebb tide. Unfortunately, the hydraulic structures proposed in this study to improve water management have not yet been implemented.

To assess good hydrologic conditions in the Mesopotamian marshlands under different water uses scenarios, a hydrologic model for the Al-Hammar marsh was developed in integration with the water resources system model of the Euphrates and Tigris river basins and a regional hydro-climate model of the Tigris and Euphrates watershed (RegHCMTE) by Kavvas et al. (2011)., The authors suggested treating the Euphrates and Tigris basins as one hydrologic unit that can sustain the Al-Hammar marsh under severe hydroclimate conditions. The study presented a methodology for the comprehensive scientific assessment of the watershed’s water resources. This approach is

interesting, but it is difficult to deal with Euphrates and Tigris rivers as one hydrologic unit because there is a technical and legal dispute between Iraq and neighbouring countries about whether the Tigris and Euphrates rivers form one basin or two basins.

Ohara *et al.* (2011) studied the effects of water resource utilisation on the dynamic water balance of the watersheds by performing several case studies of the Euphrates and Tigris River basins. The results found that: Irrigation in Iraq and Syria can be effectively met by various constant-discharge water releases from Turkey dams after providing the Turkish sector's water demands. The complex Samarra-Thartar (regulator and barrage) might be useful to provide significant freedom for optimising water allocation in this region by diverting water from the Tigris to the Euphrates. The cooler climate in the upstream sector of the watershed compared with the downstream parts makes storing water in the upstream area to be more effective due to the reduced evaporation from the water surface in reservoirs, as well as due to the smaller surface area per storage volume in the dams of the upstream Euphrates and Tigris regions. Water diversion from the Tigris to the Euphrates through the Samarra-Thartar complex may provide significant freedom to optimise water allocation in this region. Additionally, a considerable amount of water evaporates from the reservoirs because of the arid climate in the lower Tigris-Euphrates River basin.

A summary of the reviewed articles concerning water management in the Al-Hammar marsh, these studies did not take into account the water volume supply and the spatial distribution of inundation and ET. Also, the limitation of many of these studies is that they were made before the environmental problem started due to the use of brackish water for re-flooding, resulting in salt accumulation in the marsh.

4 MONITORING AND CLASSIFICATION OF WETLANDS

The land cover for wetlands in arid and semi-arid regions is very dynamic due to extreme driving factors, like high temperature, vapour deficit in the air, extreme rainfall events, and floods on feeding rivers, which led to rapid and dramatic changes in the water and vegetation cover in wetlands. The supervised and unsupervised methods cannot be applied because these methods need detailed information and many training data.

To understand these systems and support their management, a simple, robust, and fast classification and monitoring method is required with adjustment of the threshold, which can be done with very little field data.

Remotely sensed data are optimal to cover the large spatial extent of the wetlands and overcome issues related to the limited access to certain regions. This chapter suggests a new approach for classifying marshlands and monitoring land cover changes in them. The analysis is based on a hierarchical classification of optical indices: the Normalized Difference Water Index (NDWI) (McFeeters, 1996), the Normalised Difference Moisture Index (NDMI) (Gao, 1996), and the Normalised Difference Vegetation Index (NDVI) (Tucker, 1979). Compared to the UNEP methodology (UNDP, 2010), the proposed approach results in three extra classes: wet soil, dry soil, and open water.

The study area (Al-Hammar marsh in southern Iraq) was chosen because this marsh was going through drastic changes (drying out) in the nineties. Using this approach will help to improve water management in the marsh.

4.1 Approach Description

Characterisation of wetlands in the optical part of the electromagnetic spectrum is typically achieved by analysing the key land cover units' spectral characteristics based on their visible and infrared reflectance. The separation of open water, vegetation, and soils is best achieved using the red (0.60–0.69 μm) and near-infrared (0.70–1.30 μm) wavelength ranges (Siegmund and Menz, 2005). Water shows relatively low or no reflectance in near-infrared and maximum reflectance in the blue wavelength range. Chlorophyll in healthy vegetation is a good absorber of electromagnetic energy in the visible spectrum, especially in red, and strongly reflects in the near-infrared. The different vegetation types show well-detectable differences in these characteristics. Bare soil has a gradually increasing reflectance from the visible range through the near infrared to

the middle infrared, depending on soil characteristics (texture, moisture content, and organic content). Historically, a combination of analogue panchromatic and infrared photography has been used for such analysis, although now digital multiband scanners have become the preferred medium (Verhoeven, 2008). A wide range of aerial and space-borne satellite imaging systems provide data over this spectral range but differ substantially in their temporal imaging frequency (overpasses per year), swath diameter, spatial resolution, and cost. The selection of imaging systems is enforced by a trade-off between these variables and must be attuned to the study's objectives, not vice versa.

In 2010, UNEP, UNDP, and CRIM suggested a method based on NDVI to classify marshlands, and thresholds have been developed to describe the status of marsh vegetation. The UNEP study (UNDP, 2010) showed that NDVI values greater than 0.125 represented vegetation cover. Sparse vegetation was found to correspond to NDVI values between 0.125 and 0.25, while medium-density vegetation was associated with NDVI values between 0.25 and 0.5. Dense vegetation was found to occur in areas with NDVI values above 0.5. Unfortunately, areas with NDVI values between 0.125 and 0.25 (sparse marshland vegetation) showed large commission errors, falsely expanding marshland areas. The errors resulted mainly from the inability of the NDVI to differentiate between submerged sparse water vegetation and sparse terrestrial vegetation. Consequently, there was a need to initially delineate the marshland areas as a function of their wetness before classifying the vegetative cover status in **Figure 11**. Thresholding of NDMI was used to delineate areas with high levels of soil moisture (Hunt and Rock, 1989). NDMI values greater than zero were identified as wet regions (Rokni *et al.*, 2014). Regions covered with open water were identified by their MNDWI values: regions with an MNDWI value greater than zero were defined as open water (Xu *et al.*, 2006; Ji, Zhang and Wylie, 2009; Fisher, Flood and Danaher, 2016).

4.2 Indices calculation

Three spectral-based indices were generated and used to assess the temporal variability in the inundation area of the marshes as well as the health of the vegetation coverage. The formulas of the indices used in this study are listed in **Table 1**.

Table 1: Spectral indices used to assess the Iraqi marshlands.

Index	Equation	
NDVI	$NDVI = \frac{(NIR-R)}{(NIR+R)}$	(Tucker, 1979)
NDMI	$NDMI = \frac{(NIR-SWIR_1)}{(NIR+SWIR_1)}$	(Gao, 1996)
MNDWI	$MNDWI = \frac{(Green-SWIR_1)}{(Green+SWIR_1)}$	(Xu, 2006)

NIR: Near-infrared (Band 4 in Landsat 5 and 7; Band 5 in Landsat 8); R: Red (Band 3 in Landsat 5 and 7; Band 4 in Landsat 8); B: Blue (Band 1 in Landsat 5 and 7; Band 2 in Landsat 8); $SWIR_1$: Shortwave infrared (Band 5 in Landsat 5 and 7; Band 6 in Landsat 8); Green: (Band 2 in Landsat 5 and 7; Band 3 in Landsat 8).

The spatial extent of the marshlands over time was assessed based on the methodology presented in **Figure 11**. This region was defined as the spatial extent of the marsh in each satellite image.

This methodology checked every pixel in the study area. The open-water regions were identified as pixels with NDWI values greater than zero. Non-water but wetted cells were then divided into vegetated areas and wet soils. If the NDWI value is less than zero, then other indices are checked. If NDWI < zero, then the wetted regions in the marsh are identified by excluding all areas with an NDMI < zero, considering it as a dry area or no marsh. However, if NDMI > 0, then it is considered vegetated area or wet but non-vegetated area (wetted soils) in marshlands and compared with NDVI indices.

Vegetated areas were selected as wet regions (NDMI >0) and NDVI > 0.125. Vegetated areas were further classified into densely vegetated (NDVI>0.5), medium- (0.25<NDVI<0.5) and low-density vegetation (0.125<NDVI<0.25) based on the UNEP-defined NDVI thresholds (UNDP, 2010) (**Table 2** and **Figure 12**), A model in ArcGIS 9.2[1] is used to present this methodology to develop the condition of raster for every single pixel, as shown in **Figure 11**. The raster layer is converted to the vector layer to calculate each class area (**Appendix 1**).

[1] ArcGIS 9.2 version is sufficient for this study.

Table 2: Comparison of land cover categories based on remote sensing in this study and the habitat types of the Al-Hammar marsh (1: UNDP 2010, 2: Salim et al. 2009, 3: Al-Hilli 1977).

RS categories	NDVI[1]	habitat type[2]	dominant plants[3]
water		rooted submerged, halophytic and free-floating vegetation, non-vegetated river and canal (pondweed)	*Ceratophyllum demersum* with, *Myriophyllum verticillatum*
dense vegetation	>= 0.5	flooded communities (reedbed)	*Phragmites australis*
medium density vegetation	>0.25, <0.5	flooded communities (reedbed)	*Typha domigensis*
low-density vegetation	>0.125, <0.25	flooded communities (reedbed)	*Schoenoplectus litoralis*
wet soil		terrestrial vegetation-schrub	*Carex* spp., *Juncus* spp., *Tamarix* spp.
dry area		non-vegetated desert	*Salsola* spp., *Bienertia cycloptera, Hammada elegans*, etc.

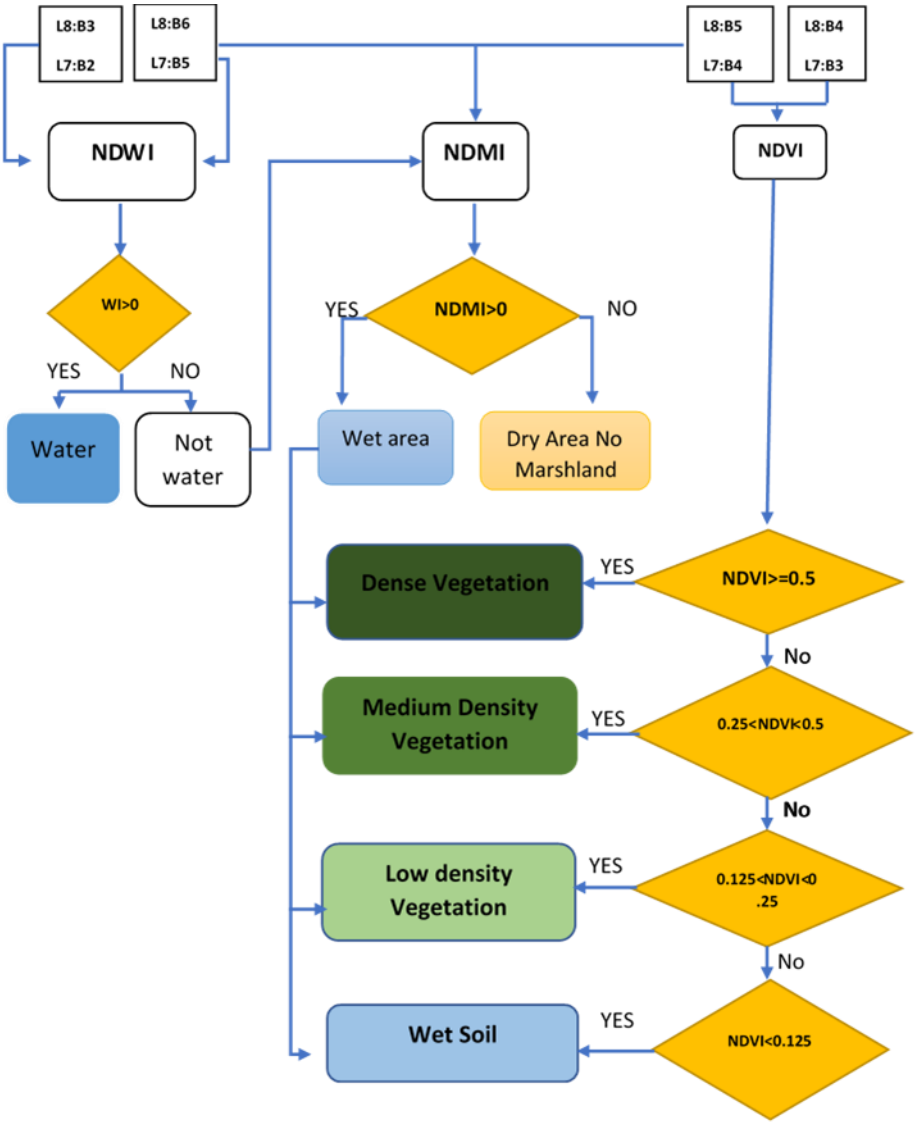

Figure 11: Method for identifying marshland extents, open waters, and vegetated areas.

*Figure 12: Photographs of land cover for the study area of typical habitats of the Al-Hammar marsh (**1**) Water with pondweeds. (**2**) Phragmites australis community. (3) Typha domigensis community. (**4**) Schoenoplectus litoralis community. (**5**) Vegetation of wet soils. (Photos by Al-Maliki).*

4.3 Data Download and Pre-processing

Images from three Landsat sensors (Thematic Mapper, TM, Enhanced Thematic Mapper, ETM, and Operational Land Imager, OLI) were used to create the time series of landcover maps. In their sun-synchronous polar orbits, Landsat satellites overpass the study area regularly (16 days; coverage over the entire study period inevitably incorporates data from all sensors and precludes simple radiometric comparison between scenes).

Ultimately, the selected available scenes with path/row (166/039) and pixel resolution (30 m*30 m) for each month with cloud cover less than 10% from six years 1991 (before degradation), 2002 (after degradation), and 2017 were selected for the analysis. A full breakdown of the data acquired is presented in (**Appendix 1**). A total of 29 Landsat images were collected for the Al-Hammar marsh. The available Landsat data for Al-Hammar are non-uniform over the analysis time. The Landsat images show a significant change in the vegetation cover in the Al-Hammar marsh over time.

Available data download for surface reflectance image products for Landsat TM, ETM+, and OLI of the study area were obtained from the USGS Earth Explorer website, http://earthexplorer.usgs.gov. Monthly monitoring was proposed for detecting the marshland

status, and because of the cloud cover problem, 58 images were available. The data used were level 2 data, which are atmospherically corrected. The atmospheric correction was based on the USGS Landsat Ecosystem Disturbance Adaptive Processing System (LEDAPS) algorithm (Masek *et al.*, 2006).

4.4 Results and Discussion

Based on the methodology, the spatial extent of the marshlands was assessed in each satellite image. A visual inspection reveals the extraordinary degree of spatial changes in its extent and vegetation cover during the study period. After a strong presence of vegetation in 1991, the 2002 image shows a near-complete lack of vegetation in the Al-Hammar marsh, while there is again vegetation cover in 2017.

The marsh lost a large portion of its vegetation cover in the year 2002 as a result of drainage and desiccation activities carried out by the Iraqi regime during that period. **Figures 13**, **14**, and **15** show the spatial distribution for the six classes for 1991, 2002, and 2017, respectively. The area covered with water dropped from more than 800 km^2 in 1991 to less than 20 km^2 in 2002 **Figure 16**. Fortunately, recent restoration efforts reversed some of these losses. In the past four years (2015-2018), the vegetated area has been above the 500 km^2 mark 75% of the time, as shown in **Figure 16**. A close observation of the vegetation density across three years, namely, 1991, 2002, and 2017, indicates the dramatic degradation that the Al-Hammar experienced in 2002 **Figure 16** The marshland lost all vegetation. The impact of the marsh restoration appears from 2015 until 2018. However, at the marshland level, the 2018 vegetation coverage and water are still lower than that of 1991 **Figure 16**. Vegetation and water between April and September covered between 1150 and 1430 km^2 of the marshland in 1991; levels in 2018 have not managed to grow beyond 1150 km^2 for water and vegetated area (**Appendix 2**).

Moreover, the composition of the vegetation changed, whereby the levels of high and medium-density vegetation dropped compared with the sparsely vegetated. Between April and September, vegetation covered 400 and 570 km^2 in 1991, less than 50 km^2 in 2002, and 170–490 km^2 in 2018. Moreover, the vegetation composition experienced a change, whereby the levels of high- and medium-density vegetation dropped compared to the sparsely vegetated area. The proposed approach can monitor the changes regarding water and land cover with time for the marshlands. **Figure 17** shows an example of open water change between different years.

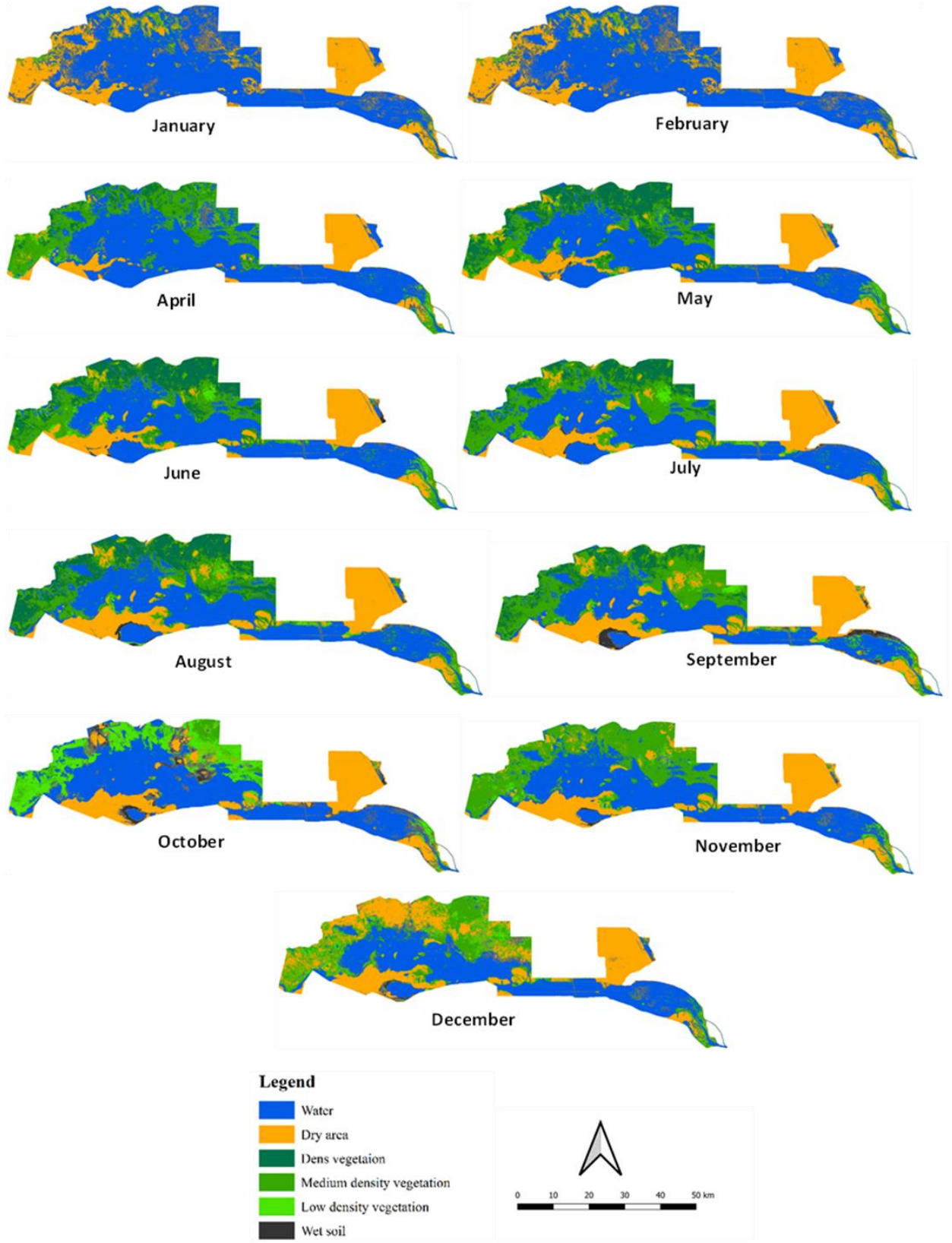

Figure 13: The extent of the marshland before the drains in (1991).

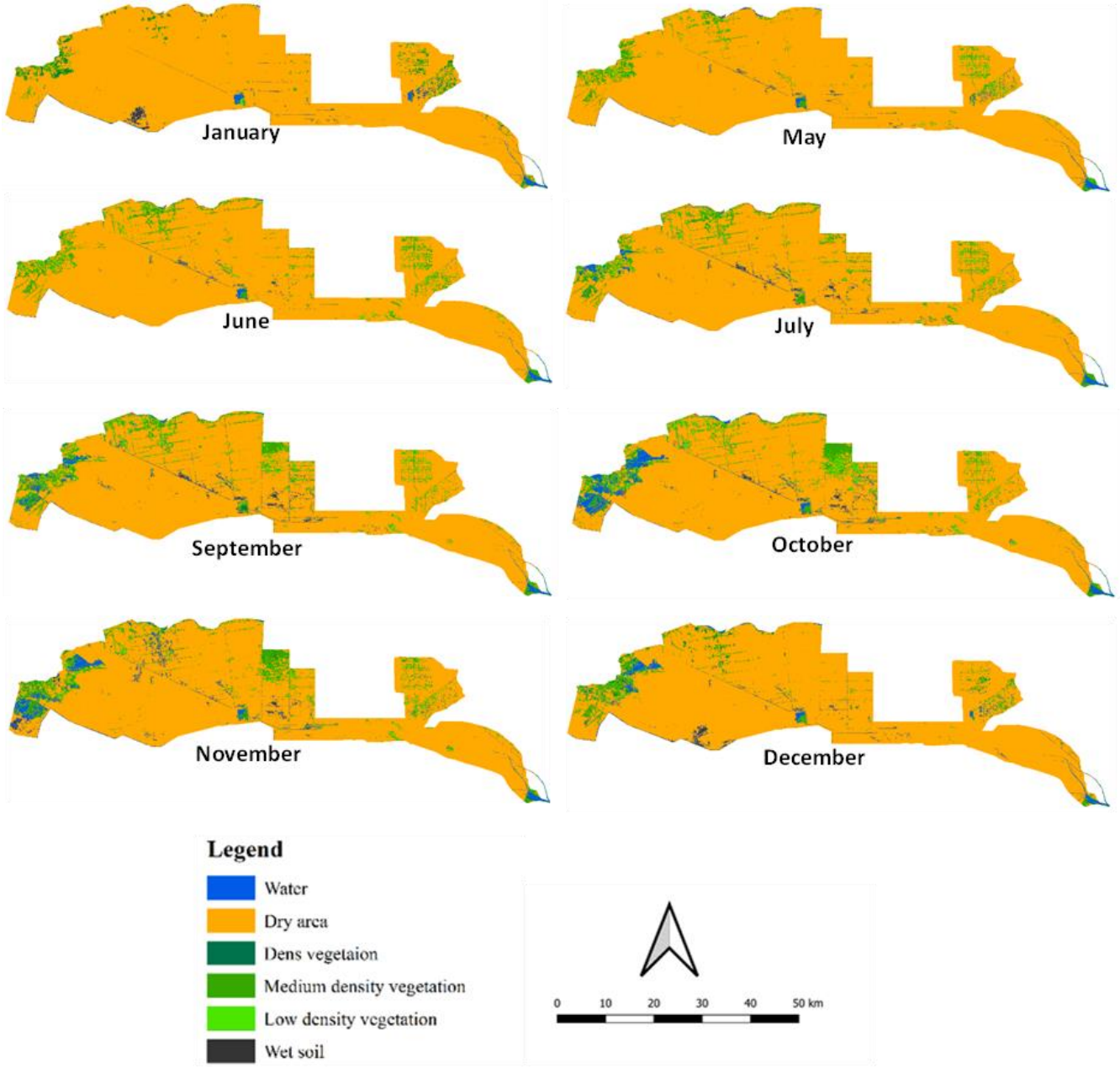

Figure 14: The extent of the swamp after the drains in (2002).

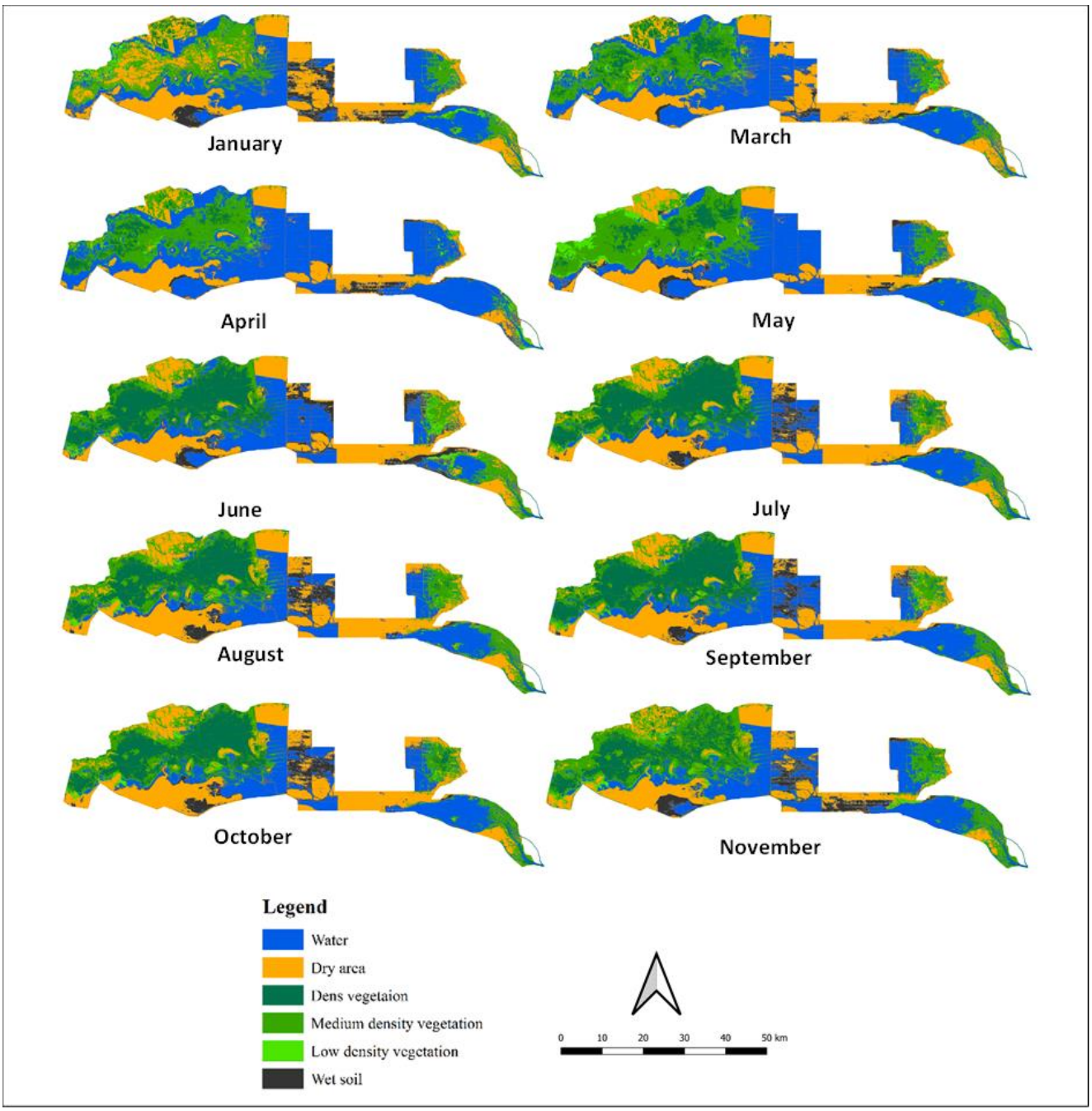

Figure 15: The extent of the marsh after the restoration in (2017).

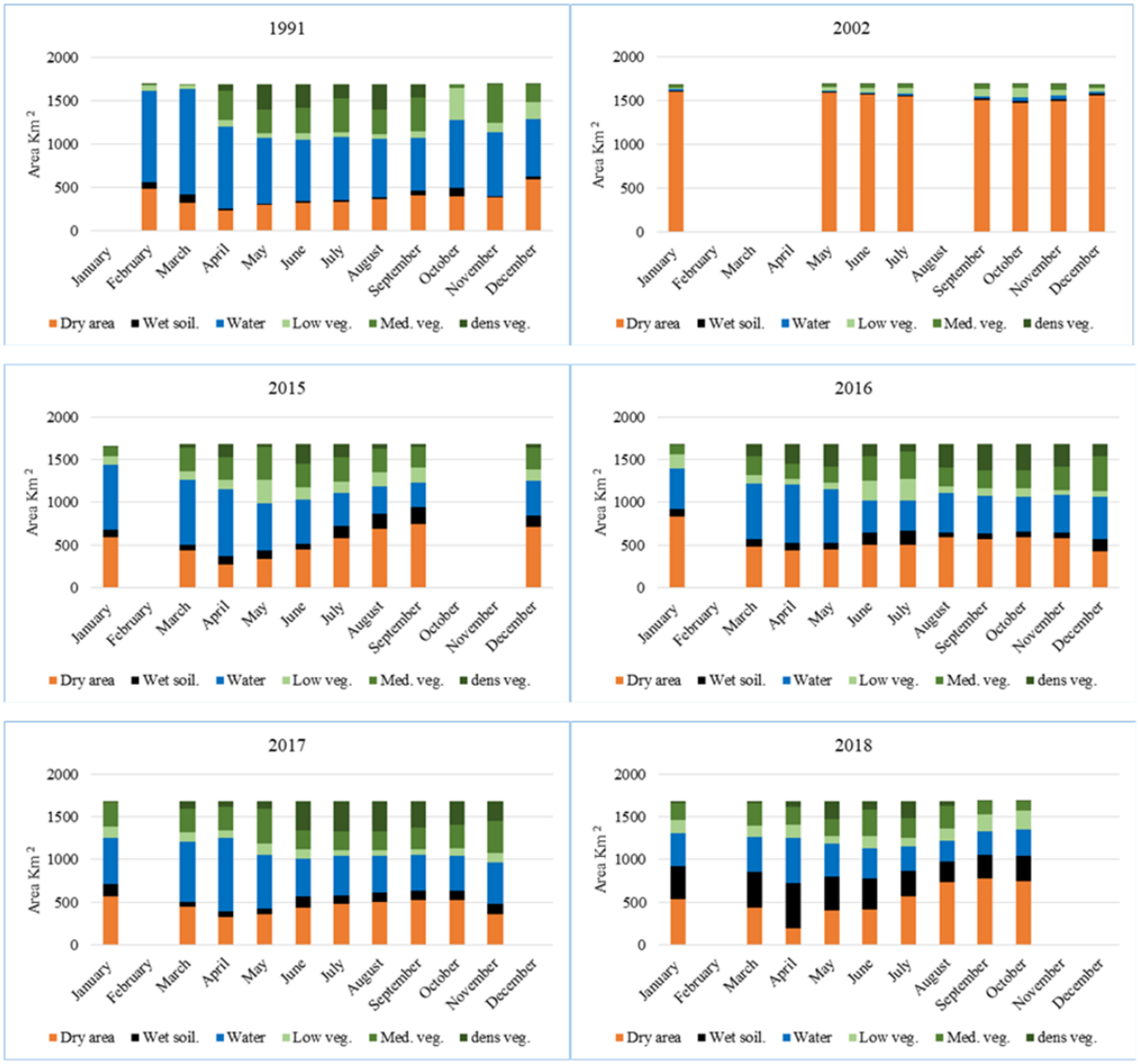

Figure 16: Monthly changes in vegetation type and water cover areas in the Al-Hammar marshland: comparison between 1991, 2002, 2015, 2016, 2017, and 2018.

Figure 17 shows the monthly change in the area of open water in the marsh in 1991, 2002, 2015, 2016, 2017, and 2018. The area of open water in 2017 is higher than in 1991 because the marsh area reduced from 4500 km^2 in 1991 to 1600 km^2 after 2003 due to the availability of water before 1991, the open water, after a while, turned into a different class of vegetation after 2003, where open water depends on the flood season. Generally, the open water areas were higher during the winter months compared with the summer months because of the high evapotranspiration.

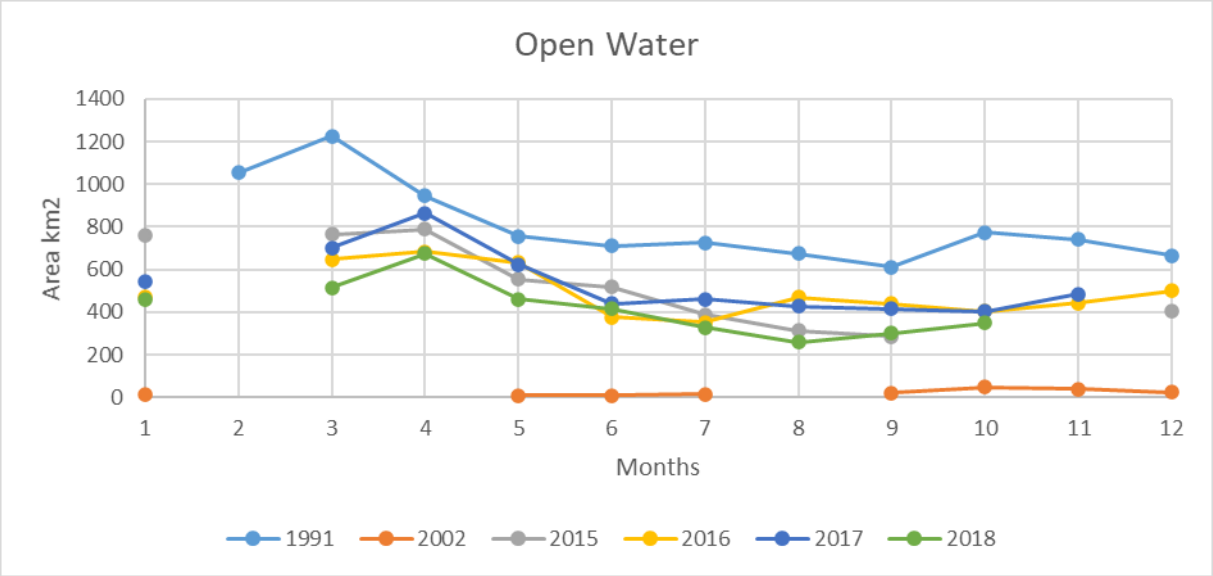

Figure 17: Changes in the open water class in the years 1991, 2002, 2015, 2016, 2017, and 2018.

In the past four years (2015–2018), the vegetated area has been above the 500 km^2 mark 75% of the time. Open water in 2017 is higher than in 1991 because the marsh area was reduced from 4500 km^2 in 1991 to 1600 km^2 after 2003. Generally, the open water areas were higher during the winter months than the summer months because of high evapotranspiration.

Figure 18 shows the total of the changing areas in different marsh classes in 1991, 2002, and 2017. In 1991 the open water class was more frequent, while in 2002, the marsh almost disappeared except for small agricultural field close to main canals fed the marsh.

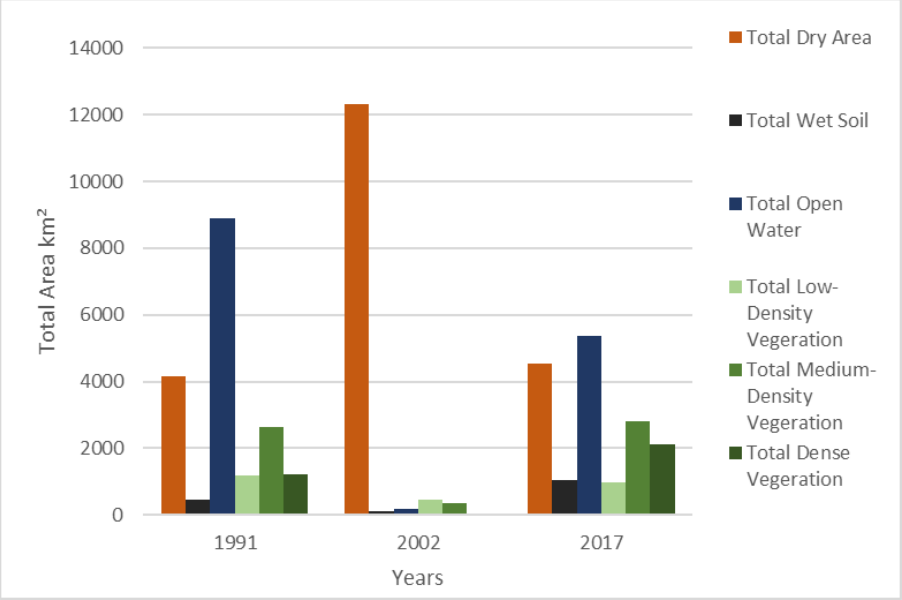

Figure 18: Land cover in the Al-Hammar marsh in 1991, 2002, and 2017.

4.5 Evapotranspiration Concepts

For clarity, the following subsections summarise the most important evapotranspiration types (concepts).

5.5.1 Evapotranspiration (***ET***)

ET is a generic term that refers to the amount of water evaporated from the surface, that is, the soil, water bodies, and plants (Jensen 2007; Perry 2009). This term is used when referring to the process in general, without specifying its type.

4.5.2 Reference Evapotranspiration (***ET_0***)

According to Allen et al. (1998a), reference ET is the ET from a hypothetical grass surface with approximately 0.12 m crop height, completely covering the soil, free of diseases, and well-watered.

Several empirical methods, such as Blaney–Criddle, Hargreaves equation, Turca (Chauhan 2009), and the Modified Penman–Monteith, which is the recommended and preferred method from FAO, have been developed to estimate and compute (ET_0) (Allen 1998b; Abdul Karim 2013). Most methods require an extensive meteorological data set as input, making them unsuitable for environments with scarce, insufficient, and limited data (Trajkovic 2005; Ren 2016). Thus, simplified methods are usually used in such environments but need calibration locally.

4.5.3 Potential ET (***ET_p***)

According to Perry (2009), the ET_p of a particular crop is the maximum ET from the crop without a deficit in the water supply. ET_0 is the ratio of the PET of a crop other than grass and is the crop coefficients *Kc* factor (Allen 1998a; Abdul Karim 2013).

4.5.4 Actual ET (***ET_a***)

ET_a is the actual ET that is lost into the air from a vegetated surface under the actual limiting conditions (water availability, disease, etc.). For a healthy crop without stress (e.g., in the case of fully irrigated surfaces or in wet seasons), ET_a is equal to PET (Perry 2009).

4.6 Effects of Water Availability on Land Cover

CRIMW carried out a complete set of total monthly discharge measurements for various inlets of main feeders of the marsh during 2015-2018 **Figure 19**. Thus, daily data from Al Chibaeich Metrological station located at E: 47.07, N: 30.94 **Figure 20** (maximum and minimum temperature

and relative humidity, maximum and average wind speed, sum of solar radiation and rainfall) between 2015 and 2018 and ET_0 calculator software from FAO (Food and Agriculture Organisation of the United Nations) version 3.2 (https://www.fao.org/land-water/databases-and-software/eto-calculator/en/) are used to gain average monthly reference evapotranspiration (ET); the result is shown in **Figure 20**. ET_0 reaches 300 mm per month during summer.

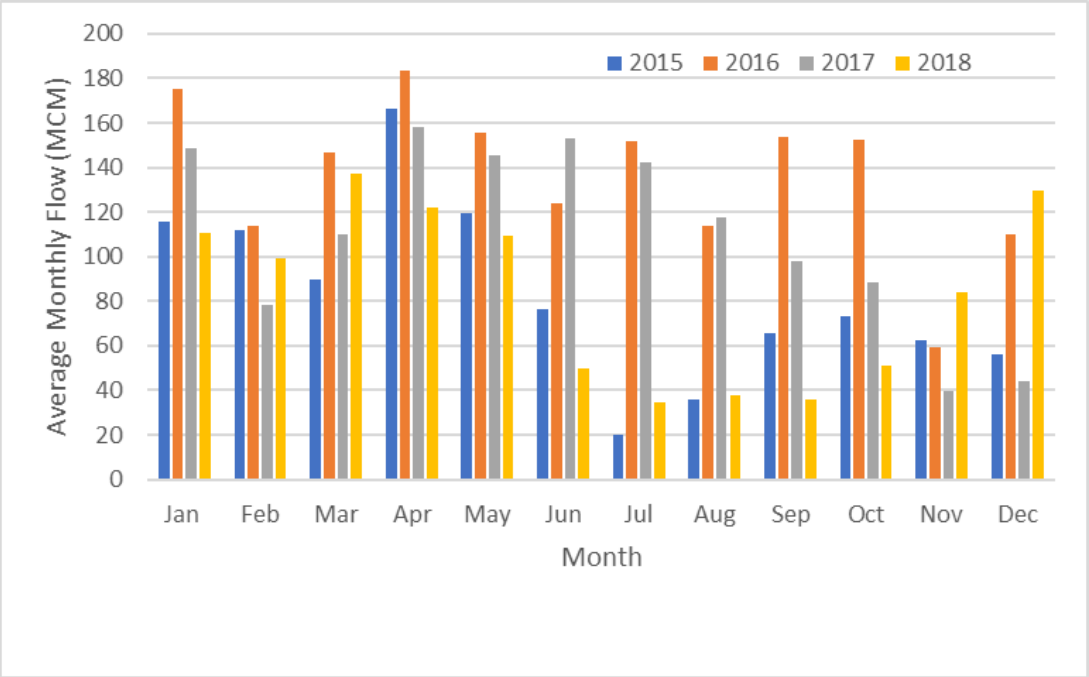

Figure 19: Average Monthly Flow Million Cubic Meters (MCM) to the marshland between 2015 and 2018; no trend is evident, and the flow depends on the marshland's upstream water control (Al-Maliki, 2018).

One of the most significant factors affecting the water cover and vegetation cover, and the water balance of the marshes in arid and semi-arid areas is evapotranspiration due to high temperatures. This condition leads to a rapid, dramatic change in water and vegetation cover. **Figure 20** shows the temperatures and evaporation for the years 2015 to 2018.

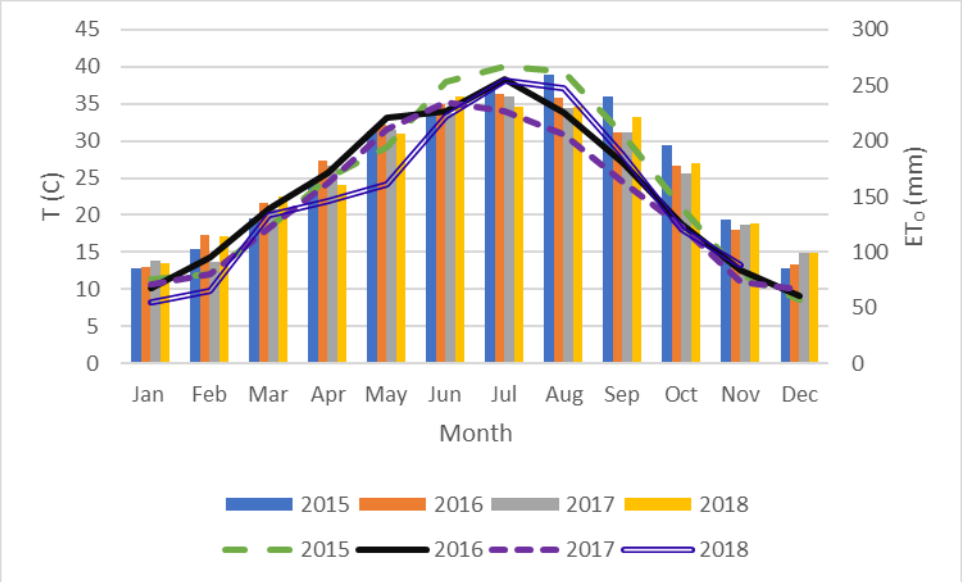

Figure 20. Average monthly reference evapotranspiration (ET) in the study area compared with the average monthly temperature between 2015 and 2018, columns are the average monthly temperature and the lines are average ET_0.

Statistical analysis was carried out to understand the relationships between the different elements of the water budget and land cover using the Statistical Package for the Social Sciences (SPSS) software. For the statistical analysis model, there are two types of variables independent variables, which mean individual variables without any influence, such as discharges, temperature, and ET_0, to see how these independent variables affect the dependent variables, which are here the six classes. In a multivariate regression analysis, the land cover categories were tested against three predictors; the total monthly flow of the feeder canals, monthly mean air temperature, and ET_0 had no impact on wet soil, low vegetation, and medium vegetation. A significant positive impact of total flow on open water cover was observed, as well as negative impacts of air temperature and evapotranspiration (**Table 3**). The minus sign in the table below indicates that there is an inverse relationship between the independent variables and the dependent variables, and the positive sign indicates that there is a direct relationship between them. For example, when open water areas increase the dry class decreases and when total inflow increases, the dense vegetation increase too.

Table 3: Results of correlation (R) between dependent and independent variables of the statistical model.

Correlations

	Dry Area	Wet Soil	Open Water	Low Vegetation	MD Vegetation	Dense Vegetation	Total Flow Discharge	Monthly Air Temperature	ET_0mm Total
Dry Area	1								
Wet Soil	0.105	1							
Open Water	-.675**	-0.221	1						
Low Vegetation	0.249	.431**	-0.316	1					
MD Vegetation	-.510**	0.079	0.008	0.127	1				
Dense Vegetation	-0.286	-0.311	-0.118	-.650**	-0.083	1			
Total Flow Discharge	-.507**	-0.269	.545**	-0.237	-0.116	0.241	1		
Monthly Air Temperature	0.088	-0.058	-.445**	0.214	-0.007	.321*	-0.103	1	
ET_0 mm Total	0.063	-0.100	-.343*	0.236	-0.039	0.230	-0.029	.954**	1

**. Correlation is significant at the 0.01 level (2-tailed).

*. Correlation is significant at the 0.05 level (2-tailed).

4.7 Sensitivity to Spatial Resolution

To analyse the effects of different spatial resolutions, two images from different sensors (Sentinel-2 with 10 m resolution and Landsat 8 with 30 m resolution) taken on the same day (24 August 2017) were compared. We analysed the western part of the study area, where the two images overlapped, and used the same method to classify the marshland. The results are shown in **Figures 21** and **22**.

The two resulting maps, resampled to 10 m spatial resolution, were compared in a confusion (error) matrix. There is 78% overall agreement between the two classified images, which can be considered a good match. The complex patchy pattern of the wetland results in relatively more mixed pixels in the Landsat image, with the coarser resolution, than in the Sentinel image, leading to more mismatch of spectrally different classes (e.g., water vs. dry soil).

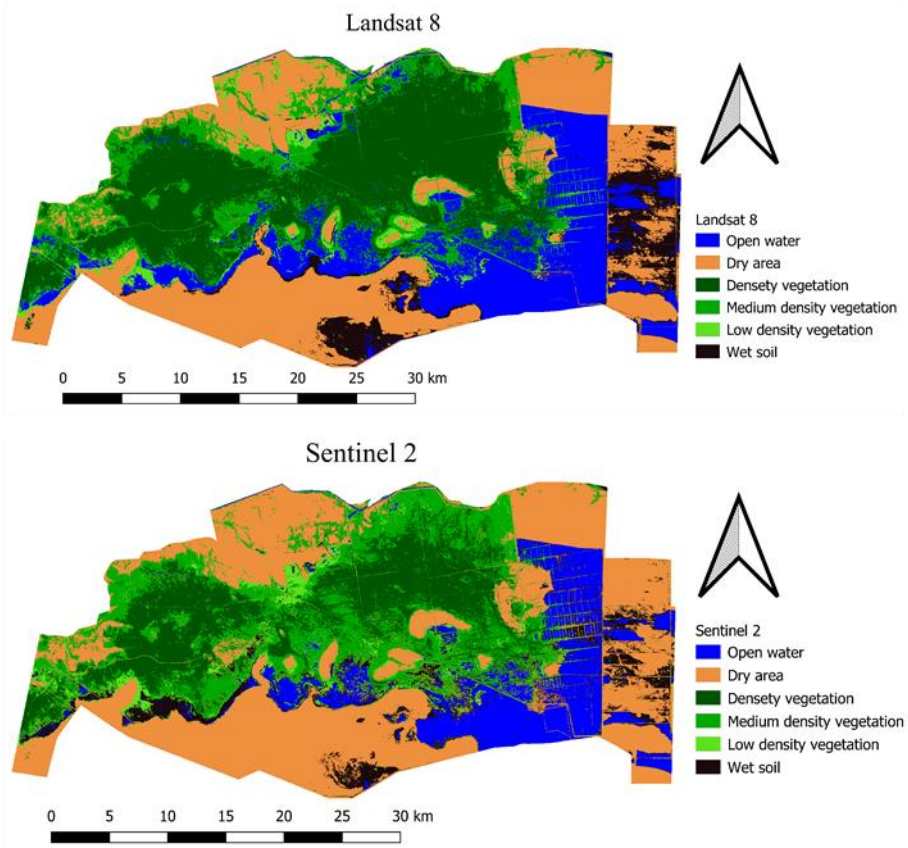

Figure 21: A comparison between the classification results for part of the study area according to the proposed approach for two types of satellite images, Landsat (a) and Sentinel 2 (b), for the same day. A significant similarity between the two images is found, and this finding confirms that the proposed approach works effectively on different satellite images.

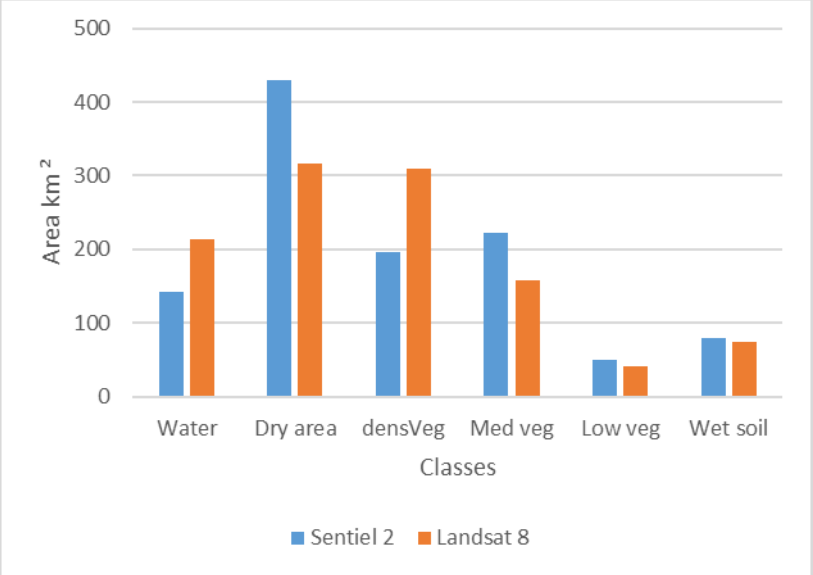

Figure 22: Compering in vegetation type and water cover in part of the Al-Hammar marsh between Landsat 8 and Sentinel 2.

5 ESTIMATING EVAPOTRANSPIRATION IN THE MARSHLANDS

This chapter presents the most common and efficient methods to calculate the actual evapotranspiration time series from satellite images and compares the results with the evapotranspiration values calculated from data of metrological stations and how integrated the data from metrological and remote sensing to calculate ET with spatial distribution instate of using calculated ET from metrological data only (Musa *et al.*, 2015). Therefore using a hydrodynamic model for more efficient water management for wetlands and open water bodies (Domeneghetti 2014).

To find an optimal model or product to estimate ET_a in marshlands, two RS data-based models (SEBS and SSEBop) using Landsat 8 images from 2016 and 2017 were chosen and compared with two ET_a products (MODIS MOD16 and FAO's WaPOR ET).

5.1 EO-based ET quantification models

Areal ET cannot be directly measured by any means. Thus, proxies and related assumptions are used in all assessment methods. RS provides several parameters, such as TIR data related to surface temperature (to calculate surface energy balance), optical data related to vegetation (to define the albedo or the resistance to evaporation in surface energy balance calculations or to use in the K_c factor methods), and microwave data related to soil moisture (to characterise water stress/availability). This list outlines the most important applications, but it cannot be considered complete since satellite images are used in a large variety of observation models.

5.1.1 Surface Energy Balance System (SEBS)

Su (2002) introduced this single-source model for calculating turbulent energy fluxes based on the surface energy balance equation. The SEBS model designed to estimate ET_a needs two types of data: the first group includes land surface albedo, emissivity, temperature, fractional vegetation coverage, and the height of vegetation (related to roughness height). These data can be retrieved from satellite images. The second group comprises air pressure, temperature, humidity, wind speed at a reference height, downward solar radiation, and downward longwave radiation. These parameters can be determined directly from meteorological data or by a model. Situ measurements are validated to observe ET with 10%–15% uncertainty (Su et al., 2005), and others show that the uncertainty is within the range of 30% (Liou and Kar, 2014).

On the basis of radiances and spectral reflectance from RS observations, the SEBS model consists of tools for estimating the land surface physical parameters, such as leaf area index, vegetation height, vegetation coverage, and roughness length for heat transfer (Su, 2002). The SEBS model calculated ET by estimating the evaporative fraction in dry and wet limits by calculating energy balance conditions.

According to Su (2002), the core equation of the SEBS model is shown in **Equations (1- 7)**.

$$R_n = \lambda E + G_0 + H \quad (1)$$

Where: R_n is the net radiation, λE is the turbulent latent heat flux (λ is the latent heat of vaporisation and E is the actual evapotranspiration), G_0 is the soil heat flux, and H is the turbulent sensible heat flux.

The calculation of net radiation flux on the land surface, R_n (W. m^{-2}), is given by **Equation (2)**.

$$R_n = (1-\propto).R_{swd} + \varepsilon.R_{lwd} - \varepsilon.\sigma.T_o^4 \quad (2)$$

Where: α is the albedo, R_{swd} is the downward solar radiation, ε is the emissivity of the surface, R_{lwd} is the downward longwave radiation, σ is the Stefan-Bolzmann constant, and T_O^4 is the surface temperature.

The soil heat flux depends on land surface characteristics, soil water content, and other factors. **Equation (3)** gives the calculation of soil heat flux by the SEBS model:

$$G_0 = R_n . (\Gamma_c + (1 - f_c).(\Gamma_s - \Gamma_c)) \quad (3)$$

Where the ratio of soil heat flux to net radiation is assumed as Γ_c = 0.05 for full vegetation canopy and Γ_s = 0.315 for bare soil. An interpolation is then performed between these limiting cases by using the fractional canopy coverage, f_c.

The calculation of sensible heat flux is calculated using **Equation (4)**:

$$H = \left((R_n - G_o) - \frac{\rho C_p}{r_{ew}} . \frac{e_s - e_a}{\gamma}\right) \Big/ \left(1 + \frac{\Delta}{\gamma}\right) \quad (4)$$

We will use SEBS to estimate evaporation fraction by making energy balance at limiting cases at the dry limit and the wet limit as shown in **Equations (5)**:

$$\Lambda_r = 1 - \frac{H - H_{wet}}{H_{dry} - H_{wet}} \quad (5)$$

Where: the H_{wet} is sensible heat flux at the wet limit and H_{dry}sensible heat flux at the dry limit.

Since the ET ratio Λ is a constant during the day, the daily ET_{a24} (mm) can be estimated using **Equations (6) and (7)**:

$$\Lambda = \frac{\lambda E}{R_n - G} = \frac{\Lambda_r . \lambda E_{wet}}{R_n - G} \quad (6)$$

$$ET_{a\ daily} = \Lambda_0^{24} \times 8.64 \times 10^7 \times \frac{R_n - G_o}{\lambda_{p\omega}} \quad (7)$$

Where: Λ_r is relative evaporation, Λ_0^{24} is the daily evaporative fraction, ρw is the density of water measured in kilograms per cubic meter. And λ is the latent heat of vaporization.

For **Equation (1)**, the energy system model has two limitations: energy availability and soil moisture availability. Hence, ET_a is at its maximum range when the conditions are wet, and the sensible heat flux is minimum. When the soil is dry near the wilting point (dry limitation), the latent heat is small and negligible or becomes zero, and the sensible heat is maximum. The available energy is the limiting factor. The evaporative fraction can be defined in the dry and wet limit conditions to achieve the turbulent energy fluxes in Equation (1). However, the evaporative fraction needs to be assumed first.

According to (Kustas and Daughtry, 1990), G_0 is mainly reliant on land cover. Thus, the ratio between dry soil limitation heat flux to total net radiation under full land cover vegetation is used to parametrise G_0, and it ranges between 0.05 for full land vegetation coverage and Γ_c is 0.315 for dry soil.

The SEBS model requires different data sets to estimate daily ET. RS multispectral images (e.g., thermal infrared, near-infrared [NIR], visible) are needed to calculate normalised difference vegetation index (NDVI), land surface temperature, albedo emissivity, the FVC, and meteorology-related data such as planetary boundary layer height (BLE), short wave incoming radiation, air pressure, air temperature, sunshine hour duration, specific humidity and wind speed at a reference height.

5.1.2 SSEBop model

Senay et al. (2007) simplified the surface energy balance equations (SEB) based on the basic assumptions of SEBAL and METRIC to estimate ET as a linear function of surface temperature. Unlike the original SEB methods, the SSEBop model does not solve for the energy balance term *H* explicitly. According to Senay et al. (2013) and on the basis of radiation balance principles for clear sky: 'dry /hot' temperature (*Th*) is used for no or limiting conditions of latent heat flux. 'Wet/

cold' temperature (*Tc*) is used for no or limiting conditions of sensible heat flux for each pixel. Senay defines differential temperature (*dT*) between two limiting conditions.

The SSEBop method needs air temperature (*Ta*, coefficient that scales the ET_0 *K*, surface temperature *Ts*), and grass reference ET (ET_0, mm) to estimate ET by assuming constant temperature difference (*dT*, *K*) for a date and location between boundary reference points (hot and cold reference conditions for each pixel) **Equation (8)** below shows ET_a calculated using SSEBop model.

$$ETa_{24} = ET_f \times K \times ET_0 \quad (8)$$

Where: ET_{a24} actual evapotranspiration for the location (mm.day^{-1}); ET_f is ET fraction; K is a coefficient that scales the ET_0 into the level of a maximum ET experienced by an aerodynamically rougher crop such as alfalfa; ET_0 is short grass reference for the location (mm. day^{-1}). ETf can be determined as:

$$ET_f = \frac{Th-Ts}{Th-Tc} = \frac{Th-Ts}{dT} \quad (9)$$

Where: Th is the estimated T_s at the idealised 'hot/dry' reference temperature value condition of the pixel for the same time period; T_s is the satellite-observed land surface temperature of the pixel, where its ET_f is being evaluated on a given image date. Tc is the estimated cold reference temperature value. (Note: Negative ET_f is set to zero). dT is defined as:

$$dT = \frac{R_n \times r_{ah}}{\rho_a \times C_p} \quad (10)$$

Where: R_n is the clear-sky net radiation; r_{ah} is the aerodynamic resistance to heat flow from a hypothetical bare and dry surface; ρ_a is the density of air ($kg.m^{-3}$); C_p is the specific heat of air at constant pressures ($1.013\ .kJ\ .kg^{-1}.C^{-1}$). Th is calculated by:

$$Th = Tc + dT \quad (11)$$

Sennay suggested some assumptions to apply SSEBop, as shown in **Table 4** (Senay et al., 2013).

Table 4: Assumptions to apply the SSEBop model.

Atmospheric pressure at sea level	101.3 kPa
ea the actual vapour pressure	1-5 kPa
P	between 80 and 1000 kPa
k scaling coefficient	1.25

5.1.3 FAO's WaPOR ET product

To improve water use efficiency, the Food and Agriculture Organisation of the United Nations (FAO) developed the WaPOR methodology and maintains the WaPOR database (FAO, 2020) at different scales. It provides open-access monthly actual ET and interception (ETIa), which can be found at https://wapor.apps.fao.org/home/WAPOR_2/2. ETIa is based on the two-source model (ETLook) described by (Bastiaanssen 2012). It uses Penman–Monteith equations (Allen 1998b) with RS data, such as solar radiation, surface albedo, NDVI, land cover, soil moisture and uses measured meteorological data (air temperature, solar radiation, wind speed and vapour pressure) for the calculation of soil evaporation, vegetation transpiration and interception.

The monthly available ETa products for 2016 and 2017 were downloaded from the database with 100 m spatial resolution for the study area.

5.1.4 MODIS ET data (MOD16)

MOD16 is an ET_a product based on an algorithm that uses the Moderate Resolution Imaging Spectroradiometer (MODIS) sensor data, meteorological data from the Global Modelling and Assimilation Office, and a satellite-based soil moisture product. MOD16 values represent the sum of evaporation from canopy stomata, interception and bare soil. The algorithm is based on the modified Penman–Monteith equation and uses the estimated canopy surface, aerodynamic conductance terms and soil moisture defined by a set of semiempirical equations developed by Mu, Zhao and Running (2011) for different land cover types. These equations require calibration for ET_a measurements with situ ET_a, such as eddy flux towers, and depend on the accuracy of the land cover type. However, uncertainty in some ET estimates from different models can range from 10% to 30%, and maximum absolute errors are 24% of the ET measurements (Mu, Zhao and Running, 2011).

Monthly ETa MOD16 data were downloaded with 1000 m spatial resolution for 2016 and 2017 and clipped for the study area from https://lpdaac.usgs.gov/.

5.2 Implementation of the SEBS models

The following subsections describe the data processing for the parameterisation of the SEBS model.

5.2.1. Satellite data acquisition and preprocessing

To compute actual evapotranspiration in SEBS and SSEBop models, different open-source satellite data products were used as inputs in the models. In this study, all available images for the

years 2015, 2016, and 2017 for SEBS and 2016 and 2017 for SSEBop were used for calculating evapotranspiration in the marshland, so 50 images from Landsat 8 have been chosen for this purpose with cloud cover less than 10% for SEBS and 19 for SSEBop, data used in this study were level 2 data which is atmospherically corrected.

The scenes for the study area were downloaded with path/row 166/039 and pixel resolution 30m*30m for each month for two years, 2016 and 2017, with cloud cover less than 10%. A full breakdown of the data acquired is presented in (**Appendix 3**). In total, 50 Landsat Images were collected for the Al-Hammar marsh. Further open-source satellite data products were used as inputs in the models, as listed in (**Appendix 4**). Data for the test area were extracted using QGIS and the boundary shapefile.

5.2.2 Parameters derived from satellite data

Landsat 8 land surface temperature

Shortly after launch, the USGS raised concerns about the quality of Landsat 8 thermal bands 10 and 11, which were affected by radiation outside the instantaneous field of view (USGS, 2016). USGS advises users to use only band 10 because band 11 is affected by light from neighbouring pixels and use the split-window algorithm suggested by (Jimenez-Munoz 2009; USGS 2016). In this study, only band 10 was used to calculate the land surface temperature.

Normalised Difference Vegetation Index (NDVI)

The NDVI was derived from OLI bands 4 (red spectrum ranges respectively) and 5 (near-infrared (NIR) at surface reflectance values using **Equation (12)**.

$$NDVI = \frac{\rho_5 - \rho_4}{\rho_5 + \rho_4} \quad (12)$$

Where: (ρ_5) is the reflectance in band 5, (ρ_4) is the reflectance in band 4.

Fraction of Vegetation Cover (FVC)

FVC can be derived from the maps of NDVI. In this study, FVC was estimated as proposed by Jiménez-Muñoz et al. (2009) for fully vegetated cover and bare soil and presented in **Equation (13)**.

$$FVC = \frac{NDVI - NDVI_S}{NDVI_v - NDVI_S} \quad (13)$$

Where: $NDVI_s$ represents NDVI of bare soil, *NDVI* is the value of the actual pixel and $NDVI_v$ corresponds to the NDVI value of the full vegetation canopy coverage.

Land surface emissivity map

Land surface emissivity (ε) is the broadband land surface emissivity and was computed for Landsat imagery using **Equation (14)** which was proposed by (Sobrino, Jiménez-Muñoz and Paolini, 2004), and this equation is generally valid and parameterisation by fitting to data.

$$\varepsilon = 0.004 \times FVC + 0.986 \quad (14)$$

Albedo

Albedo is the reflectivity of the surface in a broad-spectrum range. It expresses the reflected proportion of the incoming radiation, which is a function of the absorbed radiation (Liang, 2001). In this study, the broadband albedo was computed from the Landsat 8 (OLI sensor) algorithm, from the visible and near-infrared bands 2 to 7 based on Equation (15). This equation is generally valid and parameterisation by fitting to data.

$$\alpha_{short} = 0.362\rho_2 + 0.13\rho_4 + 0.373\rho_5 + 0.085\rho_6 + 0.072\rho_7 - 0.0018 \quad (15)$$

Where: α_{short} is the shortwave albedo, and ρ_i is the reflectance of bands *i*=2, 4, 5, 6, and 7.

5.2.3 Metrological Ground Station Data

The following daily data were used from the Al Chibaeich Metrological station, located at E: 47.07, N: 30.94 in the marsh **Figure 23**. The maximum and average wind speed, maximum and minimum temperature, and relative humidity. Furthermore, the sum of solar radiation, rainfall and sunshine hours were collected from the An Nassiriyah station, located at E: 46.14, N: 31.05. The data sets cover the period from 2015, 2016, and 2017.

Figure 23: Al Chibaeich Metrological station.

Hydrological data

A complete set of total monthly discharge measurements of million cubic meters (MCM) for various inlets of main feeders of the marsh was carried out by CRIMW during 2016-2017.

5.3 Analysis of the ET Quantification Models and Products Results

The following subsections describe the ET_a quantification results of the Al-Hammar marsh.

5.3.1 SEBS Model: Temporal and Spatial Variation of ET

Used Integrated Land and Water Information System (ILWIS) software from the International Institute for Geo-Information Science and Earth Observation (ITC) University of Twente Netherlands (www.itc.nl/ilwis/download/ilwis33) for calculating the spatial ET_a for all images in (**Appendix 3**). **Figure 24-26** shows the temporal and spatial variation of ET_a defined by the SEBS model in the study area during 2015, 2016, and 2017. The results, as expected, showed spatial distribution of ET_a values variations over the study area and higher ET_a in the summer than in winter. The maximum daily ET_a values are located where the dense vegetation is in the centre of the study area during summer, but during winter, ET_a is higher when the area consists of a mixture of open water and low vegetation cover. For 2015 the maximum in July was 9.97 mm day $^{-1}$ and in December 2.45 mm day $^{-1}$; for 2016, the ET_a was 9.83 mm day $^{-1}$ for July and 2.74 for December, and for 2017 the ET_a was 9.93 mm day $^{-1}$ for July and 3.53 mm day $^{-1}$ for December. The minimum ET_a during the study time was 0 mm day $^{-1}$ and located where the soil is very dry in agricultural areas in the north or inside the marsh when the houses. SEBS worked well in the areas with

different land cover types, i.e., open water, vegetation, bare soil, and wet soil, and there is no missing data of ET_a in any pixel. The ET_a close to Al Chibaeich metrological station ranged between 1.01 and 9.98 mm day^{-1} during the three years, with a maximum ET_a on July 18, 2015.

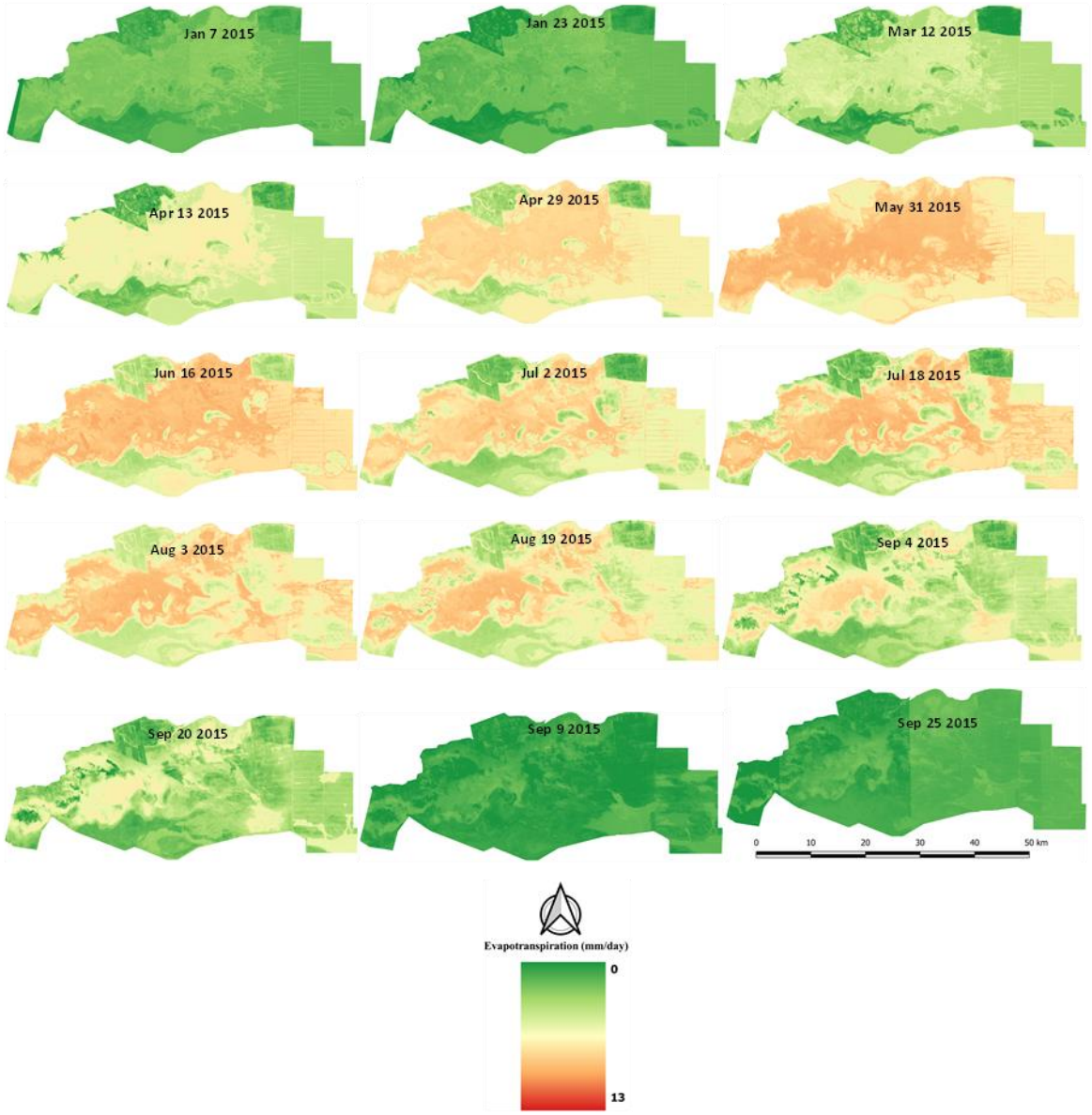

Figure 24: High-resolution daily ET_a map calculated by the SEBS model from satellite data acquired in 2015.

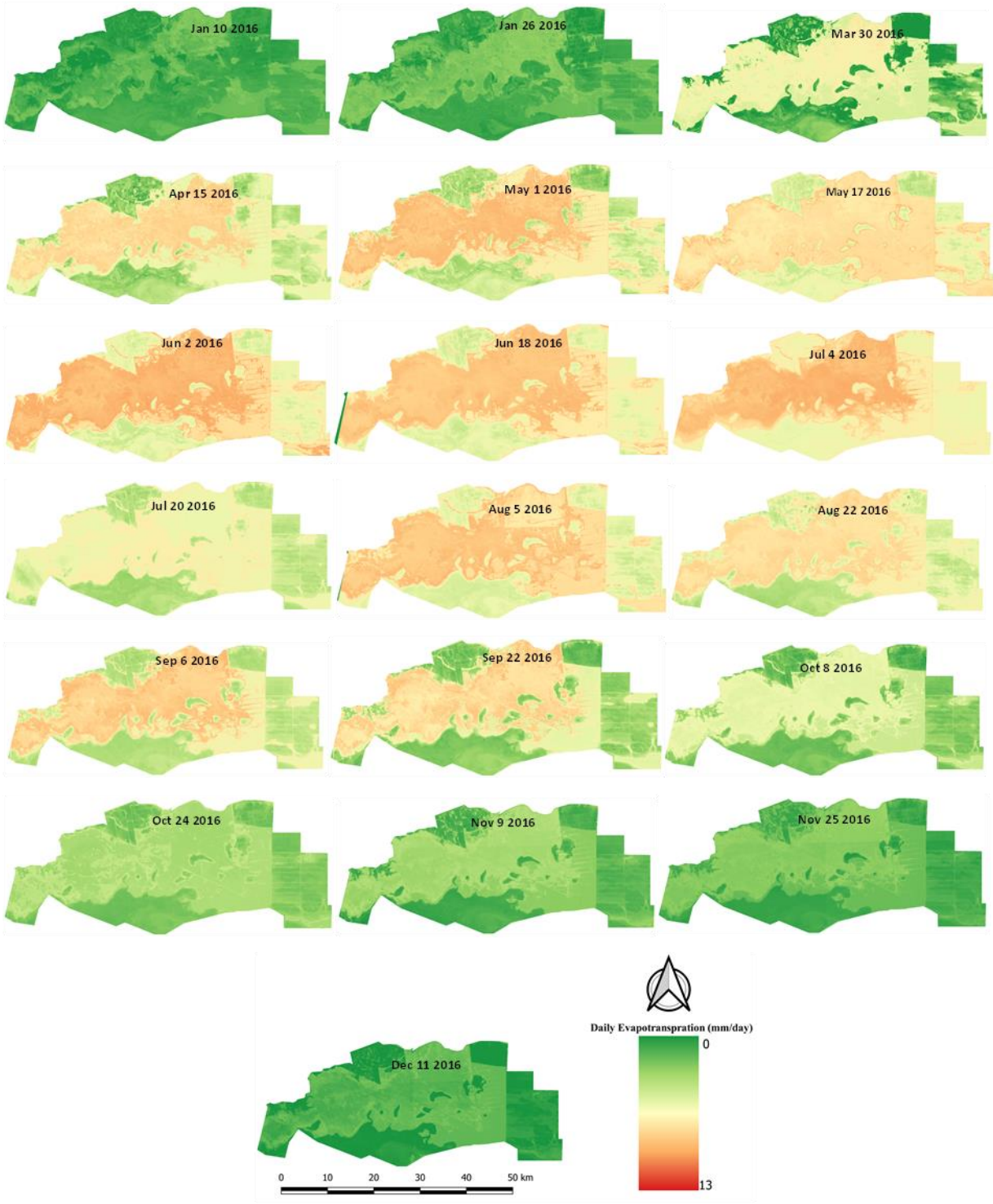

Figure 25: High-resolution daily ETa map calculated by the SEBS model from satellite data acquired in 2016.

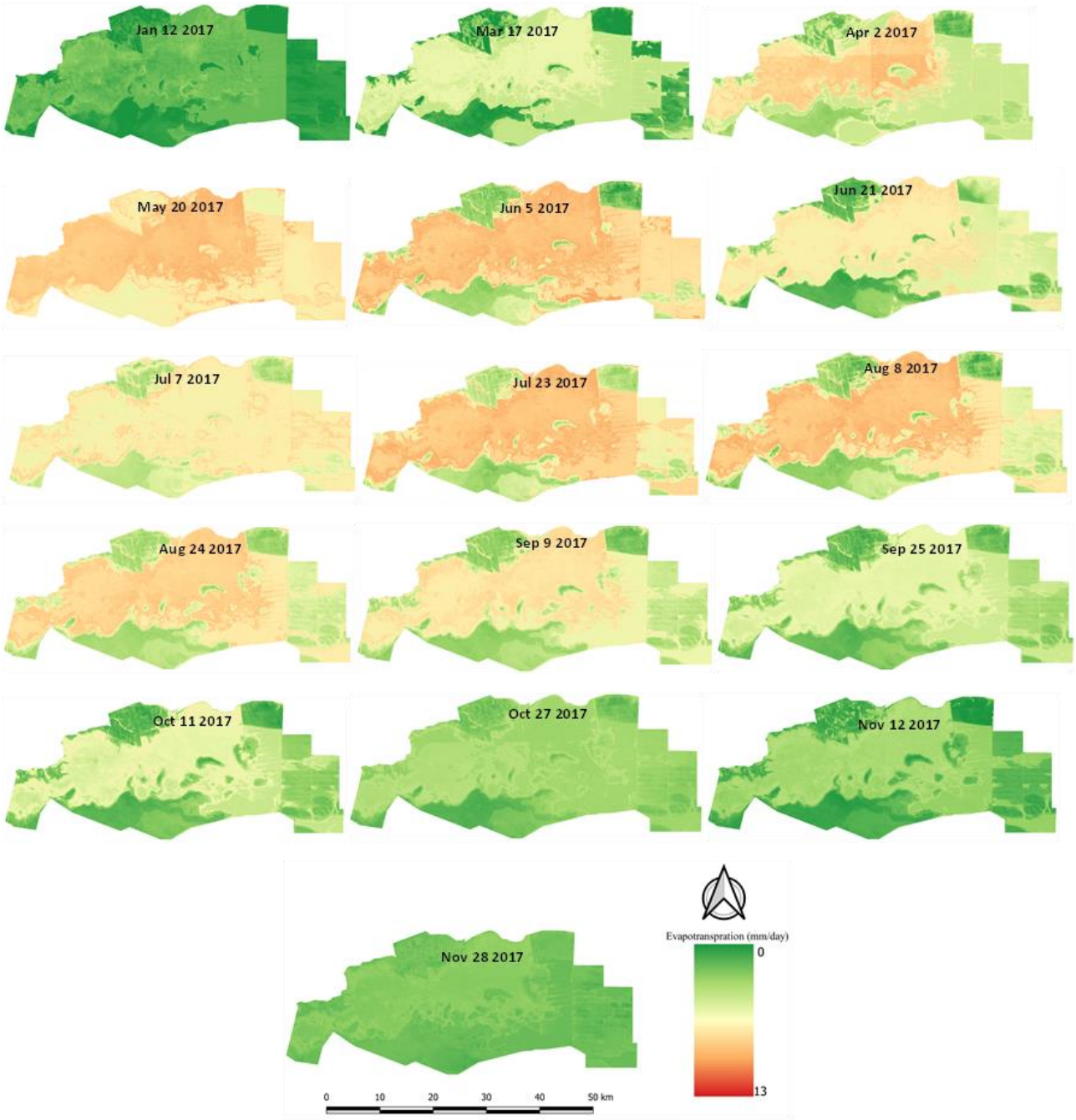

Figure 26: High-resolution daily ET_a map calculated by the SEBS model from satellite data acquired in 2017.

5.3.2 SSEBop Model: Temporal and Spatial Variation of ET

The Python code belonging to the Iraq Ministry of Water Resources (Baghdad, Iraq) and data from the Global Data Assimilation System (GDAS) were used to calculate the spatial distribution of ET_a from 19 satellite images in 2016 and 2017 for comparison with the SEBS model. **Figures. 27** and **28** shows the temporal and spatial variation of ET_a defined by the SSEBop model in the study

area during this period. There is convergence in the values for the months corresponding to the length of the years of study; there is some distinction in ET_a over 2016 and 2017.

Separating the evaporation of the open water from the ET in the area covered with vegetation was difficult in the SSEBop model results. The images from SSEBop showed missing data (practically in open water areas for some months), as shown by red circles in the **Figure 25**. For 2016, the maximum in July was 11.6 mm day $^{-1}$ and in January 2.1 mm day $^{-1}$; for 2017, the ET_a was 11.3 mm day $^{-1}$ for July and 2.74 for December. The minimum ET_a during the study time was 0 mm day $^{-1}$ and located where the soil is very dry in the agriculture area in the north or inside the marsh where the villages are located. Thus, the SSEBop was used to calculate short grass reference ET_0 in the global data product by GDAS, and the scaling coefficient *K* in Equation 8 needed to be adjusted by using ET_0 from the local metrological station. GDAS is a gridded product available every 6 hours (Senay 2008). The ET_a close to Al Chibaeich metrological station during the two years ranged from 0.75–8.75 mm day^{-1}, and the maximum ET_a was 11.6 mm day^{-1} on July 4 2016.

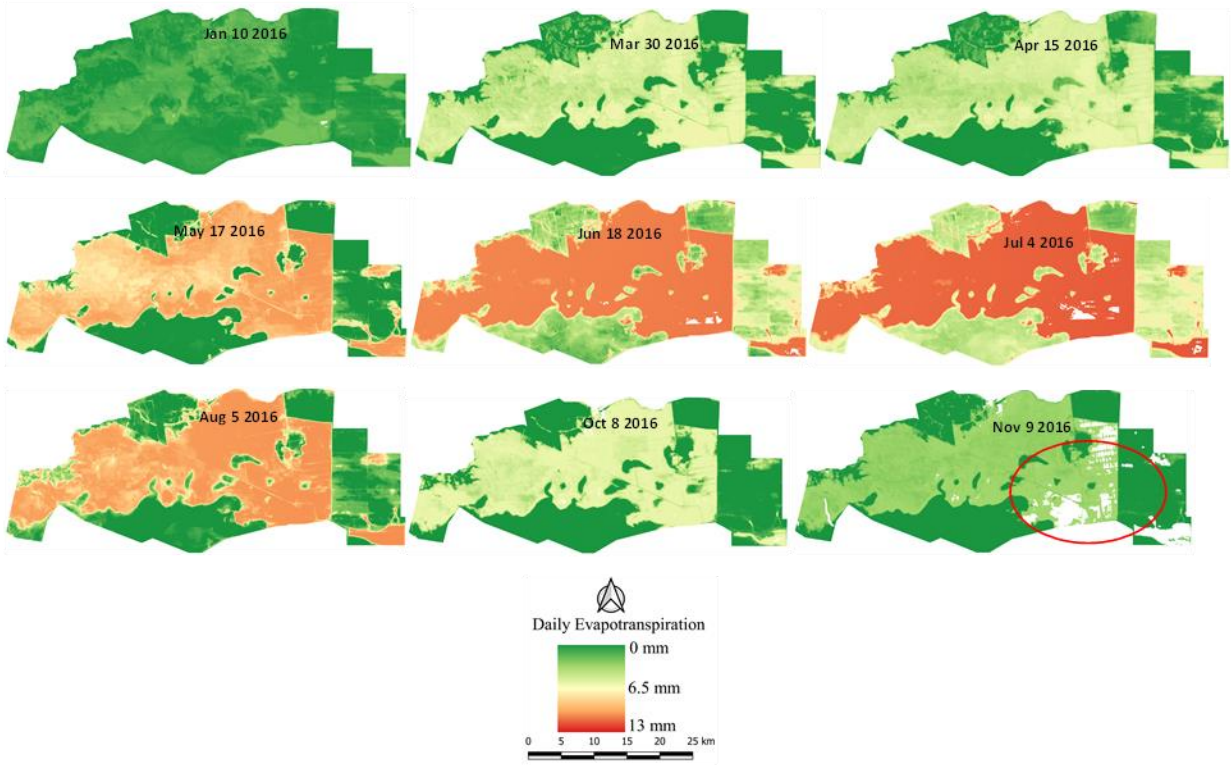

Figure 27: High-resolution maps of daily ETa calculated by the SSEBop model from satellite data acquired in 2016.

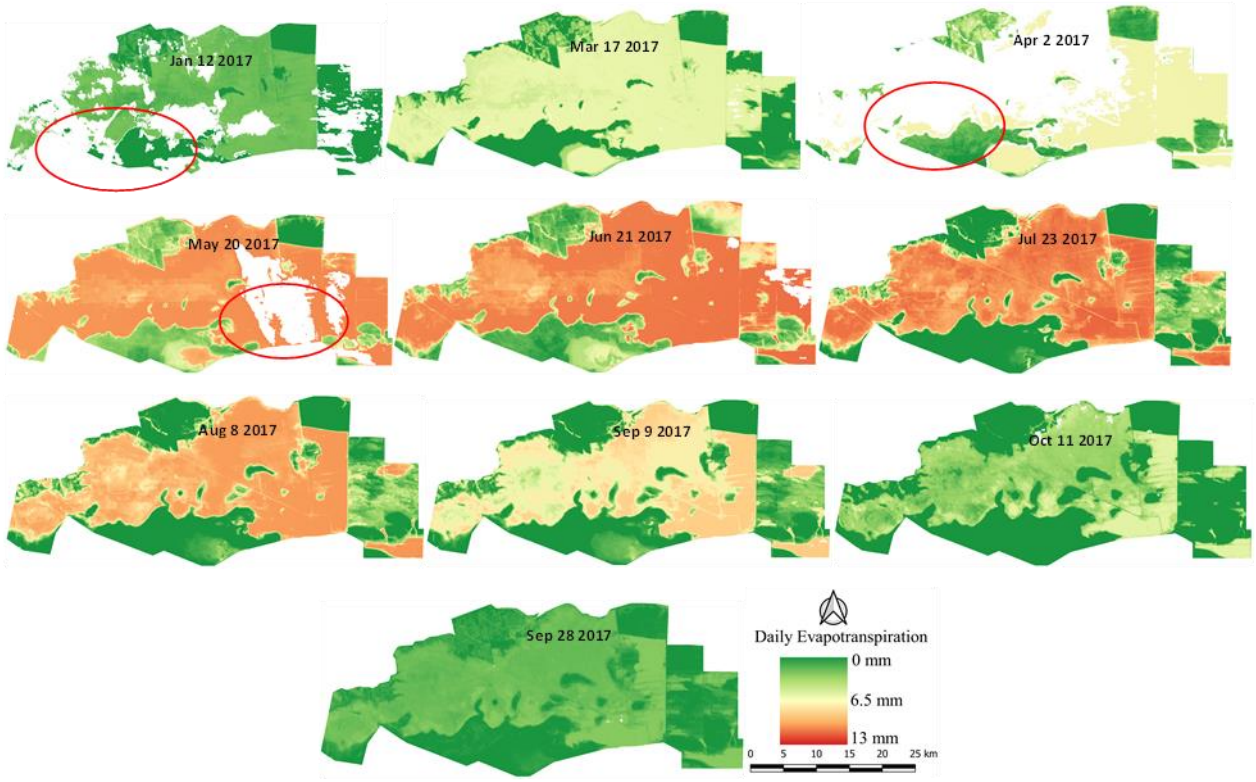

Figure 28: High-resolution maps of daily ETa calculated by the SSEBop model from satellite data acquired in 2017.

5.3.3 FAO's WaPOR product: Temporal and Spatial Variation of ET

The WaPOR ETI_a product showed spatial and temporal variations. **Figures. 29** and **30** shows the monthly ETI_a during 2016 and 2017.

The product showed spatial distribution of ET_a values varies over the study area and showed higher ET_a in the summer than in winter. Generally, during the summer, the maximum daily ET_a values are located when the dense vegetation is in the centre of the study. In the winter maximum, ETa from the area is mixed between open water and low vegetation cover. In 2016 the maximum ETa in June was 10.8 mm day $^{-1}$, and the minimum in December was 2.5 mm day $^{-1}$; in 2017, the maximum ETa was 11.5 mm day $^{-1}$ for July, and the minimum was 2.7 mm day $^{-1}$ in January. The product record minimum ETa is 0 mm day $^{-1}$ during 2016 and 2017 in different areas, especially in the south when the wet and dry soil is mixed.

The monthly ET_a close to Al Chibaeich metrological station varied during the two years from 0.43 to 4.49 mm day^{-1}, and the maximum ET_a was reached in June 2017. However, the product showed systematically lower values of ET_a compared to the models.

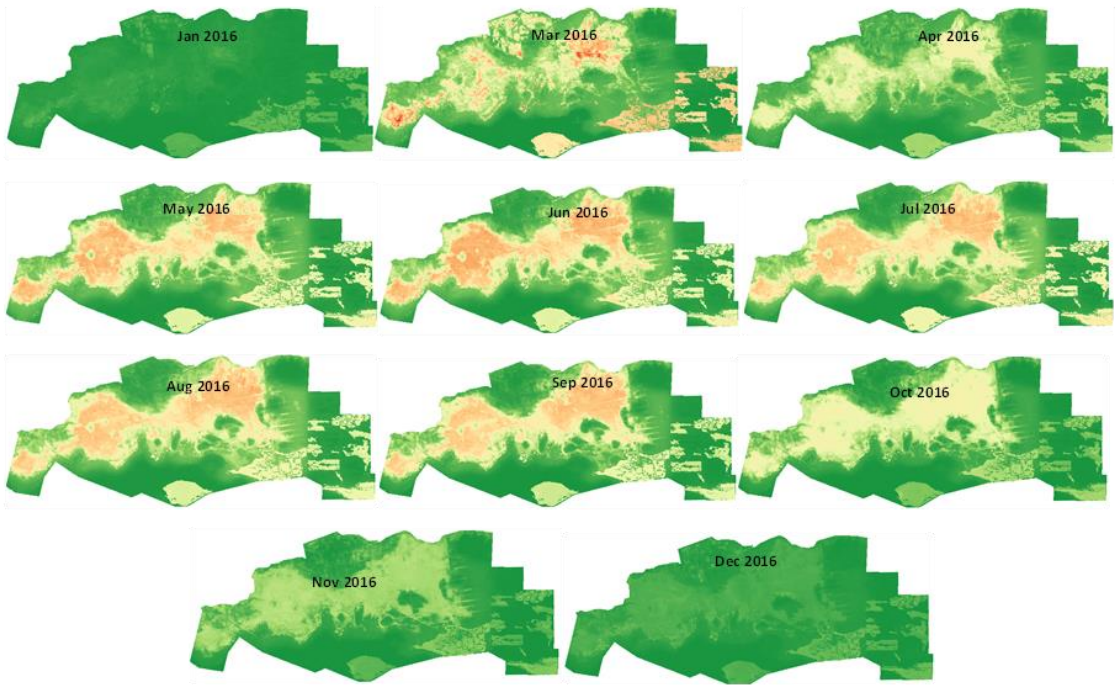

Figure 29: (FAO's WaPOR) a daily ET_a product derived from monthly ET_a during 2016.

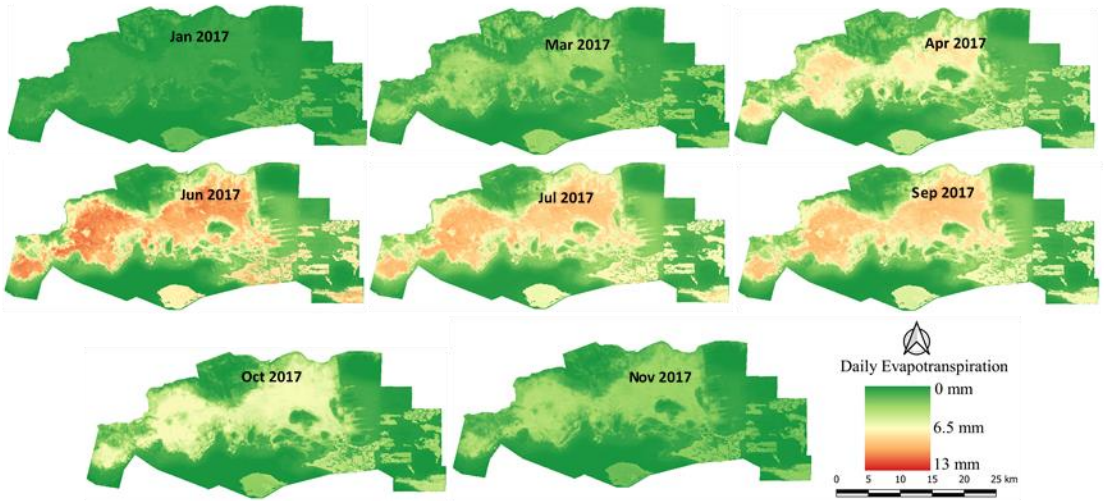

Figure 30: (FAO's WaPOR) a daily ET_a product derived from monthly ET_a during 2017.

5.3.4 MOD16 product: Temporal and Spatial Variation of ET

The product showed spatial distribution of ET_a values varies over the study area and showed higher ET_a in the summer than in winter. The maximum daily ET_a values are located at the dense vegetation in the center of the study area during summer and winter, and one image showed missing data and masked practically in an open water area (red circle on July 2016 in **Figures. 31** and **32**, which shows the ET during 2016 and 2017). For 2016, the maximum in July was 13 mm day $^{-1}$ and the minimum was in January, 2 mm day $^{-1}$; for 2017, the ET_a was 13 mm day $^{-1}$ for July and 2.7 mm day^{-1} in January. The minimum ET_a during the study time was 0 mm day $^{-1}$ and was located in different areas, especially in the south at pixels areas were mixed between the wet and dry soil.

The monthly ET_a close to Al Chibaeich metrological station changed during the two years from 0.64 to 8.29 mm day^{-1}, and the maximum ET_a was reached in June 2017.

The scheme shows a maximum of 13 mm day $^{-1}$, but this is energetically impossible; therefore, MOD16 in the wetlands needs to be calibrated by multiplying it with a bias fixing factor (Leonce, 2021).

The poor spatial resolution of x meter of the ET retrieved from MOD16 data is one of the most important reasons for its limited suitability for water management.

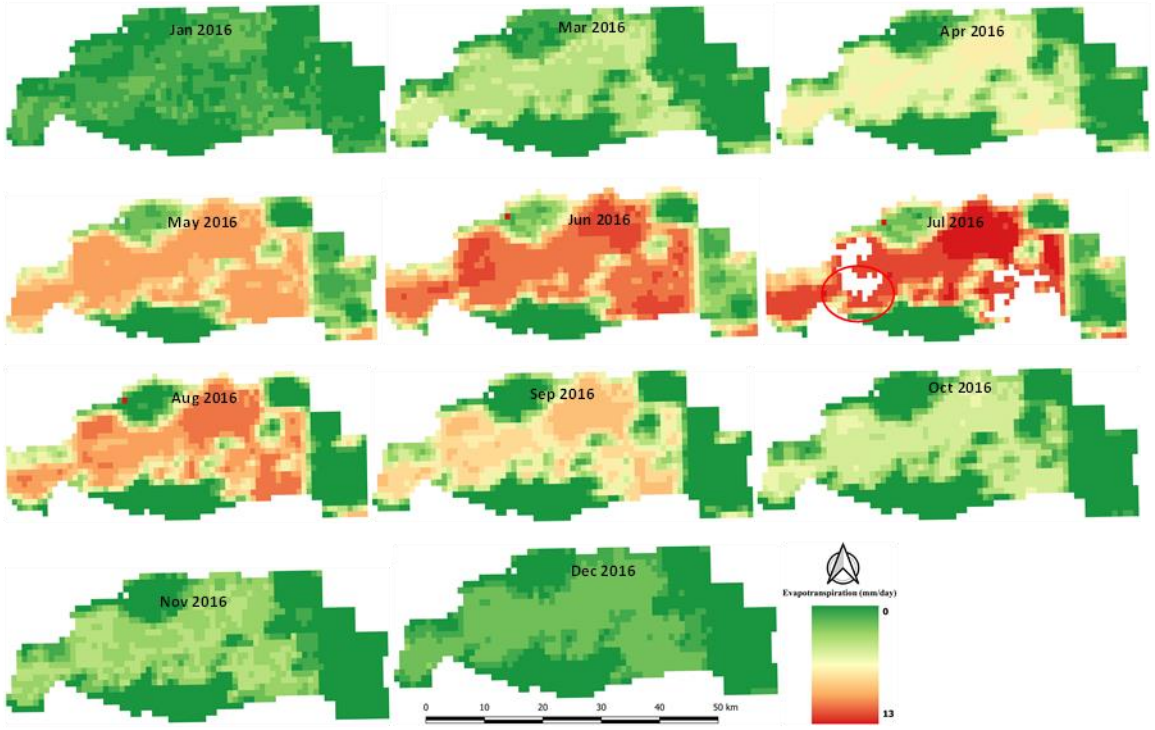

Figure 31: MOD16 ET_a product derived from monthly ET_a during 2016.

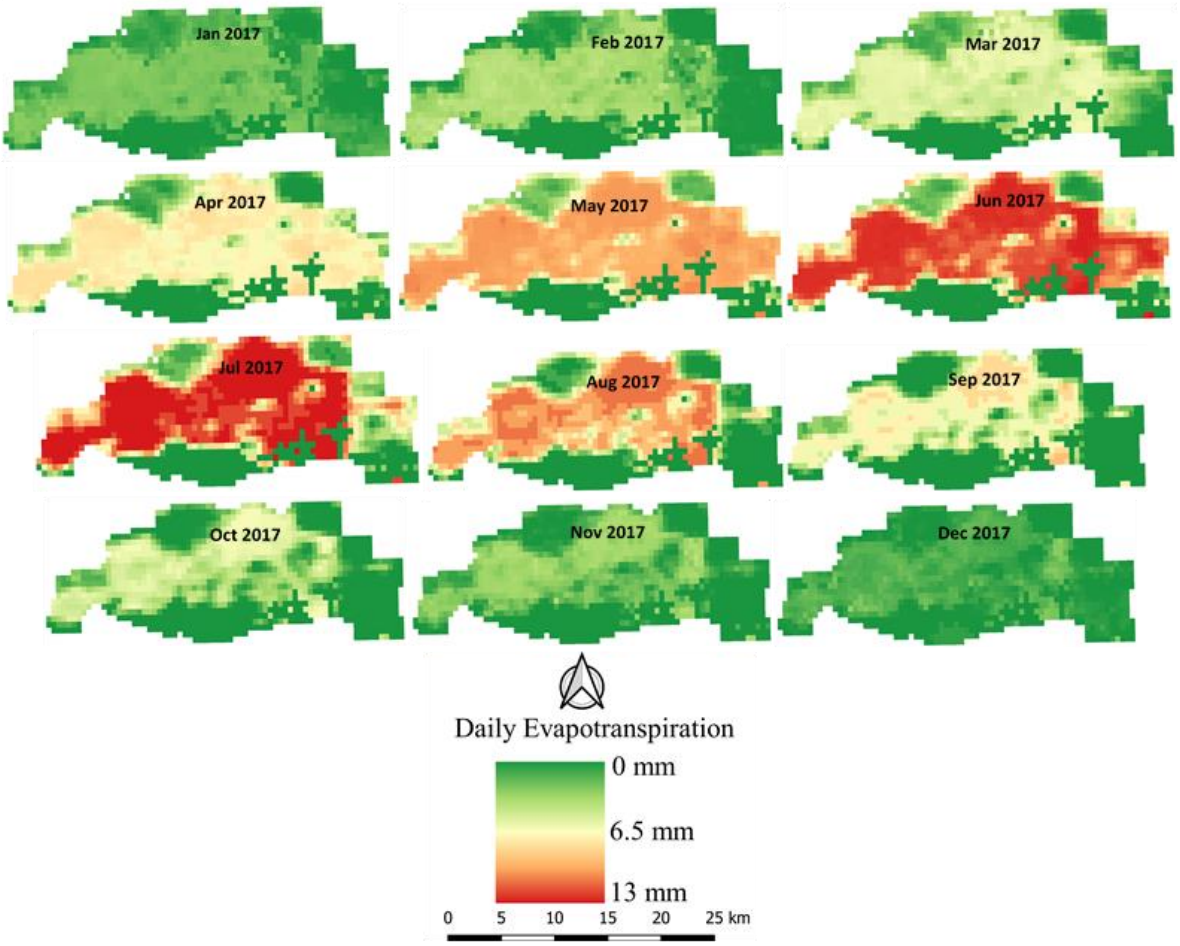

Figure 32: MOD16 ET_a product derived from monthly ET_a during 2017.

The estimated ET_a from RS and comparison with ET_0 calculated from the meteorological station during 2016 and 2017 for all models and products are presented in **Table 5**.

Table 5: Monthly ET_a estimates from SEBS, SSEBop, MOD16, WaPOR, and calculated ET_0 at the Al Chibaeich metrological station for the years 2016 and 2017.

Date	SEBS ETa	SSEBop ETa	Mod16 product ETa	FAO product ETa	ETo
1/10/2016	1.21	0.75	0.64	0.43	2.1
3/30/2016	4.14	3.06	2.2	1.23	5.4
4/15/2016	6.06	3.19	3.46	2.27	5.6
5/17/2016	7.12	5.8	6.51	3.53	6.9
6/18/2016	7.52	8.1	7.52	3.77	6.4
7/4/2016	7.74	8.75	7.97	3.71	8.1
8/5/2016	7.35	6.01	5.9	3.67	6.8
9/22/2016	5.53		4.32	3.37	6.6
10/8/2016	4.21	3.02	2.46	2.48	4.7
11/9/2016	2.5	1.73	1.74	1.55	3.0
12/11/2016	1.01		0.98	0.67	2.1
1/12/2017	1.38	1.29	1.37	0.62	2.8
3/17/2017	4.08	4.05	3.39	1.54	4.5
4/2/2017	5.89	4.47	7.13	3.1	5.4
5/20/2017	7.96	8.16	7.13		8.3
6/21/2017	5.54	8.28	8.29	4.49	8.9
7/23/2017	7.4	6.62	8.09	4.31	7.2
8/8/2017	6.9	5.94	5.74	4.01	6.9
9/9/2017	5.82	4.36	3.35	3.44	6.0
10/11/2017	4.14	1.92	2.43	2.49	5.1
11/28/2017	2.23	1.26	1.42	1.43	1.6

5.4 Validation and Comparison of the Results

Since no in situ ET_a measurements were available in this area, the validation was carried out using the ET_0 calculated from the meteorological station at Al Chibaeich, representing the "ground truth". We compared the different ET_a maps as follows: 50 maps were calculated by SEBS, 19 calculated by SSEBop, 23 maps from MODIS ET_a products downloaded from the database, and 19 ET_a maps from the WaPOR products database were downloaded.

The ET_0 values calculated from the station should be multiplied with the coefficient K_c to calculate the ET_p, as shown in **Equation 16**. According to Allen (1998b), the K_c values for reed swamp with standing water are 1.0, 1.2, and 1.0 for K_{c_ini}, K_{c_mid}, and K_{c_end}, respectively, and for reed swamp with moist soil, the same values are 0.9, 1.2 and 0.7. The different phenological phases are usually present simultaneously in the vegetation cover of the study area. Therefore, it is assumed that in these wetlands, ET_0 and ET_p are equal. Since there is always water and no water stress is present, we can assume ET_a is equal ET_p maybe it is a little lower but not higher (i.e., no water stress is present).

$$ET_p = ET_0 \times K_c \quad (16)$$

Where: ET_p is the potential ET for the crop, K_c is the crop coefficient for the particular crop.

The ET_0 calculator software of FAO (version 3.2) was used for calculating the daily reference evapotranspiration for the analysed two years for validation.

Different statistical measures of accuracy were used to assess the performance of the models using the Statistical Package for the Social Sciences (SPSS) software. Two approaches were used. First, the corresponding ET_a values in **Table 5** were compared to the ET_0-based predictions. Second, the effects of three predictors (independent variables, explained in Section 4.6: total monthly flow, monthly mean air temperature, and total solar radiation) on the ET were analysed. Four descriptive statistical parameters were considered: root mean square error (RMSE) to estimate the errors between measured and predicted values, Pearson's correlation coefficient (r), coefficient of determination (R^2), and mean absolute error (MAE).

The comparison of calculated ET_0 with estimated ET_a from the different methods gives confidence in the generic applicability of each analysed method for ET_a estimate, since the methods effectively tracked the temporal variation of the ET_0 defined from the meteorological data **Figure 28**.

The comparison of the ET_a estimated and calculated ET_0 showed that SEBS and SSEBop models effectively tracked ET_0 variation **Figure. 33**.

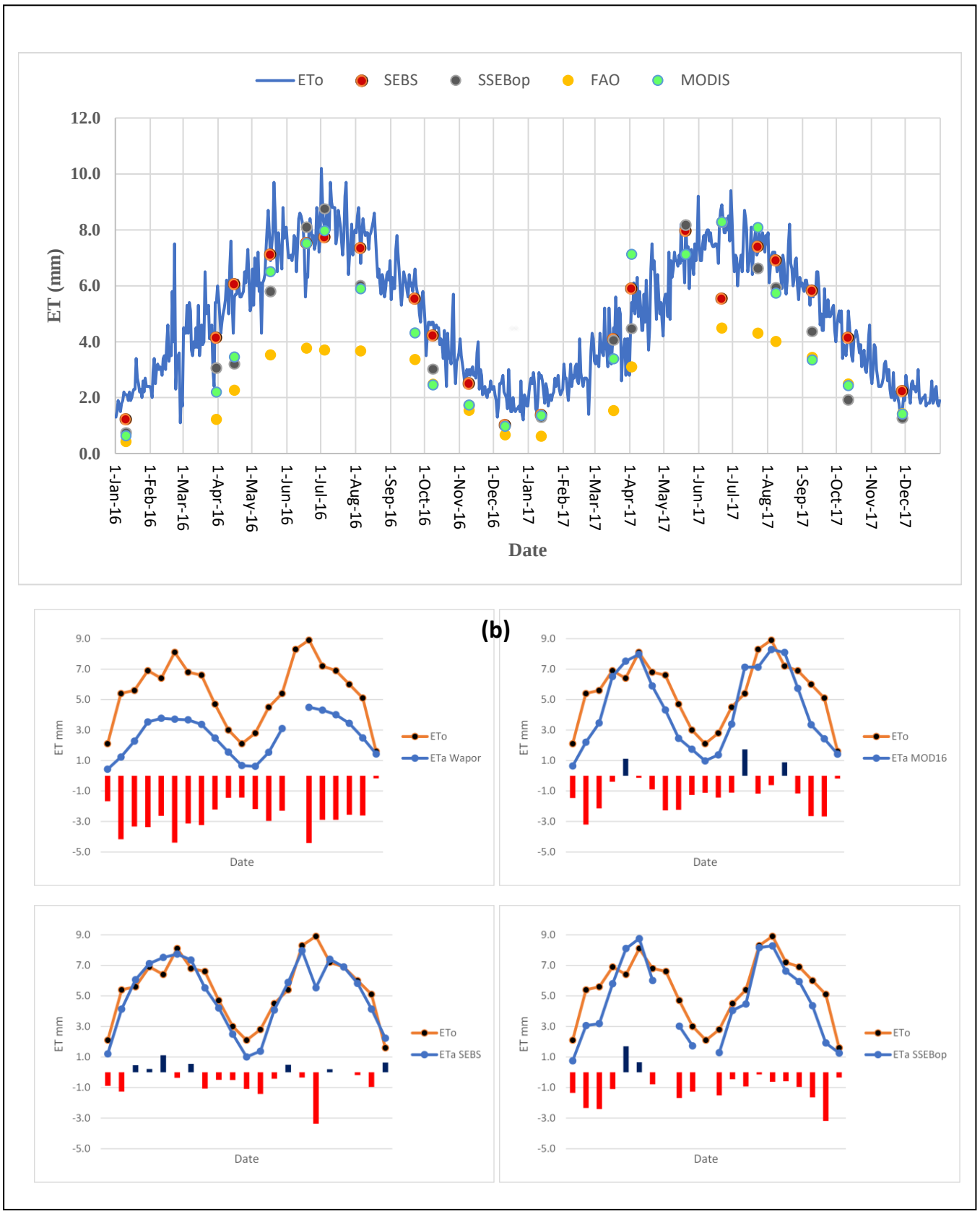

Figure 33: (a) Daily ET_0 and temporal ET_a variation satellite overpasses based on the models and products close to Al Chibaeich metrological station changed during the two years 2016 and 2017. (b) Residual of calculated ET_0 and estimated ET_a of models and products for same dates and compared with ET_0.

From **Table 5,** during winter time, evaporation from open water was higher than from vegetation. However, the SEBS model showed higher spatial variability ET_a on January 10 2016, April 2, 2016, and November 28, 2017, as compared to ET from the SSEBop model and products due to the rainy days before these dates and high residual moisture content owing and high ET_o, the values of ET_a pixels showed the SEBS model is sensitive to soil moisture, open water, and wet soil areas. Similarities were found in the spatial patterns of the SSEBop and SEBS model results during the winter, but different spatial patterns were observed during the summer. During summer, SSEBop shows higher ET_a in open water and vegetation areas than SEBS. However, the SSEBop pattern on different dates was more in agreement with SEBS than the two ET products.

The WaPOR ETI_a product showed the spatial and temporal variations, but the values were lower than SEBS, SSEBop, and ET_0 for 2 years. This product has a problem with evaporation from wet soil. Regarding the results, the WaPOR ET product is unreliable for estimating ET in this area. MOD16 product reported higher ETa values from vegetation throughout summer and winter than the SEBS and SSEBop models' values in the same locations. The SSEBop model still showed a good result and demonstrated relatively good performance. According to the results of the regression analysis, SSEBop is less linked to ET_0 than SEBS; WaPOR ET product is unreliable to estimate ET in this area, as shown in **Table 5**.

The result of RMSE, R^2, and the MAE are shown in **Tables 6** and **7**. SEBS has closer results to ET_0, and the accuracy of SEBS comes from using the data in the local metrological station. The wind speed (changing the ET process location due to water vapour displacement) and sunshine hour duration factors are important keys in estimating ET_a.

Table 6: Correlation between estimate ET for the models and products with three predictors.

	SEBS	SSEBop	WaPOR product	MOD16 product
Inflow (MCM)	0.466	0.435	0.362	0.463
Air Temperature (^oC)	0.932	0.876	0.928	0.862
Solar radiation ($MJ.m^2$)	0.921	0.798	0.842	0.789

Table 7: Comparison statistics for calculated ET_0 based on the coefficient of determination (R^2), Pearson's correlation coefficient (r), RMSE, and MAE using the models and products.

Parameters	SEBS model	SSEBop model	WaPOR product	MOD16 product
r (-)	0.944	0.939	0.930	0.903
R^2(-)	0.890	0.881	0.864	0.815
MAE (mm day^{-1})	0.239	0.449	0.926	0.851
RMSE (mm day^{-1})	0.391	0.594	1.202	1.159

6 WATER BUDGET

This chapter discusses the flows within the marsh. It is based on data obtained by in situ flow measurements, sampling, and measuring TDS on the inflow drains in the marsh. These data are combined for tracking the water movement within the wetland (hydrological routing); ET calculations from the satellite images in chapter five and the data measured in additional to the data available from MoWR and the Ministry of Environment (MoE) used in this chapter and all data are monthly.

6.1 Meteorological Data

There are three meteorological stations around Iraqi marshlands **Figure 5(c)** that provide monthly data for 1980–2017 (pan evaporation, rainfall, mean sunshine duration, minimum, mean, and maximum air temperature, relative humidity, wind speed). In 2014, the Ministry of Agriculture installed a weather station (Chibaeich metrological station) in the marsh **Figure 5(d)**, and daily data are available (rainfall, maximum, minimum, and average temperature, growing degree day, maximum and minimum humidity, average wind speed, total solar radiation, and average barometric pressure).

6.2 Evapotranspiration in the Marshlands

The region of the Al-Hammar marsh has high evapotranspiration ET_a with extreme cases of drought. There are different values of the annual average evapotranspiration published in the literature; **Figure 34** shows the average monthly pan evaporation data from 1980 till 2017 and rainfall from 1980 till 2017 for three stations, E_{pan} reached 621 mm day^{-1} in July at the Nasirya station, and the mean annual pan evaporation is 3812 mm (Center for Restoration of Iraqi Marshes, 2020). Unfortunately, this cannot be relied upon in water balance calculations because it is pan evaporation, which is higher than the evaporation from natural surfaces. **Figure 35** shows the ET_a calculated from meteorological data. The mean annual ET_a is 3011 mm (UNEP, 2006). In the present study, based on the SEBS model for the 2015–2017 period, when, according to MoWR, 2015 and 2016 were average water years and 2017 was a dry year, the mean annual evapotranspiration was 2464 mm **Figure 36.** It is noticeable that there is a difference between the distribution of monthly ET_a between the UNDP study and the present study because UNDP used the data from metrological stations, which are far more than 100 km from the study area.

6.3 Precipitation

The precipitation within Al-Hammar marsh is characterised by a dry season, about three months long, that coincides with the warm period of the year, from June to August when no rainfall occurs. Higher monthly precipitation occurs from December to January. In general, the average annual precipitation within the marsh is approximately 150 mm. The variation of precipitation in the marsh is shown in **Figure 34**.

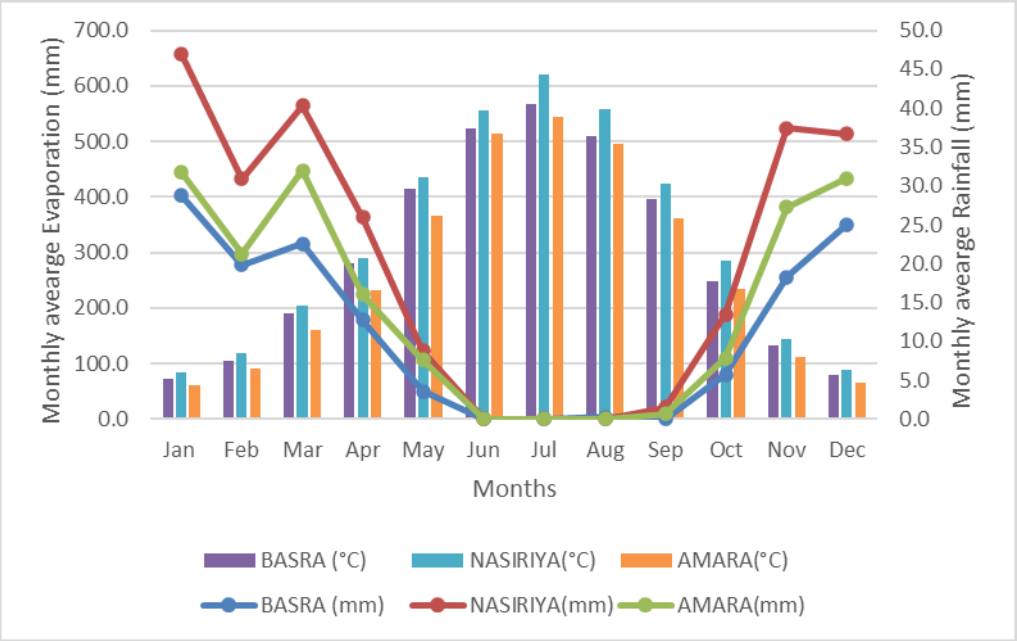

Figure 34: Average monthly pan evaporation and rainfall from 1980 till 2017 for three stations (Source of data: Ministry of Transport, Iraqi Meteorological Authority and Seismology, Iraq).

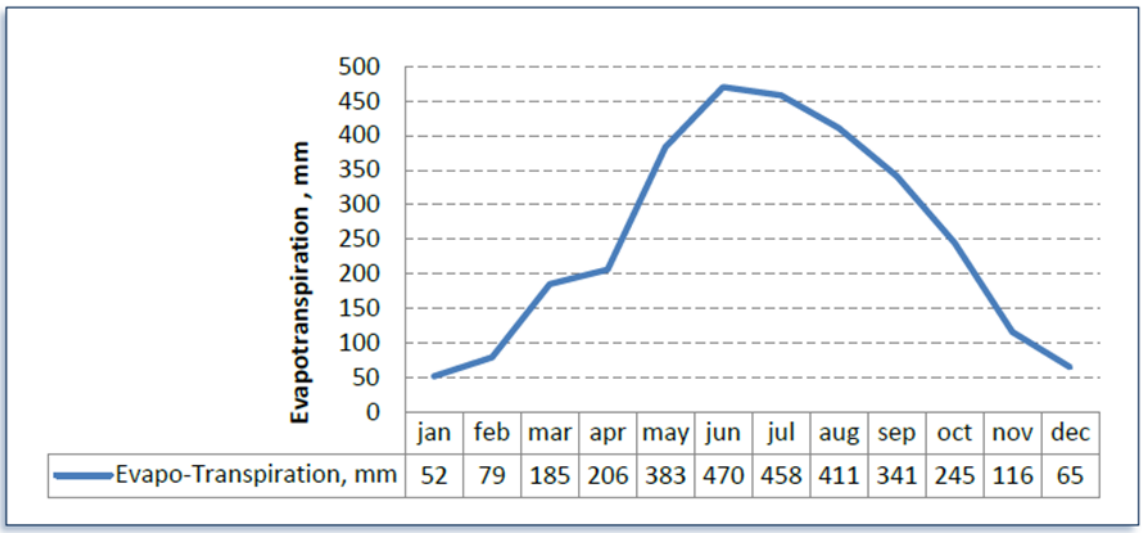

Figure 35: Monthly mean evapotranspiration within Al-Hammar marsh (CRIMW, 2007).

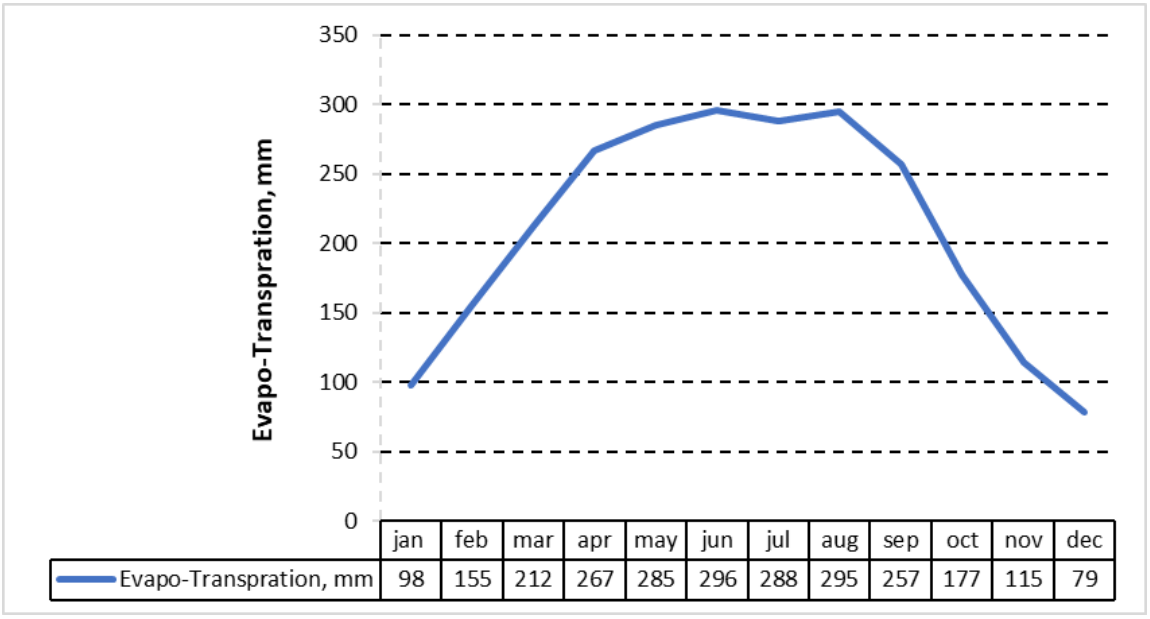

Figure 36: Monthly mean actual evapotranspiration in the Al-Hammar marsh based on the method defined in Chapter 5, using the data from 2015 till 2017.

6.4 Fieldwork

Field campaigns were carried out for collecting complementary data that are essential for this study, to understand the nature and features of the study area, and check the accuracy and reliability of the recorded data. A complete set of monthly discharge measurements for the main feeders of the marsh was carried out during 2015–2017 in cooperation with CRIMW, and water samples to define the TDS concentration were also collected.

6.4.1 Water Quantity

Monthly discharge measurements of the main feeders of the west part of the Al-Hammar marsh at the locations presented in **Figure 5** were carried out with cooperation of CRIMW during 2015-2017. An Acoustic Doppler Current Profiler (ADCP) was used for the discharge measurement. **Figure 37** shows the main feeders, and **Figure 38** shows the monthly discharge data from 2015 till 2017. **Tables 8** and **9** present the data from 2015 to 2017. The total average monthly discharge supplied to the marsh between 2015–2017 by all feeders were 32.3 m^3/s (16.7 from Euphrates feeders, **Table 8** and 15.6 m^3/s from the Al Khamissiya, **Table 9**); thus, the average discharge from the Euphrates River feeders was about 52% of the total inflow to the marsh.

Al Khamissiya

Al Kurmashia

Right of Euphrates River

Um Nakhla

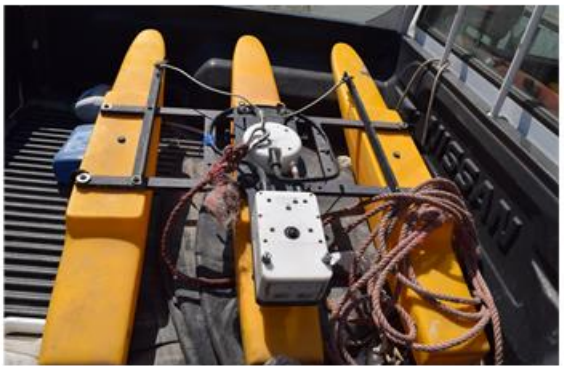

ADCP

Figure 37: The upstream feeders of the Al-Hammar marsh. The photo at the bottom shows the ADCP equipment for the discharge measurements.

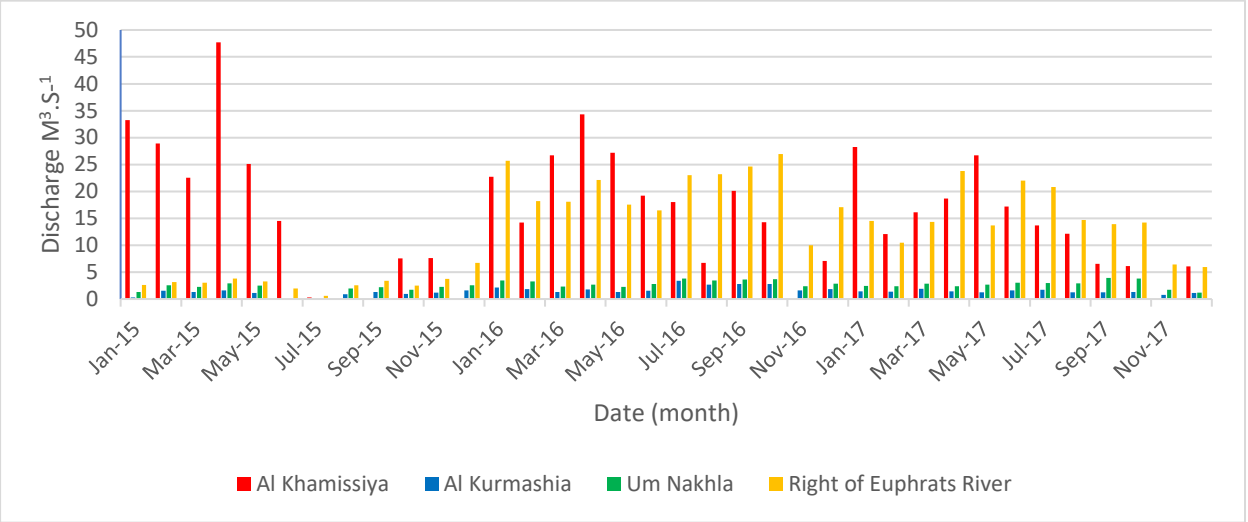

Figure 38: Monthly discharge to the Al-Hammar marsh through the feeders in m^3 s^{-1} from 2015 to 2017 (Source of data: Ministry of Water Resources, Iraq). (Al-Maliki, 2018)

6.4.3 Water Quality

The Ministry of Environment monthly measured the TDS concentrations of the Euphrates River and the MOD at the marsh border from 2010. For this study, it was decided with MoE and WoWR to add locations also inside the marsh for sampling, using YSI Water Quality Sampling and Monitoring Meters **Figure 39**. The locations of the WQ sampling are shown in **Appendix 5**. The monthly data is available for all locations from 2015 till 2017, except for the Arch Drain point, where the data is not available periodically due to security reasons. The measurement results are shown in **Figure 40** and the tables **Appendix 6** and **7**. The water samples were collected from a depth of 20 cm. The TDS concentration of the collected samples was measured using the YSI 650 MDS instrument.

Figure 39: Tools and methods used in measuring water quality. (a) YSI 650 MDS instrument (b) Sample of WQ (c) The Security Dike (d) Euphrates River (e) Al Hamedy (f) BC 3 (g) Arch Drain (h) Al Khamissiya canal (i) BC 4.

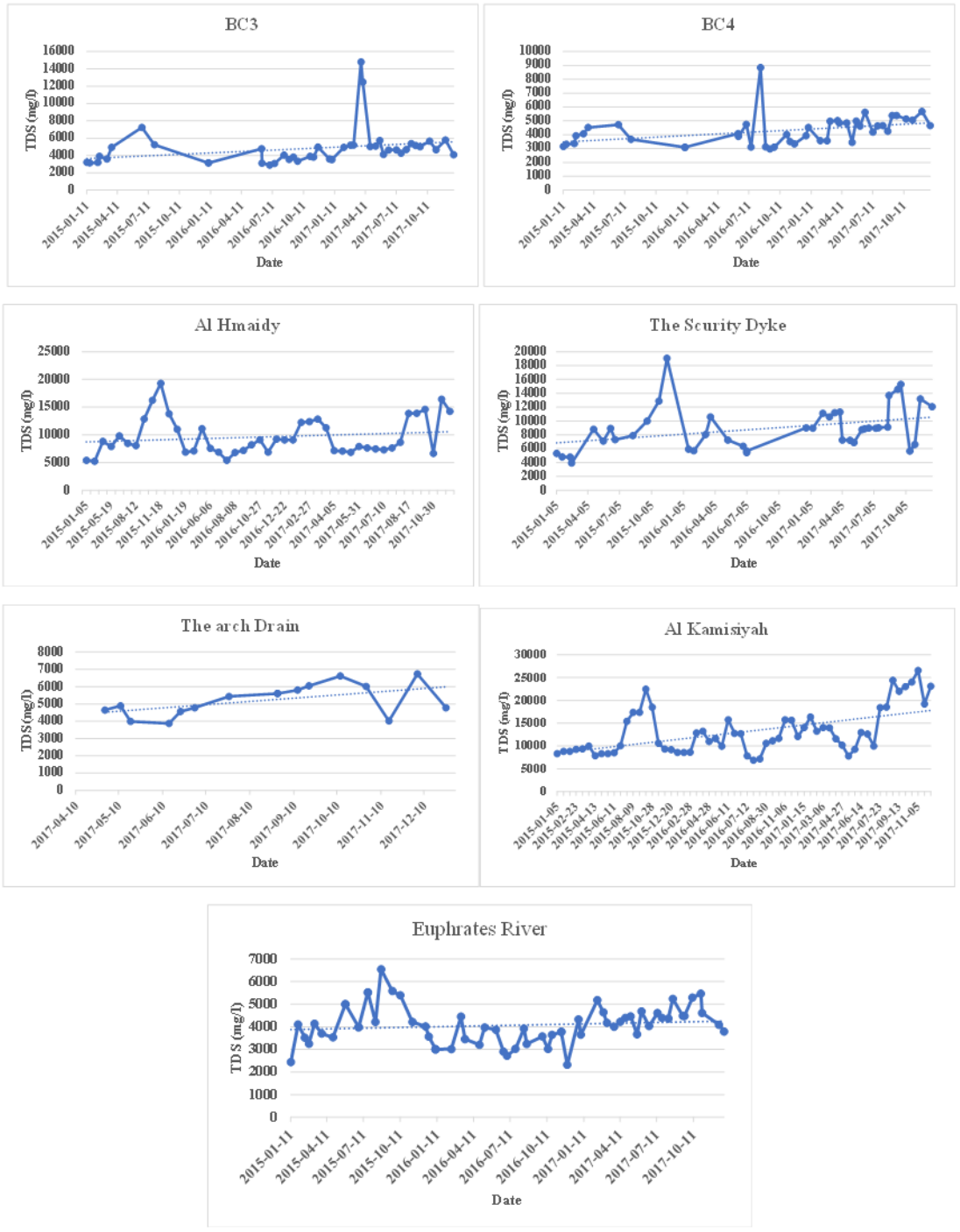

Figure 40: TDS of the Euphrates River, MOD upstream of the Al-Hammar marsh, and the sampling points inside the marsh from 2015 to 2017 (with cooperation of Ministry of Environmental, Iraq).

6.5 Water budget calculation

The field measurement showed that the TDS concentration of the feeders from the Euphrates River ranged between 2320 and 6540 mg/l with an average of 2067 mg/l. The TDS concentration of the Al Khamissiya Canal was ranging between 6900 mg/l and 26522 mg/l with an average of 13130 mg/l during the period above, so the TDS of the Al Khamissiya Canal was more than four times higher than the TDS concentration in the Euphrates River **Figure 40**.

By applying the basic principle of mass conservation, the hydrological routing of the west part of the Al-Hammar marsh was carried out. The required inflow to maintain a constant marsh area equals the evaporation from this area, plus an outflow required for flushing out some of the salts accumulated within the marsh.

Maintaining a constant area can help in flushing out the salts accumulated within the marsh when there is a surplus inflow. Moreover, maintaining a constant area helps fix the marsh's boundaries for future planning of projects. The constraints for maintaining a constant area are the sum of outflow from the marsh, including evapotranspiration subtracted the rainfall from it and the outflow to flush out the accumulated salts within the marsh, and the sum of inflow to the marsh, including the inflow of the feeders from the Euphrates River and the water of the MOD supplied by Al Khamissiya Canal.

Discussion with the experts of MoWR and the strategical study for water and land in Iraq for 2015-2035 (MoWR, 2014) show that the discharge of the feeders to the marsh from the Euphrates River varies within a range of about ± 25% of the measured discharges. Taking into account this assumption, we can prepare different operation scenarios.

The monthly actual evapotranspiration within the marsh was defined is given in **Figure 36**. The highest evapotranspiration was in June. Two factors govern the outflow required to flush out the accumulated salts within the marsh. The first is the total volume of the salt in the marsh water, and the second is how much water can be supplied from the feeders, including the Al Khamissiya Canal. The maximum design capacity of the canal is 40 m^3/s which restricts the possible inflow. The amount of outflow from the west part of the Al-Hammar marsh positively affects the concentration of the TDS within the marsh. The more outflow, the more salt is flashed out.

The water budgeting was carried out, with the constraints of

- maintaining a constant area;
- the maximum design capacity of Al Khamissiya Canal is 40 m^3/s, and
- the discharge of the feeders of the marsh from the Euphrates River varies within a range of about ±25% of the measured discharges **Table 8** and
- the average discharge from the Al Khamissiya canal in **Table 9**.

An example of the water budget calculation with different scenarios of water availability in the future **Table 10** shows the required inflow to maintain the maximum area of, e.g., 250 km^2 discharge of Al Khamissiya Canal is 15.6 m^3 /s, **Table 10** shows the monthly discharge can be released from the suggested outlet to reduce the salinity in the marsh, and the value of 3.6 m^3/s for June restricts a minimum outflow discharge.

With the same procedure can make different scenarios, e.g., under the condition that the feeders' discharges from the Euphrates River are 25% higher than the measured and a maximum inflow from Al Khamissiya Canal of 40 m^3/s, a maximum marsh area of 499 km^2 can be reached.

Table 8: Averages Sum of inflow to Al-Hammar marsh from Euphrates Rivers feeders from 2015-2017 m3 /s.

Month	Al Kurmashia	Um Nakhla	Right of Euphrates River canal	Sum	Sum +25%	Sum -25%
Jan.	1.3	2.4	14.3	18.0	22.5	13.5
Feb.	1.6	2.7	10.6	14.9	18.6	11.2
Mar.	1.5	2.5	11.8	15.8	19.8	11.9
Apr.	1.6	2.7	16.6	20.9	26.1	15.7
May	1.2	2.5	11.5	15.2	19.0	11.4
Jun.	1.1	2.0	13.5	16.5	20.6	12.4
Jul.	1.7	2.3	14.8	18.8	23.5	14.1
Aug.	1.6	2.8	13.5	17.9	22.3	13.4
Sep.	1.8	3.3	14.0	19.0	23.8	14.3
Oct.	1.7	3.1	14.6	19.3	24.1	14.5
Nov.	1.2	2.1	6.7	10.1	12.6	7.5
Dec.	1.5	2.2	9.9	13.6	17.0	10.2
Averages	1.5	2.6	12.7	**16.7**	20.8	12.5

Table 9: Average Discharge m3 /s of Al Khamissiya from 2015-2017.

Month	2015	2016	2017	Average
Jan.	33.25	22.7	28.25	28.07
Feb.	28.88	14.2	12.1	18.39
Mar.	22.57	26.7	16.1	21.79
Apr.	47.7	34.3	18.65	33.55
May	25.1	27.17	26.7	26.32
Jun.	14.5	19.2	17.2	16.97
Jul.	0.3	18.03	13.7	10.68
Aug.	0	6.7	12.15	6.28
Sep.	0	20.1	6.55	8.88
Oct.	7.55	14.25	6.15	9.32
Nov.	7.6	0	0	2.53
Dec.	0	7.1	6.05	4.38
Average	15.62	17.54	13.63	**15.60**

Table 10: The average release discharge from the suggested outlet to keep maintain the maximum area of 250 km^2 if the discharge of Al Khamissiya Canal is 15.6 m3 /s.

Month	Day	ET_a mm	ET_a m^3/s	Average monthly Rain fall mm	Rainfall m^3/s	Supplied Inflow from Euphrates River by Feeders m^3/s	Outflow m^3/s
Jan.	31	98	9.1	2.6	0.01	18.0	24.51
Feb.	28	155	16.0	10.9	0.04	14.9	14.59
Mar.	31	212	19.8	12.8	0.04	15.8	11.64
Apr.	30	267	25.7	4.3	0.01	20.9	10.90
May	31	285	26.6	0.2	0.00	15.2	4.20
Jun.	30	296	28.5	0.0	0.00	16.5	3.60
Jul.	31	288	26.9	0.0	0.00	18.8	7.50
Aug.	31	295	27.5	0.0	0.00	17.9	6.00
Sep.	30	257	24.8	0.0	0.00	19.0	9.80
Oct.	31	177	16.5	8.7	0.03	19.3	18.43
Nov.	30	115	11.1	5.6	0.02	10.1	14.62
Dec.	31	79	7.3	16.4	0.05	13.6	21.95
Averages		210	20	5.1	0.02	16.67	12.30

The calculation is made on monthly bases just to provide order on the magnitude, we can use actual evapotranspiration calculated in this study from satellite images and with develop two-dimensional hydrodynamic and water quality transport model with different scenarios and then analyses the results for the west part of the Al-Hammar marsh to know the optimum location of the outlet and to simulate the distribution of the salt inside the marsh. The final decision about the area of the marsh and the target water quality parameters of the restoration is beyond the objectives of the present research; it has to be defined by the MoWR.

7 CONCLUSIONS AND SUGGESTIONS FOR THE FUTURE RESEARCH

7.1 Classification

In wetlands of arid and semi-arid regions, the land cover is very dynamic due to extreme driving factors, like high temperature, vapour deficit in the air, extreme rainfall events and floods on feeding rivers.

The revival of marshlands is based on the incoming flows affected by upstream agricultural and hydrological conditions.

Extreme meteorological and flooding conditions in arid and semi-arid regions result in rapid and dramatic changes in the water and vegetation cover in wetlands. To understand these systems and support their management, a robust classification and monitoring method is required. The above-described methodology can support examining management and restoration plans for marshlands/wetlands.

A classification approach was presented for monitoring marshlands by a hierarchical application of NDVI, NDMI, and NDWI indices calculated based on optical satellite images. The proposed automatic classification results in six land cover classes, namely, (1) open water, (2) dry area, (3) dense vegetation, (4) medium-density vegetation, (5) low-density vegetation, and (6) wet soil. The proposed method uses optical indices calculated from level-2 data, allowing the use of generic thresholds.

Optical indices have been used for wetland mapping by several authors already (e.g., (Kääb *et al.*, 2016; Mandanici and Bitelli, 2016; Jiang *et al.*, 2018; Al Shehhi and Kaya, 2021; Varga *et al.*, 2021)). The approach proposed here uses a combination of the indices, exploiting the strength of each of them in optimally separating different land cover types. The advantage of the method is the use of fine-tuned, time-independent thresholds for systematic and automated mapping.

For long-term monitoring, time series of Landsat images were exploited for classifying and monitoring the Al-Hammar marsh (Iraq) over a period of 26 years. To estimate the sensitivity of the method to the spatial resolution of the images, a comparison was made with the classification result of a Sentinel-2 image. Spectral differences did not affect the comparison since the Landsat data can be combined into a systematic time series with Sentinel-2 images (Kääb *et al.*, 2016; Mandanici and Bitelli, 2016). Differences can be attributed to the patchy land cover pattern of the Al-Hammar marsh, resulting in more mixed pixels at the 30 m resolution of the Landsat 8 images. In general, it can be concluded that the coarser resolution of the Landsat images provides sufficient accuracy for defining

the land cover categories, but the much longer time series of the Landsat sensor is superior in monitoring long-term changes.

Statistical analysis was carried out to identify the direct relationships between selected variables affecting the water balance (total monthly inflow discharge, monthly air temperature, and ET) and the formation of land cover classes. A significant positive correlation between total inflow and open water cover was found. This shows that the flooding process is fast; open water cover is formed in the same month as the inflow. There was no direct effect of inflow on vegetation cover detected since the emergence of vegetation after flooding occurs with a time delay. The reaction of vegetation cover to flooding dynamics will be a topic for further analysis.

Significant negative correlations between water cover and air temperature and evapotranspiration were also observed. This proves that these climatic factors affect water cover directly due to the shallowness of the water. For maintaining stable wetland conditions, a sufficient water depth has to be achieved and maintained.

The implemented monitoring approach allowed the analysis of the flooding dynamics for a longer period, i.e., from 1991 to 2018.

The results demonstrated the changes within the marshes over the last 28 years. This analysis sheds light on the timing of major changes and allows the identification of the primary forcing variables. It was demonstrated that up until 2002, the total area covered by water and vegetation decreased by 90% of the area in 1991. As a result of the re-wetting efforts after 2003, recovery was observed, but the wetland extent did not reach the area of the baseline year of 1991.

The monitoring results demonstrate the rapid pace of degradation within the Al-Hammar marsh over the last two decades. These results may provide insights used for appropriate water management for habitats.

The results showed that the proposed methodology could efficiently classify marshlands and be used in different wetlands by changing the threshold for NDVI, NDMI, and NDWI.

The results prove that this approach is suitable for classifying marshlands with land cover types of water, dry soil, wet soil, and different densities of vegetation. Combining the long time series of Landsat images with new satellite data can also be recommended to provide more accurate classifications and increase revisiting times.

There is potential to develop our methodology to include other indices and other landcover groups.

7.2 Evapotranspiration

One of the most significant drivers affecting the water cover, vegetation cover and water balance of the marshes in arid and semi-arid areas is evapotranspiration.

Various models increasingly use satellite imagery to measure ET and water use in watersheds at a large scale. The performance of these models depends on various factors, such as input data and model structure. Under these circumstances, selecting suitable models for the study area is challenging. Our study evaluated two ET models, SEBS and SSEBop, and global ET products WaPOR and MOD 16, by comparing ET_0 from a metrological station. SEBS and SSEBop models performed reasonably well in estimating ET_a.

Our comparison shows that the average ET_0 for 21 dates is 5.44 mm. On the basis of the results, the average ET_a values for SSEB, SSEBop, WaPOR and Mod16 are 5.03, 4.56, 2.60 and 4.38, respectively. The ET_a estimate showed that SEBS and SSEBop models effectively tracked ET_0 variation; during summer SSEBop shows higher ETa in open water and vegetation areas Compared with SEBS. The correlation between SEBS and ET_0 was the highest, and the SSEBop model needs to calibrate the *K* value. The WaPOR ETIa product showed the spatial and temporal variations, but the values were lower than SEBS, SSEBop and ET_0 during 2 years. This product has a problem with evaporation from the wet soil. Regarding the results, the WaPOR ET product is unreliable for estimating ET in this area, and MOD16 has an extremely coarse resolution. These products are unsuitable to use in small areas, and separating different ET from open water, vegetation and wet soil is difficult at this level of resolution. The higher ET_a for MOD16 from vegetation during summer and winter, MOD16 product recorded higher ET than the SEBS and SSEBop models value in some areas.

The results in estimating ET from the SEBS model are comparable with the SSEBop model, although SEBS is more complex and needs many input data.

Comparing the data with ET_0 calculated from the data of the meteorological station showed that the R^2, RMSE and MAE values for the SEBS model are 0.89, 0.391 mm and 0.239, respectively, and are 0.881, 0.594 mm, and 0.449 for SSEBop, respectively. The SEBS model performed reasonably well in estimating ET_a with RMSE less than 0.5 mm day^{-1} **Tables 11** and **12**. Users should be careful in using the WaPOR and MOD16 products in marshland areas.

The accuracy of SEBS comes from using the data of the local metrological station. The wind speed (changing the ET process location due to water vapour displacement) and sunshine hour duration factors are important keys in estimating ET_a.

7.3 Calculated Water Balance

The results of the hydrological routing under the condition of the measured discharges showed that an inflow from Al Khamissiya Canal of 15.6 m^3/s and an annual average of the outflow of 33.6 m^3/s are required to maintain 250 km^2 of the west part of Al-Hammar marsh. Under the condition that the feeders' discharges from the Euphrates River are 25% higher than the measured and a maximum inflow from Al Khamissiya Canal of 40 m^3/s, a maximum marsh area of 499 km^2 can be reached. To maintain 250 km^2 of the marsh, when the discharges of the feeders from the Euphrates River are 25% higher than their measured values, the required flow from Al Khamissiya Canal is 11.5 m^3/s. Moreover, the required inflow from the Al Khamissiya Canal to maintain a minimum area of 250 km^2 in the west part of the Al-Hammar marsh of when the discharges of the feeders from Euphrates River are 25% less than their measured values, is 19.7 m^3/s. Finally, in reducing the discharges of the feeders from the Euphrates River by 25%, the maximum area can reach up to 427 km^2 with a maximum discharge of Al Khamissiya Canal of 40 m^3/s.

7.4 Suggestions for the future research

The following recommendations were suggested for further studies:

- The demonstrated classification method uses empirically defined and validated thresholds which might be fine-tuned with machine learning techniques and optical indices-based classification accuracies can be improved significantly.
- Definition of how RS can be used for environmental impacts in marshlands.
- Investigation of the effects of groundwater quantity and its quality in the west part of Al-Hammar marsh.
- Develop and analyse the results of a two-dimensional hydrodynamic and water quality transport model for the west part of the Al-Hammar marsh.

8 New scientific results

A new scientific result of the dissertation can be summarised for the following five thesis:

1. I developed an optical indices-based hierarchical classification method for automatic land cover mapping to monitor the wetlands.
2. I proposed an optimum data processing method that locates the ET model as more sensitive in spatial and temporal.
3. I prepared and modified the actual ET curve that can be used in future water management studies.
4. I integrated and optimised the management data from different sources for feeding the regions with scarcity data.
5. I calculated the marsh's water balance to pinpoint the region that can be protected when water is abundant.

9 THESIS SUMMARY

Worldwide diminishing water resources lead to environmental water scarcity, especially in the arid and semi-arid climatic areas. This leads to the need of efficient water management and monitoring methods.

In this study, the test area was the Al-Hammar marsh in the southern part of Iraq. This marsh was exposed to draining measures in the nineties. It also strongly depends on upstream water management activities in its catchment, inside and outside Iraq. Many of these measures focused on controlling and altering natural hydrology for the retention of water. The west part of Al-Hammar marsh was supplied with the effluent agricultural brackish water of the Main Outfall Drain (MOD), in order to address the water shortage problem and avoid complete drying up. Resultingly, salts started to accumulate in the marsh.

Classifying marshlands in these regions and creating a land cover map is not a simple target. The dynamics of marshes is high, inundation and vegetation cover rapidly change due to the dynamics of the many drives affecting the marshlands, such as high evapotranspiration, temperature, and variation of inflow from rivers. In this study, we suggested a new approach for classifying the marshlands by a hierarchical classification of NDVI, NDMI, and NDWI. The results showed that the proposed method can efficiently classify marshlands. It can be used in other marshlands too, but the threshold for NDVI, NDMI, and MDWI have to be adjusted.

One of the major components of water balance (WB) in these zones is evapotranspiration (ET). ET estimation from wetlands (marshlands) in these areas plays a main role in water management. Information about it is needed for preserving marshlands, to take into account the imbalance between precipitation and potential evapotranspiration. For estimating ET, this study used Landsat images and the SEBS and SSEBop models for estimate ET_a, and ET_a products from MODIS (MOD16) and FAO's WaPOR system. These actual evapotranspiration from models and products were compared to ET_0 defined by the Penman-Monteith method using metrological data measured at a meteorological station nearby the test area by assumed that in these wetlands, ET_0 and ET_p are equal. Since there is always water and no water stress is present, we can assume ET_a is equal ET_p maybe it is a little lower but not higher (i.e., no water stress is present).

All the compared models and products captured the trends in the temporal and spatial variations of ET. The SEBS and SSEBop models showed R more than 0.9 and low. RMSE for SEBS is less than 0.391 mm day^{-1} and for SSEBop is less than 0.594 mm day^{-1}; whereas the MOD16 and WaPOR

products had high RMSE, 1.159 mm day^{-1} and 1.202 mm day^{-1}, respectively. SEBS is a more complex model and needs many data for parameterisation but it reasonably estimates ET in the marshlands, while SSEBop is simpler and faces some problems to calculate ET from open water. Its scaling coefficient (k) needs to be calibrated for the application site. In the case of mixed pixels, it is not easy to separate the evaporation from open water bodies and the evaporation from vegetation. The results show that the use of WaPOR ET products in marshlands is not advisable, because it underestimates ET. Due to its coarse spatial resolution, MOD16 is not suitable for small wetlands.

Using ET_a time series from satellite images and field discharge measurements, a water budget calculation scheme was developed for the Al Hammar Marsh, which is suitable for developing scenarios for the restoration and management of the wetland.

Two scenarios were demonstrated, for maintaining selected sizes of inundated areas with a need for flushing salt out from the wetland. Constraints in water supply and of climatic conditions were considered. The results can provide a basis for 2D hydrodynamic modelling for studying the water quality distribution within the marsh.

The presented research shows how ET-base data can be integrated into workflows for the management of wetlands in in situ data-scarce semi-arid regions.

10 REFERENCES

Abbas, A. and Ziboon, A. R. T. (2009) 'Using Remote Sensing and Gis Technique to Study Soil Physical Properties for Hour Al-Hammar (South of Iraq)', *Engineering and Technology*, 28(1), pp. 164–180.

Abdul Karim, S. N. A. *et al.* (2013) 'FAO 56 Model and Remote Sensing for the Estimation of Crop-Water Requirement in Main Branch Canal of the Bhadra Command area, Karnataka State', *Journal of the Indian Society of Remote Sensing*, 41(4), pp. 883–894. doi: 10.1007/s12524-012-0238-z.

Al-Ansari, N., Knutsson, S. and Ali, A. (2012) 'Restoring the Garden of Eden, Iraq', *Journal of Earth Sciences and Geotechnical Engineering*, 2(1), pp. 53–88.

Al-Hmedawy, H. (2008) *Geomorphological Study of Haur Al-Hammar and adjacent area Southern Iraq using remote sensing data and GIS techniques*. PhD thesis, University of Baghdad (unpublished).

Al-Maliki, S. (2017) *Annual report on water resources in Iraq (internal report)*. Baghdad, Iraq.

Al-Maliki, S. (2018) *Annual report on water resources in Iraq (internal report)*. Baghdad, Iraq.

Al-Mosewi, T. J. K. (2009) 'Water quality of Al-Hammar marsh South Iraq', *Journal of Engineering*, 15(3), pp. 3999–4008.

Al-Saad, H. T. *et al.* (2010) 'Water quality of the Iraqi southern marshes', *Mesopot. J. Mar. Sci*, 25(2), pp. 79–95. Available at: https://www.researchgate.net/profile/Ali_Douabul/publication/260105401_Water_quality_of_the_Iraqi_southern_marshes/links/54a64cf60cf256bf8bb4e0d5.pdf.

Al-Saboonchi, A. *et al.* (2011) 'On the Current and Restoration Conditions of the Southern Iraqi Marshes: Application of the CCME WQI on East Hammar Marsh', *Journal of Environmental Protection*, 02(03), pp. 316–322. doi: 10.4236/jep.2011.23035.

Al-Shamary, A. (2012) 'Water quality study for Southern part of Al- Hammar marsh', *Iraqi Journal For water agriculture, No.2,* 7(Basrah, (in Arabic)), pp. 205–224.

AL-Shamary A.Ch (2012) 'Water quality study for Southern part of Al- Hammar marsh', *Iraqi Journal For water agriculture, No.2,* 7(Basrah, (in Arabic)).

Allen, R. *et al.* (2011) 'Satellite-based ET estimation in agriculture using SEBAL and METRIC', *Hydrological Processes*, 25(26), pp. 4011–4027. doi: 10.1002/hyp.8408.

Allen, R. G. *et al.* (1998a) 'Crop evapotranspiration - Guidelines for computing crop water requirements - FAO Irrigation and drainage paper 56 By', pp. 1–15.

Allen, R. G. *et al.* (1998b) 'Fao,1998', *Irrigation and Drainage Paper No. 56, FAO*, p. 300. doi: 10.1016/j.eja.2010.12.001.
Altinbilek, D. (2004) 'Development and management of the Euphrates - Tigris basin', *International Journal of Water Resources Development*, 20(1), pp. 15–33. doi: 10.1080/07900620310001635584.
Amin, A. A. (2008) 'Proposed Hydrological Scenarios for Restoration of Al-Hammar Marsh', (1), pp. 1–15.
Aoki, C. and Kugaprasatham, S. (2009) *Support for environmental management of the Iraqi marshlands, UNDP*. UNEP Publication DTI/1171/JP. United Nations Environment Programme Nairobi, Kenya.
Bashford, K. E., Beven, K. J. and Young, P. C. (2002) 'Observational data and scale-dependent parameterizations: Explorations using a virtual hydrological reality', *Hydrological Processes*, 16(2), pp. 293–312. doi: 10.1002/hyp.339.
Bastiaanssen, W. G. M. *et al.* (1998) 'A remote sensing surface energy balance algorithm for land (SEBAL)', 213.
Bastiaanssen, W. G. M. *et al.* (2005) 'SEBAL model with remotely sensed data to improve water-resources management under actual field conditions', *Journal of Irrigation and Drainage Engineering*, 131(1), pp. 85–93. doi: 10.1061/(asce)0733-9437(2005)131:1(85).
Bastiaanssen, W. G. M. *et al.* (2012) 'Surface energy balance and actual evapotranspiration of the transboundary Indus Basin estimated from satellite measurements and the ETLook model', *Water Resources Research*, 48(11), pp. 1–16. doi: 10.1029/2011WR010482.
Bastiaanssen W.G.M. *et al.* (1998) 'A remote sensing surface energy balance algorithm for land (SEBAL): 1. Formulation', *Journal of Hydrology*, 212–213(1–4), pp. 198–212. doi: 10.1016/S0022-1694(98)00253-4.
Becker, R. H. (2014) 'The stalled recovery of the Iraqi marshes', *Remote Sensing*, 6(2), pp. 1260–1274. doi: 10.3390/rs6021260.
Bhattarai, N. *et al.* (2016) 'Evaluating five remote sensing based single-source surface energy balance models for estimating daily evapotranspiration in a humid subtropical climate', *International Journal of Applied Earth Observation and Geoinformation*. Elsevier, 49, pp. 75–86.
Center for Restoration of Iraqi Marshes (2017) *CRIMW*. Baghdad, Iraq.
Center for Restoration of Iraqi Marshes (2020) *CRIMW*. Baghdad, Iraq.
Chauhan, S. and Shrivastava, R. K. (2009) 'Performance evaluation of reference evapotranspiration estimation using climate based methods and artificial neural networks', *Water Resources*

Management, 23(5), pp. 825–837. doi: 10.1007/s11269-008-9301-5.
Chávez, J. L. *et al.* (2009) 'Radiometric surface temperature calibration effects on satellite based evapotranspiration estimation', *International Journal of Remote Sensing*, 30(9), pp. 2337–2354. doi: 10.1080/01431160802549393.
CIDA, C. I. D. A. (2010) *Managing for change: the present and future state of the marshes of southern Iraq*. Canada-Iraq Marshlands Initiative.
CRIM (2007) *Study of Improving the Environmental Present Condition of Southern Marshes, Hydrological and Water Quality Study*. Baghdad, Iraq.
CRIM (2010) *Possibility of Using the Water of the main Outfall Drain to Restore Al Hammar Marsh after Operating the Pumping Station in Al Nassiriyah.*
CRIMW (2007) *" Restoration of Al-Hammar Marsh Study ", Prepared in cooperation with the Al-Tawasul International Company for Engineering Design and Consultants and The Consulting Bureau of the Iraqi Engineers Union, Iraq.* Baghdad.
Domeneghetti, A. *et al.* (2014) 'The use of remote sensing-derived water surface data for hydraulic model calibration', *Remote Sensing of Environment*. Elsevier Inc., 149, pp. 130–141. doi: 10.1016/j.rse.2014.04.007.
FAO (2020) *WaPOR database methodology: Version 2 release, WaPOR database methodology*. Rome. doi: 10.4060/ca9894en.
Fisher, A., Flood, N. and Danaher, T. (2016) 'Comparing Landsat water index methods for automated water classification in eastern Australia', *Remote Sensing of Environment*. Elsevier Inc., 175, pp. 167–182. doi: 10.1016/j.rse.2015.12.055.
Gao, B.-C. (1996) 'NDWI—A normalized difference water index for remote sensing of vegetation liquid water from space', *Remote Sensing of Environment*, 58(3), pp. 257–266.
Glenn, E. P., Nagler, P. L. and Huete, A. R. (2010) 'Vegetation index methods for estimating evapotranspiration by remote sensing', *Surveys in Geophysics*, 31(6), pp. 531–555. doi: 10.1007/s10712-010-9102-2.
Gokmen, M. *et al.* (2013) 'Assessing groundwater storage changes using remote sensing-based evapotranspiration and precipitation at a large semiarid basin scale', *Journal of Hydrometeorology*, 14(6), pp. 1733–1753. doi: 10.1175/JHM-D-12-0156.1.
Gowda, P. H. *et al.* (2008) 'ET mapping for agricultural water management: Present status and challenges', *Irrigation Science*, 26(3), pp. 223–237. doi: 10.1007/s00271-007-0088-6.
Guarasci, B. L. (2011) 'Biodiversity and ecosystem management in the Iraqi Marshlands–screening

study on potential world heritage nomination', *Journal of Chemical Information and Modeling*, 53(9), pp. 1689–1699. doi: 10.1017/CBO9781107415324.004.
Guarasci, B. L., Garstecki, T. and Amr, Z. (2011) 'Biodiversity and ecosystem management in the Iraqi Marshlands–screening study on potential World Heritage Nomination', *Amman, Jordan: IUCN*, 53(9), pp. 1689–1699. doi: 10.1017/CBO9781107415324.004.
Guo, M. *et al.* (2017) 'A review of wetland remote sensing', *Sensors (Switzerland)*. Multidisciplinary Digital Publishing Institute, 17(4), pp. 1–36. doi: 10.3390/s17040777.
Hashesh, T. S. and Ahmed, B. A. (2018) 'Using GIS and remote sensing to study water quality changes and spectral analysis for AL-Hawizah marshes, South of Iraq', *Iraqi Journal of Science*, 59(3C), pp. 1757–1768. doi: 10.24996/ijs.2018.59.3c.20.
Hassan, Z. D. (2012) 'Using Remote Sensing Techniques and Geographic Information Systems (Gis) in Sequences Study To Al-Hammar Marsh / South of Iraq for the Period (1973-2010)(in Arabic)', *IRAQI JOURNAL OF DESERT STUDIES*, 4(1).
Hunt, E. R. and Rock, B. N. (1989) 'Detection of changes in leaf water content using Near- and Middle-Infrared reflectances', *Remote Sensing of Environment*, 30(1), pp. 43–54. doi: 10.1016/0034-4257(89)90046-1.
Jana, C. *et al.* (2016) 'Application of SEBAL model to estimate evapotranspiration in Doon Valley, India', *Indian Journal of Soil Conservation*, 44(2), pp. 191–197.
Jensen, M. E. (2007) 'Beyond irrigation efficiency', *Irrigation Science*, 25(3), pp. 233–245. doi: 10.1007/s00271-007-0060-5.
Ji, L., Zhang, L. and Wylie, B. (2009) 'Analysis of dynamic thresholds for the normalized difference water index', *Photogrammetric Engineering & Remote Sensing*, 75(11), pp. 1307–1317. doi: 10.14358/PERS.75.11.1307.
Jiang, W. *et al.* (2018) 'Multilayer perceptron neural network for surface water extraction in landsat 8 OLI satellite images', *Remote Sensing*, 10(5), pp. 1–22. doi: 10.3390/rs10050755.
Jimenez-Munoz, J. C. *et al.* (2009) 'Revision of the single-channel algorithm for land surface temperature retrieval from landsat thermal-infrared data', *IEEE Transactions on Geoscience and Remote Sensing*, 47(1), pp. 339–349. doi: 10.1109/TGRS.2008.2007125.
Jones, C. *et al.* (2008) 'Hydrologic impacts of engineering projects on the Tigris-Euphrates system and its marshlands', *Journal of Hydrology*, 353(1–2), pp. 59–75. doi: 10.1016/j.jhydrol.2008.01.029.
Jung, H. C. *et al.* (2019) 'Uncertainties in evapotranspiration estimates over west Africa', *Remote*

Sensing, 11(8), p. 892. doi: 10.3390/rs11080892.
Kääb, A. *et al.* (2016) 'Glacier remote sensing using sentinel-2. part I: Radiometric and geometric performance, and application to ice velocity', *Remote Sensing*, 8(7). doi: 10.3390/rs8070598.
Kalma, J. D., McVicar, T. R. and McCabe, M. F. (2008) 'Estimating land surface evaporation: A review of methods using remotely sensed surface temperature data', *Surveys in Geophysics*, 29(4–5), pp. 421–469. doi: 10.1007/s10712-008-9037-z.
Kavvas, M. L. *et al.* (2011) 'A study of water balances over the Tigris-Euphrates watershed', *Physics and Chemistry of the Earth*. Elsevier Ltd, 36(5–6), pp. 197–203. doi: 10.1016/j.pce.2010.02.005.
Kustas, W. P. and Daughtry, C. S. T. (1990) *Estimation of the soil heat flux/net radiation ratio from spectral data*, *Agricultural and Forest Meteorology*. doi: 10.1016/0168-1923(90)90033-3.
Leonce, N. J. (2021) *Combining satellite-based et time series with integrated modeling of a wetland*. MSc Thesis, University of Twente, Netherlands.
Liang, S. (2001) 'Narrowband to broadband conversions of land surface albedo I: Algorithms', *Remote sensing of environment*, 76(2), pp. 213–238. doi: 10.1016/S0034-4257(02)00068-8.
Liou, Y. A. and Kar, S. K. (2014) 'Evapotranspiration estimation with remote sensing and various surface energy balance algorithms-a review', *Energies*, 7(5), pp. 2821–2849. doi: 10.3390/en7052821.
Mandanici, E. and Bitelli, G. (2016) 'Preliminary comparison of sentinel-2 and landsat 8 imagery for a combined use', *Remote Sensing*, 8(12). doi: 10.3390/rs8121014.
Mas, J.-F. (1999) 'Monitoring land-cover changes: a comparison of change detection techniques', *International Journal of Remote Sensing*, 20(1), pp. 139–152.
Masek, J. G. *et al.* (2006) 'A Landsat surface reflectance dataset for North America, 1990-2000', *IEEE Geoscience and Remote Sensing Letters*, 3(1), pp. 68–72. doi: 10.1016/S0168-1273(87)10004-9.
McFeeters, S. K. (1996) 'The use of the normalized difference water index (NDWI) in the delineation of open water features', *International Journal of Remote Sensing*, 17(7), pp. 1425–1432. doi: 10.1080/01431169608948714.
MoWR (2014) *Strategy for Water and Land Resources in Iraq*. Baghdad, Iraq.
Mu, Q., Zhao, M. and Running, S. W. (2011) 'Improvements to a MODIS global terrestrial evapotranspiration algorithm', *Remote Sensing of Environment*. Elsevier Inc., 115(8), pp. 1781–1800. doi: 10.1016/j.rse.2011.02.019.

Munro, D. C. and Touron, H. (1997) ‘The estimation of marshland degradation in southern Iraq using multitemporal Landsat TM images’, *International Journal of Remote Sensing*. Taylor & Francis, 18(7), pp. 1597–1606. doi: 10.1080/014311697218304.

Musa, Z. N., Popescu, I. and Mynett, A. (2015) ‘A review of applications of satellite SAR, optical, altimetry and DEM data for surface water modelling, mapping and parameter estimation’, *Hydrology and Earth System Sciences*, 19(9), pp. 3755–3769. doi: 10.5194/hess-19-3755-2015.

New Eden Team (2006) *New Eden master plan for the integrated water resources management in the Marshland area, Main Report, Iraqi Ministries of Environment, Water Resources Municipalities and Public Works with cooperation of the Italian Ministry for the Environment and Territory and Free Iraq Foundation*.

Oberg, J. W. and Melesse, A. M. (2006) ‘Evapotranspiration dynamics at an ecohydrological restoration site: An energy balance and remote sensing approach’, *Journal of the American Water Resources Association*, 42(3), pp. 565–582. doi: 10.1111/j.1752-1688.2006.tb04476.x.

Ohara, N. *et al.* (2011) ‘Water Balance Study for the Tigris-Euphrates River Basin’, *Journal of Hydrologic Engineering*, 16(12), pp. 1071–1082. doi: 10.1061/(ASCE)HE.

Partow, H. *et al.* (2005) *Iraqi Marshlands observation system*. Nairobi, Kenya.

Perry, C. *et al.* (2009) ‘Increasing productivity in irrigated agriculture: Agronomic constraints and hydrological realities’, *Agricultural Water Management*, 96(11), pp. 1517–1524. doi: 10.1016/j.agwat.2009.05.005.

Polhamus, A., Fisher, J. and Tu, K. (2013) ‘What controls the error structure in evapotranspiration models?’, *Agricultural and Forest Meteorology*. Elsevier B.V., 169, pp. 12–24. doi: 10.1016/j.agrformet.2012.10.002.

Ren, X. *et al.* (2016) ‘Daily Reference Evapotranspiration for Hyper-Arid to Moist Sub-Humid Climates in Inner Mongolia, China: I. Assessing Temperature Methods and Spatial Variability’, *Water Resources Management*. Water Resources Management, 30(11), pp. 3769–3791. doi: 10.1007/s11269-016-1384-9.

Roerink, G. J., Su, Z. and Menenti, M. (2000) ‘S-SEBI: A simple remote sensing algorithm to estimate the surface energy balance’, *Physics and Chemistry of the Earth, Part B: Hydrology, Oceans and Atmosphere*, 25(2), pp. 147–157. doi: 10.1016/S1464-1909(99)00128-8.

Rokni, K. *et al.* (2014) ‘Water feature extraction and change detection using multitemporal landsat imagery’, *Remote Sensing*, 6(5), pp. 4173–4189. doi: 10.3390/rs6054173.

Safiah, S. (2010) ‘Al-Hammar Marsh Water Hydro Chemical Changes and their Negative Effect (in

Arabic)', *Journal of Basrah Art*, 54(Basrah, (Arabic)).
Saleh, S. A. H. (2012) 'Temporal Change Detection of AL-Hammar Marsh–IRAQ Using Remote Sensing Techniques', *Open Access Scientific Reports*, 1(6), pp. 1–6. doi: 10.4172/scientificreports.
Salih, S. A., Ziboon, A. and Salman, A. A. (2006) 'Application of Remote Sensing and GIS Techniques for Surface Soil Description of AL-Hammar Marsh (Southern of Iraq)', in *Conference: ACIT 2007, At: Lattakia, Syria*, pp. 26–28.
Salim, Š. M. (1962) 'Marsh dwellers of the Euphrates delta', *Monographs on Social Anthropology*. The Athlone Press, 23(8), p. 157.
Senay, G. B. *et al.* (2007) 'A Coupled Remote Sensing and Simplified Surface Energy Balance Approach to Estimate Actual Evapotranspiration from Irrigated Fields', *Sensors*, 7(6), pp. 979–1000.
Senay, G. B. *et al.* (2008) 'Global daily reference evapotranspiration modeling and evaluation', *Journal of the American Water Resources Association*, 44(4), pp. 969–979. doi: 10.1111/j.1752-1688.2008.00195.x.
Senay, G. B. *et al.* (2013) 'Operational Evapotranspiration Mapping Using Remote Sensing and Weather Datasets: A New Parameterization for the SSEB Approach', *Journal of the American Water Resources Association*, 49(3), pp. 577–591. doi: 10.1111/jawr.12057.
Al Shehhi, M. R. and Kaya, A. (2021) 'Time series and neural network to forecast water quality parameters using satellite data', *Continental Shelf Research*. Elsevier Ltd, 231(October), p. 104612. doi: 10.1016/j.csr.2021.104612.
Siegmund, A. and Menz, G. (2005) 'Fernes nah gebracht–Satelliten-und Luftbildeinsatz zur Analyse von Umweltveränderungen im Geographieunterricht', *Geographie und Schule*, 154(4), pp. 2–10.
Sobrino, J. A., Jiménez-Muñoz, J. C. and Paolini, L. (2004) 'Land surface temperature retrieval from LANDSAT TM 5', *Remote Sensing of Environment*, 90(4), pp. 434–440. doi: 10.1016/j.rse.2004.02.003.
Su, H. *et al.* (2005) 'Modeling evapotranspiration during SMACEX: Comparing two approaches for local- and regional-scale prediction', *Journal of Hydrometeorology*, 6(6), pp. 910–922. doi: 10.1175/JHM466.1.
Su, Z. (2002) 'The surface energy balance system (SEBS) for estimation of turbulent heat fluxes', *Hydrology and Earth System Sciences*, 6(1), pp. 85–100. doi: 10.5194/hess-6-85-2002.
Tabari, H. *et al.* (2012) 'Spatial distribution and temporal variation of reference evapotranspiration in arid and semi-arid regions of Iran', *Hydrological Processes*, 26(4), pp. 500–512. doi:

10.1002/hyp.8146.
Tiner, R. W., Lang, M. W. and Klemas, V. V (2015) *Remote sensing of wetlands: applications and advances*. CRC Press.
Trajkovic, S. (2005) 'Temperature-based approaches for estimating reference evapotranspiration', *Journal of irrigation and drainage engineering*. American Society of Civil Engineers, 131(4), pp. 316–323.
Tucker, C. J. (1979) 'Red and photographic infrared linear combinations for monitoring vegetation', *Remote Sensing of Environment*, 8(2), pp. 127–150. doi: 10.1016/0034-4257(79)90013-0.
UNDP (2010) *Iraqi Marshlands Observation System*. Nairobi, Kenya: United Nations Environment Programme.
UNEP (2001) *The Mesopotamian Marshlands: Demise of an Ecosystem, Division of Early Warning and Assessment, United Nations Environment Program (UNEP) Nairobi, Kenya*. Geneva, Switzerland. Available at: http://www.grid.unep.ch/activities/sustainable/tigris/marshlands/%0AUNEP/DEWA/GRID.
UNEP (2009) *Support for environmental management of the Iraqi marshlands*. NEP Publication DTI/1171/JP. United Nations Environment Programme, Nairobi, Kenya.
USGS (2016) *Landsat 8*. Available at: https://www.usgs.gov/core-science-systems/nli/landsat/landsat-8?qt-science_support_page_related_con=0#qt-science_support_page_related_con.
Varga, O. G. *et al.* (2021) 'Validation of visually interpreted corine land cover classes with spectral values of satellite images and machine learning', *Remote Sensing*, 13(5), pp. 1–24. doi: 10.3390/rs13050857.
Verhoeven, G. (2008) 'Imaging the invisible using modified digital still cameras for straightforward and low-cost archaeological near-infrared photography', *Journal of Archaeological Science*, 35(12), pp. 3087–3100. doi: 10.1016/j.jas.2008.06.012.
Vinez, M. and Leonard, S. (2010) 'The Iraq marshlands: the loss of the garden of Eden and its people', in *PLSI-3443*. Illinois, USA. doi: https://pol.illinoisstate.edu/downloads/conferences/2011/LeonardIraqMarshes.pdf.
Wan, Z. and Li, Z. L. (1997) 'A physics-based algorithm for retrieving land-surface emissivity and temperature from eos/modis data', *IEEE Transactions on Geoscience and Remote Sensing*, 35(4), pp. 980–996. doi: 10.1109/36.602541.
Wu, X. *et al.* (2015) 'Evaluation of irrigation water use efficiency using remote sensing in the

middle reach of the Heihe river, in the semi-arid Northwestern China', *Hydrological Processes*, 29(9), pp. 2243–2257. doi: 10.1002/hyp.10365.
Xie, P. and Arkin, P. A. (1997) 'A 17-Year Monthly Analysis Based on Gauge Observations, Satellite Estimates, and Numerical Model Outputs', *Bulletin of the American Meteorological Society*, 78(11), pp. 2539–2558. doi: 10.1175/1520-0477(1997)078<2539:GPAYMA>2.0.CO;2.
Xu, C. yu *et al.* (2006) 'Analysis of spatial distribution and temporal trend of reference evapotranspiration and pan evaporation in Changjiang (Yangtze River) catchment', *Journal of Hydrology*, 327(1–2), pp. 81–93. doi: 10.1016/j.jhydrol.2005.11.029.
Xu, H. (2006) 'Modification of normalised difference water index (NDWI) to enhance open water features in remotely sensed imagery', *International Journal of Remote Sensing*, 27(14), pp. 3025–3033. doi: 10.1080/01431160600589179.
Yesuph, A. Y. and Dagnew, A. B. (2019) 'Land use/cover spatiotemporal dynamics, driving forces and implications at the Beshillo catchment of the Blue Nile Basin, North Eastern Highlands of Ethiopia', *Environmental Systems Research*. Springer Berlin Heidelberg, 8(1). doi: 10.1186/s40068-019-0148-y.

APPENDIX

Appendix 1: Landsat data type and acquisition dates.

Date of Acquisition	Sensor Type	Date of Acquisition	Sensor Type	Date of Acquisition	Sensor Type
1991-02-22	TM	2015-03-12	OLI	2017-03-17	OLI
1991-03-10	TM	2015-04-13	OLI	2017-04-02	OLI
1991-04-11	TM	2015-05-31	OLI	2017-05-20	OLI
1991-05-29	TM	2015-06-16	OLI	2017-06-21	OLI
1991-06-14	TM	2015-07-18	OLI	2017-07-23	OLI
1991-07-16	TM	2015-08-19	OLI	2017-08-08	OLI
1991-08-17	TM	2015-09-20	OLI	2017-09-09	OLI
1991-09-18	TM	2015-12-09	OLI	2017-10-11	OLI
1991-10-20	TM	2016-01-10	OLI	2017-11-28	OLI
1991-11-21	TM	2016-03-30	OLI	2018-01-15	OLI
1991-12-23	TM	2016-04-15	OLI	2018-03-20	OLI
2002-01-27	ETM	2016-05-17	OLI	2018-04-05	OLI
2002-05-03	ETM	2016-06-18	OLI	2018-05-23	OLI
2002-06-12	ETM	2016-07-04	OLI	2018-06-08	OLI
2002-07-14	ETM	2016-08-05	OLI	2018-07-10	OLI
2002-09-08	ETM	2016-09-22	OLI	2018-08-11	OLI
2002-10-26	ETM	2016-10-08	OLI	2018-09-12	OLI
2002-11-11	ETM	2016-11-09	OLI	2018-10-14	OLI
2002-12-29	ETM	2016-12-11	OLI		
2015-01-23	OLI	2017-01-12	OLI		

Appendix 2: shows the monthly land cover classification area for each class in KM^2 for 1991, 2002, 2015, 2016, 2017, and 2018, respectively.

Marshland cover	Jan	Feb	Mar	Apr	May	Jun	Jul	Aug	Sep	Oct	Nov	Dec
Dry area	-	486	323	235	298	322	337	366	412	394	380	587
Wet soil.	-	74	91	18	15	16	16	17	52	106	18	38
Water	-	1054	1225	947	755	712	724	676	611	773	742	666
low-density vegetation	-	63	44	78	58	72	61	57	73	372	102	195
medium density vegetation	-	7	2	337	269	294	384	281	393	39	442	197
densely vegetated	-	0	0	69	288	267	161	287	143		0	0

Marsh land cover	Jan	Feb	Mar	Apr	May	Jun	Jul	Aug	Sep	Oct	Nov	Dec
Dry area	1598		-	-	1592	1570	1543	-	1506	1469	1490	1559
Wet soil.	14				8	6	15.2		19.98	21.55	23	17.7
Water	14		-	-	11	9	15	-	20	48	41	25
low density vegetation	12		-	-	39	57	69	-	89	98	66	36
medium density vegetation	32		-	-	34	41	41	-	47	46	62	42
densely vegetated	13		-	-	0	0	1	-	2	1	2	5

Marshland cover	Jan	Feb	Mar	Apr	May	Jun	Jul	Aug	Sep	Oct	Nov	Dec
Dry area	595	-	435	268	340	443	577	688	745	-	-	712
Wet soil.	84	-	67	99	95	74	143	184	195	-	-	135
Water	760	-	766	788	554	520	388	314	287	-	-	408
low density vegetation	104	-	99	113	274	143	138	168	176	-	-	126
medium density vegetation	112	-	273	264	388	273	285	270	244	-	-	255
densely vegetated	11	-	43	153	31	231	154	59	36	-	-	48

Marshland cover	Jan	Feb	Mar	Apr	May	Jun	Jul	Aug	Sep	Oct	Nov	Dec

Dry area	833	-	476	433	446	504	498	595	566	591	585	428
Wet soil.	89	-	98	93	76	139	167	50	69	72	56	141
Water	474	-	647	684	631	376	354	470	441	405	444	500
low density vegetation	162	-	99	70	77	230	256	76	86	96	58	68
medium density vegetation	109	-	217	172	192	292	324	213	211	211	276	407
densely vegetated	16	-	147	232	262	138	85	279	310	310	265	140

Marshland cover	Jan	Feb	Mar	Apr	May	Jun	Jul	Aug	Sep	Oct	Nov	Dec
Dry area	565	-	443	331	355	439	482	504	522	525	364	-
Wet soil.	142	-	61	62	74	135	97	113	111	115	119	-
Water	542	-	702	865	624	440	461	427	417	405	486	-
low density vegetation	138	-	108	87	130	104	65	66	76	87	105	-
medium density vegetation	283	-	280	276	410	221	221	221	249	272	381	-
densely vegetated	13	-	89	62	90	345	356	353	309	279	228	-

Marshland cover	Jan	Feb	Mar	Apr	May	Jun	Jul	Aug	Sep	Oct	Nov	Dec
Dry area	630	-	541	250	478	490	649	789	848	843	-	-
Wet soil.	458	-	516	675	460	415	328	258	301	351	-	-
Water	458	-	516	675	460	415	328	258	301	351	-	-
low density vegetation	184	-	157	196	102	167	117	147	221	249	-	-
medium density vegetation	244	-	332	278	235	373	254	284	171	124	-	-
densely vegetated	21	-	29	81	250	112	230	63	2	1	-	-

Appendix 3: Landsat data type and acquisition dates.

Date of Acquisition	Sensor Type	Date of Acquisition	Sensor Type	Date of Acquisition	Sensor Type
2015-01-07	OLI	2016-03-30	OLI	2017-01-12	OLI

2015-01-23	OLI	2016-04-15	OLI	2017-03-17	OLI
2015-01-12	OLI	2016-05-01	OLI	2017-04-02	OLI
2015-04-13	OLI	2016-05-17	OLI	2017-05-20	OLI
2015-04-29	OLI	2016-06-02	OLI	2017-06-05	OLI
2015-05-31	OLI	2016-06-18	OLI	2017-06-21	OLI
2015-06-16	OLI	2016-07-04	OLI	2017-07-07	OLI
2015-07-02	OLI	2016-07-20	OLI	2017-07-23	OLI
2015-07-18	OLI	2016-08-05	OLI	2017-08-08	OLI
2015-08-03	OLI	2016-08-21	OLI	2017-08-24	OLI
2015-08-19	OLI	2016-09-06	OLI	2017-09-09	OLI
2015-09-04	OLI	2016-09-22	OLI	2017-09-25	OLI
2015-09-20	OLI	2016-10-08	OLI	2017-10-11	OLI
2015-12-09	OLI	2016-10-24	OLI	2017-10-27	OLI
2015-12-25	OLI	2016-11-09	OLI	2017-11-12	OLI
2016-01-10	OLI	2016-11-25	OLI	2017-11-28	OLI
2016-01-26	OLI	2016-12-11	OLI		

Appendix 4: Open-source satellite and product used and their sources.

Product	Source
Landsat 8 images	http://earthexplorer.usgs.gov.
SRTM DEM	http://earthexplorer.usgs.gov.
Planetary boundary layer height	https://cds.climate.copernicus.eu/cdsapp#!/dataset/reanalysis-era5-single-levels?tab=overview
Surface pressure	https://cds.climate.copernicus.eu/cdsapp#!/dataset/reanalysis-era5-single-levels?tab=overview
2m temperature	https://cds.climate.copernicus.eu/cdsapp#!/dataset/reanalysis-era5-single-levels?tab=overview
Mean surface downward short-wave radiation flux	https://cds.climate.copernicus.eu/cdsapp#!/dataset/reanalysis-era5-single-levels?tab=overview
Specific humidity	https://cds.climate.copernicus.eu/cdsapp#!/dataset/reanalysis-era5-pressure-levels?tab=overview

Appendix 5: The location of water quality sampling feeders of Al-Hammar marsh.

Number	Name of location	Location of outlet	
		East	North
1	BC 3	3420844	691726
2	BC 4	3420338	678659
3	Al Hamedy	3411700	659794
4	The Security Dike	3409755	653035
5	Al Khamissiya	3402000	647000
6	Arch Drain	3407000	648000
7	Euphrates River	3435451	618380

Appendix 6: TDS of Euphrates River 2015-2017.

Date	TDS (mg/I)	Date	TDS (mg/I)
Jan-15	3486.5	Aug-16	2400
Feb-15	3789.5	Sep-16	2375
Mar-15	3748	Oct-16	2175
Apr-15	3632	Nov-16	2238
May-15	4571	Dec-16	
Jun-15	4700	Jan-17	2237
Jul-15	4650	Feb-17	2750
Aug-15	4902	Mar-17	2600
Sep-15	3938.5	Apr-17	2310
Oct-15		May-17	2430
Nov-15		Jun-17	2337
Dec-15	2640	Jul-17	2549
Jan-16	2375	Aug-17	2890
Feb-16	2442	Sep-17	2700
Mar-16	2812	Oct-17	
Apr-16	1984.5	Nov-17	

May-16	2511	Dec-17	
Jun-16	2570	Jul-17	2549
Jul-16	2050	Aug-17	2890

Appendix 7: TDS of Al Kamissiyah canal 2015-2017.

Date	TDS (mg/I)	Date	TDS (mg/I)
5/1/15	8330	12/7/16	7840
27/1/15	8825	25/7/16	6900
15/2/15	8815	8/8/16	7150
23/2/15	9260	30/8/16	10590
15/3/15	9379	29/9/16	11144
30/3/15	9992	23/10/16	11690
13/4/15	7868	6/11/16	15760
19/5/15	8312	30/11/16	15645
19/5/15	8312	28/12/16	12098
11/6/15	8539	15/1/17	14050
28/6/15	10066	8/2/17	16350
28/7/15	15400	21/2/17	13230
9/8/15	17360	6/3/17	14050
9/8/15	17360	16/3/17	14000
9/9/15	22460	5/4/17	11590
28/10/15	18500	27/4/17	10200
18/11/15	10580	3/5/17	7800
7/12/15	9338	29/5/17	9255
20/12/15	9200	14/6/17	12960
19/1/16	8600	22/6/17	12623
19/1/16	8600	13/7/17	9988
28/2/16	8611	23/7/17	18430
8/3/16	12870	2/8/17	18533
28/3/16	13230	24/8/17	24400

28/4/16	11010	13/9/17	22000
9/5/16	11630	20/9/17	23010
10/6/16	9956	29/10/17	24040
11/6/16	15760	5/11/17	26552
13/6/16	12780	13/12/17	19200
29/6/16	12680	17/12/17	23120

11 ACKNOWLEDGMENTS

All research of this PhD dissertation was funded by:

Tempus Public Foundation (TPF) / Stipendium Hungaricum Scholarships Program.

THANKSGIVING AND DEDICATION

The content of this PhD dissertation would not have been possible without the help and support of many.

To my creator (Allah)

I am more than thankful to Allah for his blessing and help during my PhD research period.

To my family

I thank and dedicate my PhD degree to my father's soul.

I also want to express my sincere gratitude to Dr.Habil.ZoltánVEKERDY, my Ph.D. supervisor, throughout the whole process, Dr. Vekerdy was a Ph.D. supervisor and a big brother and a friend for me while I am away from home. For always supporting my Ph.D. study and related research and for the patient guidance, motivation, and immense knowledge he provided throughout my time as his student.

A special thank you to Dr. Istvan Waltner for his encouragement.
A special thanks to the head of our PhD school, Professor Erika Micheli.

I am also thankful to the PhD office at Szent Istvan University for their continued help when I asked for any documentation or papers for the ministry of higher education in Iraq.

Many thanks to the Hungarian people and Government, The Ministry of Human Capacities, Tempus Public Foundation (TPF) for granting me the PhD scholarship under the frame of Stipendium Hungaricum (SH) for providing the funding that allowed me to undertake my doctoral research and attend international conferences.

To my friends

Many thanks to my dear friends Dr.Mohammed AL-Nussairawi, Jafar Al-Aomari, and Taha Ibrahim for your support, …Thank you very much.